MINERALOGICAL AND GEOCHEMICAL STUDIES OF AGBAJA IRONSTONE FORMATION NUPE BASIN, CENTRAL NIGERIA

BY

AKINLOLU FESTUS ABIMBOLA
B.Sc.(Hons), M.Sc. (Ilorin)

A THESIS IN THE DEPARTMENT OF GEOLOGY
SUBMITTED TO THE POSTGRADUATE SCHOOL IN PARTIAL
FULFILMENT OF THE REQUIREMENTS FOR THE
AWARD OF THE DEGREE OF

DOCTOR OF PHILOSOPHY

OF THE
UNIVERSITY OF IBADAN

JULY 1994

ABSTRACT

Agbaja Ironstone Formation of the Lokoja district, Central Nigeria occurs within the Upper Cretaceous sedimentary sequences of the NW-SE trending Nupe Basin. Three lithostratigraphic units were delineated; Lokoja Sandstone (the oldest), Patti Formation and Agbaja Ironstone Formation. Lokoja Sandstone rests unconformably on the basement complex and grades from conglomerate to arkosic sandstone. Patti Formation consists of intercalations of sandstone, siltstone and carbonaceous mudstone units. Agbaja Ironstone Formation is made up of colites, pisolites and bog ore.

Textural studies show a very finely to very coarsely skewed mesokurtic sands for Lokoja Sandstone and leptokurtic for Patti Formation. ZTR index value ranges from 61 to 81% for Lokoja Sandstone and 83 to 95% for the Patti Formation. Higher ZTR index value for Patti Formation indicates a relative higher mineralogical maturity over the Lokoja Sandstone. These sedimentological studies indicate a basement source for the sedimentary materials deposited under low energy short fluvial regime, that evolved into two facies; alluvial fans and flood basin.

Four petrographic varieties of the Agbaja Ironstone Formation were identified; ooidal pack-ironstone, pisoidal pack-ironstone, detrital mud-ironstone and breccia mud-ironstone Kaolinite ooids are spherical, oblong and fragmented, usually with pseudomorphs of goethite after pyrite at the core. Goethite pisoids cemented in kaolinitic to goethitic matrix are elliptical, oval, subspherical in shape and composite in nature. Constituent minerals of the mud-ironstone are kaolinite, quartz and heavy minerals. Paragenetic studies show that pyrite, siderite, kaolinite, quartz, mica and heavy minerals are the initial minerals of the ironstone while secondary enrichment minerals are goethite, hematite, goyazite-crandallite, bolivarite and boehmite. Chemistry of these minerals further classified them into ferritic kaolinite, kaolinitic ferrite and ferrite.

SiO_2 ranges between 23.71 and 56.41% and Al_2O_3 between 22.01 and 36.54% in all the unferruginized portions of the Agbaja ironstone. But both components can be as low as 0.22% in the ferruginized equivalent. SiO_2 and Al_2O_3 contents are highest in the mud-ironstone varieties and lowest in the pack-ironstone varieties. Fe_2O_3 content increases from about 1.59% in the unferruginized to about 97.54% in the ferruginized equivalents, for all the petrographic varieties. The highest concentration of

Fe_2O_3 is in the pisoidal pack-ironstone. P_2O_5 values range between 0% in the unferruginized to 5.10% in the ferruginized portions, and often increase with increasing Fe_2O_3 contents. MgO, CaO, MnO, Na_2O and K_2O are generally less than 1.0% in all the petrographic varieties.

Element mobility during ferruginization indicates that iron enrichment is accompanied by a parallel depletion in SiO_2 and Al_2O_3, moderate to extreme reduction in CaO, MgO, MnO, Na_2O and K_2O and a significant gain in P_2O_5. This relationship confirms the supergene nature of the replacement process (desilicification, removal of alumina and iron enrichment process (ferruginization)).

Sedimentological, mineralogical and geochemical studies provided evidences for a kaolinitic precursor for the ironstone deposit, contrary to the earlier proposed chamositic precursor. Also the presence of pseudomorphs of pyrite in nuclei and as incorporation into the concentric laminae of ooids are reliable indicators for a possible accretionary model for the formation of ooids and pisoids prior to ferruginization. Two ferruginization periods unrelated to lateritization were established; first won enrichment is supply due to oxidation of the initial pyrite/siderite and reconcentration of absorbed FeOOH in the lattice structure

of kaolinite; second period is linked to the presence of bacteria (framboids) which is oxidised to form iron phosphate complex in the bog ore. The Fe and P were remobilised into the underlying pack-ironstone by descending meteoric water.

ACKNOWLEDGEMENT

wife, Eniola Margaret Abimbola for her darling support and endurance during the course of this study.

CERTIFICATION

This is to certify that this study was carried out in the Department of Geology, University of Ibadan, Ibadan, by Mr. Akinlolu Festus Abimbola.

_____

T.A. Badejoko, B.Sc.(Hons),
M.Sc., Ph.D. (Ibadan), FNMGS
Professor,
Department of Geology
University of Ibadan
Ibadan

Supervisor

_____

A.A. Elueze, B.Sc. (Hons),
M.Phil, Ph.D. (Ibadan)
Reader,
Department of Geology
University of Ibadan
Ibadan

Supervisor

DEDICATION

To my children,
Folasade and **Akinlolu Jnr.**

TABLE OF CONTENTS

Page

LIST OF PLATES

LIST OF FIGURES

LIST OF TABLES

CHAPTER ONE

INTRODUCTION

1.1   General Statement

The economic growth of a nation is related to her steel consumption. The economic growth of Nigeria in the measured consumption index of steel rose from 150,000 tons in 1960 to 2.4 million tons in 1977 and 8.5 million tons in 1990. It is projected to be 30 million tons by the year 2000.

In Nigeria iron ore deposits occur within both the basement complex and sedimentary basins (Fig. 1). In the Precambrian basement complex they are found as ferruginous quartzites and/or banded iron formations (Olade, 1978; Olade and Adekoya, 1988; Mucke and Neumann, 1986). While in the sedimentary basins they occur as oolitic ironstone formations (Adeleye and Dessauvagie, 1972; Adeleye, 1979; Oresajo, 1979; Olade and Adekoya, 1988). In 1982, the Federal Government of Nigeria initiated the establishment of two integrated steel plants, namely, Delta and Ajaokuta Steel Plants with the aim of utilising the Precambrian iron ore deposits around Okene and Maru in northwestern Nigeria. But it has long been realised that these deposits may not supply the optimum need of these plants for the realisation of the country's iron and steel dream. The importance attached to this steel project and the
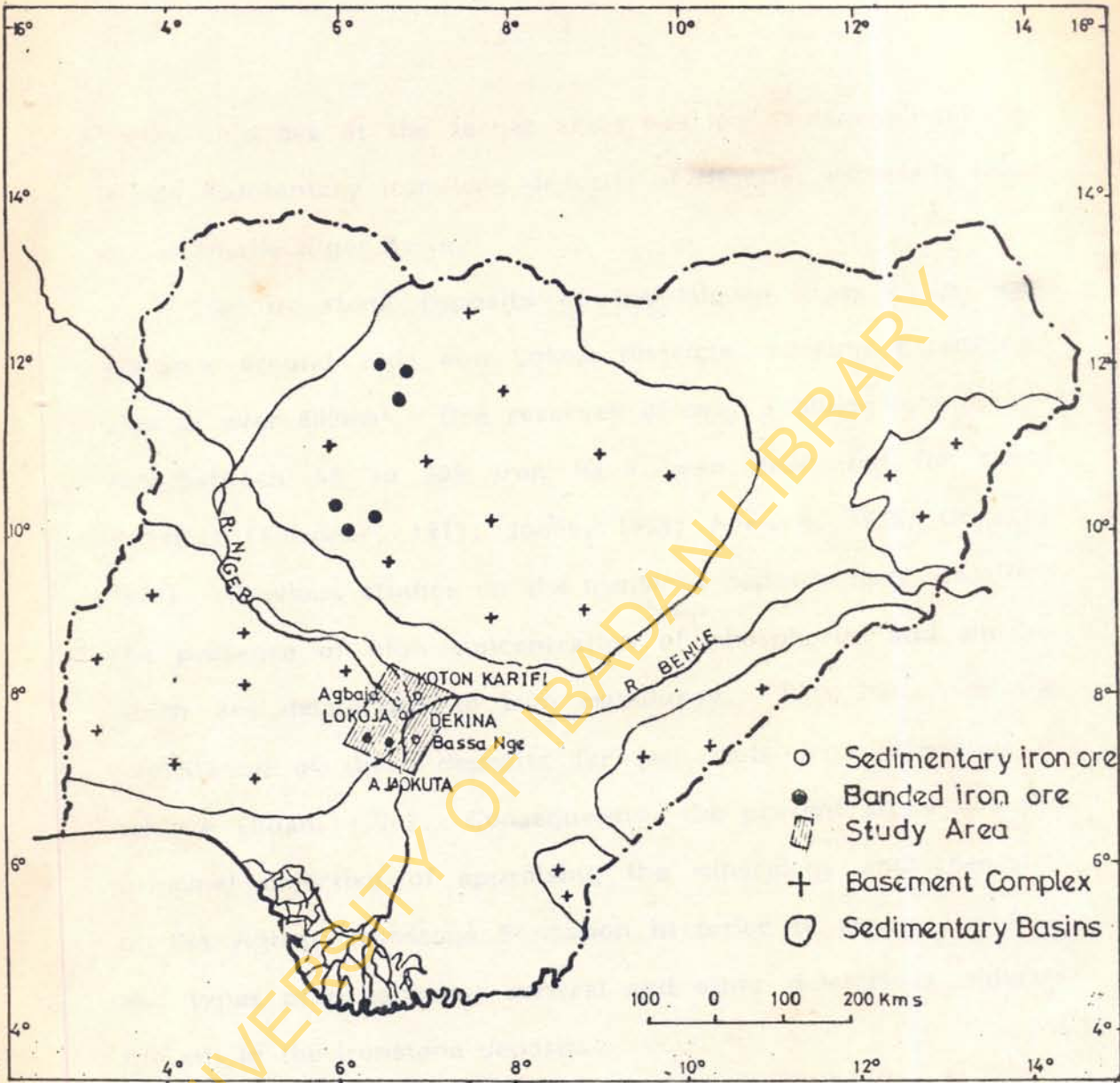
Fig. 1 Map of Nigeria showing the location of the study area

limited iron ore at the target areas has led to renewed interest in the sedimentary ironstone deposits of Nigeria, especially those of the Middle Niger Basin.

The ironstone deposits of the Middle Niger Basin cap plateaux around Bida and Lokoja districts covering a combined area of over 600km². Ore reserves of over 3 billion tons assaying between 40 to 50% iron have been delineated for these districts (Falconer, 1911; Jones, 1955; Adeleye, 1976; Oresajo, 1979). Previous studies on the ironstone deposits have identified the presence of high concentration of phosphorus and alumina which are deleterious to iron metallurgy. This has made the exploitation of these deposits for iron metallurgy impossible to achieve (Edah, 1990). Consequently, the present study has the principal objective of appraising the mineralogy and chemistry of the Agbaja Ironstone Formation in order to assess the form and types of phosphorus mineral and other deleterious minerals present in the ironstone deposits.

1.2   Objectives of the Study

The objectives of this study include:

1.   To ascertain the stratigraphic relationship of the sedimentary units of the study area, reconstruct their probable provenance and suggest their likely paleoenvironment.

2. Identify and describe the petrographic varieties and the mineral paragenesis of the ironstone deposit.

3. To establish the elemental abundance and distribution pattern in the petrographic varieties.

4. To determine the mineral chemistry of the Agbaja ironstone deposit.

5. To use all chemical and mineralogical results to propose a possible source of iron and ooids of the Agbaja ironstone deposit.

1.3 Scope and Method of Investigation

Field studies of the Lokoja area and of the Agbaja ironstone deposit was carried out on scales of 1:50,000 and 1:5,000 respectively. Samples representing rock units identified during mapping were collected for granulometry, heavy mineral studies, petrographic studies and chemical analyses. Available borehole logs and Landsat/Spot imageries were interpreted and used to complement the geological mapping.

Laboratory works involved grain size, heavy mineral and chemical analyses as well as study of polished and thin sections of ironstone and sandstone. X-ray diffratometer studies were also conducted on the powdered samples of the mudstone and

ironstone. Electron microprobe method was used for the determination of the elemental abundance and distribution in the minerals of the ironstone deposit.

1.4 Location and Accessibility

The study area, located to the eastern half of the Nupe Basin, around the confluence of rivers Niger and Benue in central Nigeria, covers an areal extent of about 400km^2. This area which lies within latitude 7°15' to 8°45'N and longitude 6°00' to 7°10'E (Fig. 1) is referred to as the Lokoja district in this study.

Three major ironstone deposits can be isolated as plateaux in the study area, namely, Agbaja Plateau (west of the confluence), Kotonkarifi Plateau (north of the confluence) and Bassa-Nge Plateau (south east of the confluence).

Agbaja Plateau is about 25km west of the Okene-Lokoja road through the Filele-Agbaja unpaved road. Kotonkarifi Plateau, 20km north of Lokoja township is about 800m east of the Lokoja-Abuja road. Bassa-Nge Plateau, located 200km east of Okene township is about 40km west of the Okene-Ayangba road (Fig. 2). Traverses were made through minor roads and footpaths which become more open for use during dry seasons when bushes were burnt.
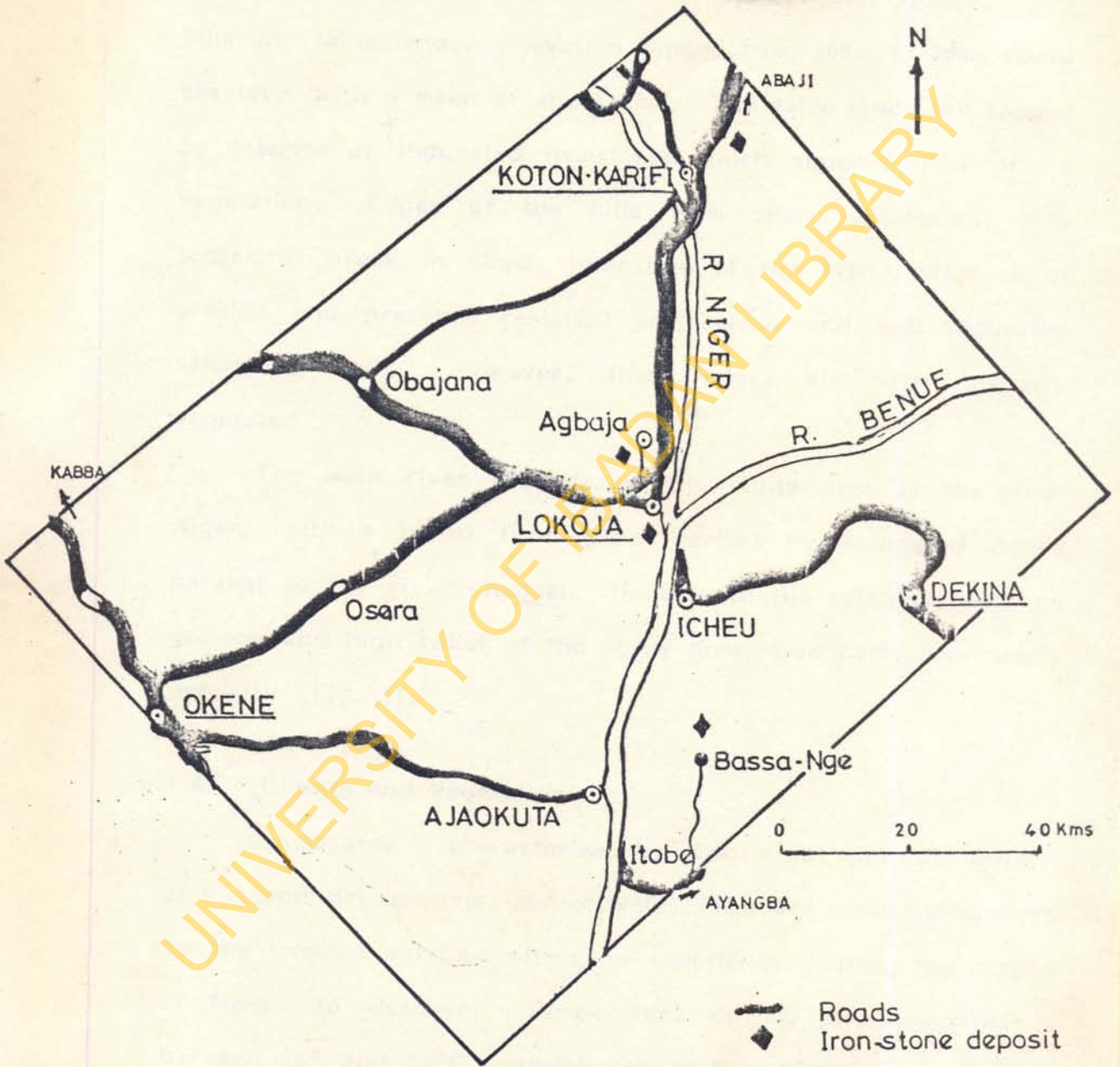
Fig. 2 : Accessibility within the study area

Roads
Iron-stone deposit

ABAJI

KOTON·KARIFI

R. NIGER

R. BENUE

Obajana

Agbaja

KABBA

LOKOJA

DEKINA

Osara

ICHEU

OKENE

Bassa-Nge

AJAOKUTA

Itobe

AYANGBA

0   20   40 Kms

N

1.5   Topography and Drainage

The study area is characterised by irregular ridges, steep hills and table lands. Elevation ranges from 200m to 750m above sea level with a mean of about 30m. The table lands are capped by laterite or indurated ironstones which support little or no vegetation. Edges of the hills form sharp escarpment with occasional break in slope, indicative of the effect/influence of erosion and presence resistant argillaceous and well indurated sandstone beds. However, these edges are often densely vegetated.

The main river that drains the study area is the river Niger, with a broad flood plain marked by elongated ponds parallel to the river channel. Hence with the relatively uniform geology and high relief of the study area, flow pattern is mainly dendritic (Fig. 3).

1.6   Climate and Vegetation

Lokoja area is characterised by about eight and four months of wet and dry seasons, respectively. The wet season influenced by the tropical maritime winds, is experienced during the months of March to October. Temperature during these months is between 18° and 32°C, rainfall ranges from 120-200mm and very high humidity which ranges from about 95% (morning) to 65%
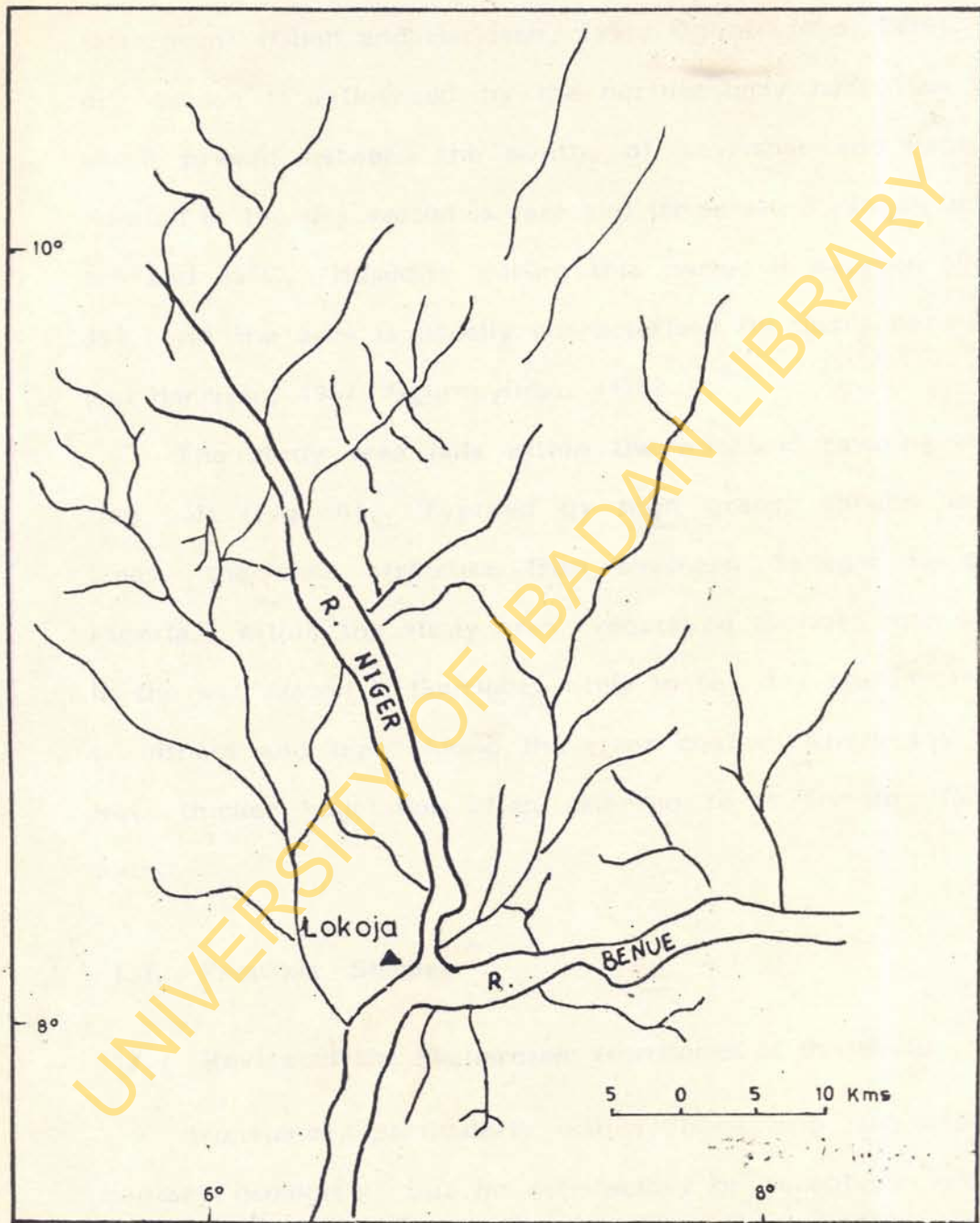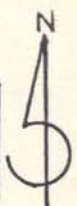
Fig. 3: Drainage pattern of the Study Area

(afternoon) (Oboli and Harrison, 1957; Oguntoyinbo, 1978). The dry season is influenced by the northeasterly harmattan winds which prevail between the months of November and February. Rainfall in the dry season is rare and temperature ranges between 30° and 35°C. Humidity during this period is between 30% and 35%, and the area is usually characterised by dusty haze (Oboli and Harrison, 1957; Oguntoyinbo, 1978).

The study area falls within the woodland savanna vegetation belt (Fig. 4). Typified by high grass, shrubs and low trees, the belt stretches from southern Senegal to central Nigeria. Within the study area, vegetation changes with season, in the wet season it flourishes while in the dry season, much of it withers and die. Along the river courses where the soil is wet, thicker vegetation often referred to as fringing forest is found.

1.7   Previous Studies

1.7.1 Review of the Phanerozoic Ironstones of the World

Ironstones, particularly oolites, have long fascinated sedimentary geologists, but no satisfactory or acceptable model has been developed for the origin of the ironstones. This failure
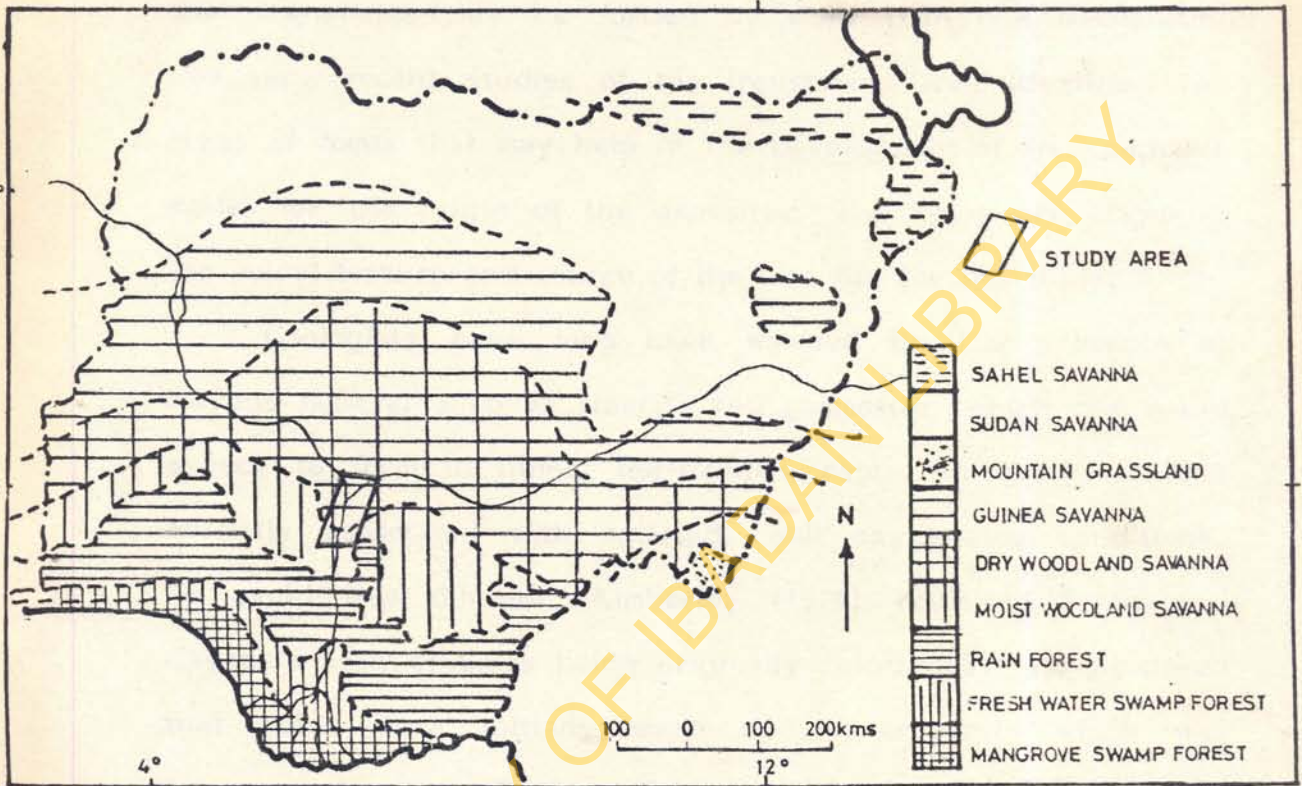
Fig 4 : Vegetation Map of Nigeria (Modified after Ileoje; 1972).

STUDY AREA

SAHEL SAVANNA
SUDAN SAVANNA
MOUNTAIN GRASSLAND
GUINEA SAVANNA
DRY WOODLAND SAVANNA
MOIST WOODLAND SAVANNA
RAIN FOREST
FRESH WATER SWAMP FOREST
MANGROVE SWAMP FOREST

100 0 100 200kms

is attributable to the absence of modern analogues and to the fact that ironstones may be formed by more than one mechanism. However, recent studies of the ironstones have identified two areas of focus that may help in the development of an acceptable model for the origin of the deposits. The areas are origin of the ooidal texture and source of the iron for the ironstone.

Geologists have long been worried by the presence of ferrous mineral such as siderite and chamosite, which one would expect to form in quiet, low-oxygen water, in oolite, a rock normally associated with agitated, well oxygenated conditions. To avoid this dilemma, Kimberley (1979) reviewed Sorby and Cayenx's idea of ooids being originally calcareous. He proposed that ooids were initially made up of aragonite which was subsequently transformed into chamosite and goethite by downward percolating meteoric waters that leached iron from the overlying organic-rich fluviodeltaic sediments. The lack of carbonate sediments in most ironstone sequences, the evidence for early formation of the ooids, and the rarity of the proposed stratigraphic succession have been cited as evidence against this model (James and Van Houten, 1979; Hallam and Braashaw, 1979; Van Houten, 1985, 1986; Kearsley, 1989; Van Houten and Hon, 1990). Another problem is the high alumina content of these

oolites.   Since aluminium is one of the least mobile elements in rocks, it is improbable for meteoric water to have added the much alumina to ironstone.

Another hypothesis assumed that the ooids are detrital, being eroded soil ooids from lateritic terrains (Siehl and Thein, 1978; Nahon et al., 1980; Madon, 1992).   This idea provides the source of the iron and the aluminum and an explanation for the texture.   However, most ironstone deposits have the core of ooids incompatible with a soil origin, such as phosphatic or calcareous shell debris or quartz grains and tangential orientation of the ooidal texture (Bhattacharyya and Kakimoto, 1982).   These arguments do not preclude a preconcentration of iron in the source area by lateritic weathering, with rearrangement into ooids in the environment of deposition.   A more likely explanation for the origin of the ooids is that chamosite formed in quiet waters are washed up into shoals possibly by storms (Knox, 1970) while goethite ooids are formed in more agitated water (James and Van Houten, 1979; Van Houten, 1985; Van Houten and Hon, 1990).

There are five ways suggested for the transportation of iron to the site of deposition (Table 1).   However, no information exists to point to any one of these as the correct mechanism for the source of iron.   However, a recent study of Ordovician

TABLE 1:   Possible mechanisms for the production of ooidal ironstone (modified after Maynard, 1983; Kimberley, 1989).

ORIGIN OF OOIDS

(i)   Replacement of pre-existing aragonite ooids by iron-bearing solutions.

(ii)   Erosions and redeposition of soil ooids and pisoids from lateritic terrains.

(iii)   Direct precipitation from sea water as true ooids.

(iv)   Formation in a quiet water environments, either as scattered ooids or mudflats or as microconcretions within the sediments, and subsequent transportation into sand bars.

SOURCE OF THE IRON

(i)   Volcanic.

(ii)   Groundwater:

    (a)   Downward – from overlying organic-rich muds

    (b)   Upward – from underlying aquifers (submarine springs)

(iii)   River water (iron – in solution, as colloids or organic complexes)

(iv)   Sea water (upwelling of deep, anoxic basin water)

(v)   Prewaters (upward diffusion of iron from underlying organic-rich sediments).

chamosite ooids in Sweden established that their iron was derived from the volcanic ash (Sturesson, 1992). Also the supply of iron by diffusion from underlying organic-rich sediments is unlikely as observed in stratigraphic successions associated with oolitic ironstone formations (James and Van Houten 1979; Hallam and Braashaw, 1979; Van Houten, 1985, 1986; Young, 1989; Van Houten and Hon, 1990). Upward-moving groundwater discharging from submarine springs could introduce iron to the depositional environment to be precipitated as primary ooids. However, submarine springs noticed in modern shelves are not associated with appreciable iron enrichment.

Transport of iron by river waters has been the most discussed hypothesis. It has been demonstrated that the dissolved iron in rivers is carried as mixture of oxide and organic matter colloids (Taylor, 1949; Hallam, 1975; Boyle et al. 1977). These are rapidly precipitated in estuaries and constitute a potential source of iron for semi-restricted near-shore basins. An alternative mode of transport of the iron is as a coating on detrital clay (Carroll 1958; Harder, 1989; Mucke, 1993; Haase, 1993) or as lateritic particles. Another source of iron is the upwelling of basinal water (exhalative model) as proposed by Kimberley (1989).

1.7.2   Review of Work Done on the Ironstone Deposits of Nigeria

The geology of the Middle Niger Valley was first studied by Falconer (1911), during a reconnaissance survey by the Mineral Surveys of Nigeria.   He characterised the various sedimentary successions of Sokoto, Bida and Lokoja as the Lokoja Series.   Although he believed that the ironstones are sedimentary in origin, but excluded them from the marine facies of the Sokoto area because the ironstones lack fossils.   However, in a separate stratigraphic and correlation studies, Tattam (1943) introduced the term Nupe Sandstone for sediments around Bida, which were referred to as shallow water unfossiliferous sediments.

The Geological Survey of Nigeria, in 1955, carried out an economic evaluation of the ironstone around Lokoja by drilling about thirty boreholes in the Agbaja plateau.   Jones (1955, 1958) sedimentological studies of these core samples revealed a conglomeratic to predominantly argillaceous sediments resting unconformably on the basement complex.   He referred to these sedimentary successions as Lokoja Sandstone and the Patti Formation.   He noted that the Patti Formation is a lateral equivalent of the lower part of the coal bearing sediments of the Abhocho-Dekina and Enugu regions.   This he took to indicate an upper Senonian age for the Patti Formation, a conclusion he

believed was confirmed by the presence of Campanian to Maestrichtian flora in the Lower Coal Measures of the adjacent Anambra Basin. The Lokoja Sandstone was described as an arenaceous facies of the shales which underlie the western fringe of the Cross River plain at Enugu.

A more detailed picture of the stratigraphy and sedimentation history of the basin emerged from the works of Adeleye (1971) and Adeleye and Dessauvagie (1972). They gave the sedimentary successions of the basin around Bida and their lateral equivalents in Lokoja and Dekina.

Four formations were recognisable in the central part of the basin, all of which are of Campanian to Maestrichtian in age (Adeleye, 1971; Adeleye and Dessauvagie, 1972). These formations are Bida Sandstone (oldest), Sakpe Ironstone, Enagi siltstone and Batati Ironstone (youngest). The lateral equivalents of these formations in the Lokoja district are the Lokoja Sandstone (oldest), Patti Formation and Agbaja Ironstone (Fig. 5). Summaries of these were also presented in the works of Adeleye and Halstead (1972); Adeleye (1973; 1975a); Kogbe (1976); Adeleye (1979) and Agyingi (1991). The established sedimentary successions demonstrate fluvial, braided alluvial fans in poorly drained flood plains (Adeleye, 1973; Ladipo et al. 1988, 1993;
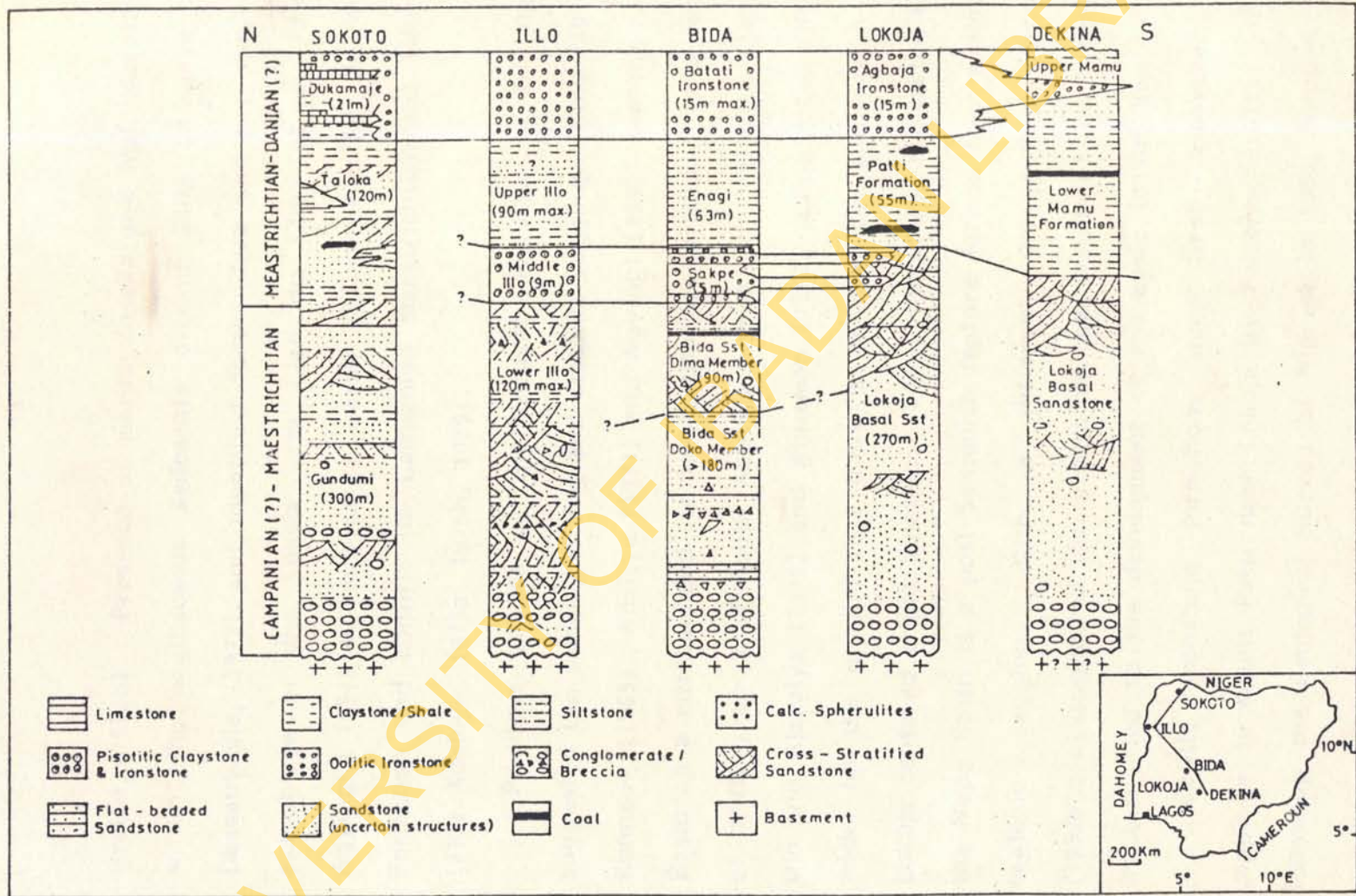
Fig. 5 : Generalised stratigraphical correlation of the Campanian – Maestrichtian Strata of the Nupe Basin (modified after Adeleye, 1973)

Braide, 1992b). Presence of marine fossils and leaf impressions within the argillaceous sediments around Bida (Adeleye and Dessauvagie, 1972) and identified foraminifera and palynomorphs assemblage of the Lokoja area (Jan du Chen et al., 1978; Agyingi, 1991) all suggest a marsh environment for the Patti Formation and confirm its Campanian Maestrichtian age (Murat, 1972; Adeleye, 1975a, 1975b, 1979).

Previous studies on the tectonic evolution of the basin suggested two models; rifting and cratonic sagging. King (1950), Kennedy (1965), Adeleye (1971) and Agyingi (1991) saw the Nupe Basin as a rift-bounded tensional structure produced as a result of drifting apart of South America and Africa. Holmes (1975), Ojo and Ajakaiye (1976) and Whiteman (1982) opposed the rifting model on the ground that there is no available evidence for a Lokoja centered triple junction. They, therefore, suggested that the Nupe Basin is a post-Santonian feature formed from a simple cratonic sagging. With a different perspective, Braide (1992a,b,c) suggested that a possible reactivation of the basement fractures led to the development of the basin in the Santonian.

Oolitic ironstone formations were first discovered as cappings to Mount Patti near Lokoja by Falconer (1911). In a follow-up the Geological Survey of Nigeria in 1955, mapped out

an extensive oolitic ironstone deposits similar to those of Mount Patti around the rivers Niger-Benue confluence. Twenty nine exploratory boreholes totalling 550.6m in depth were drilled to evaluate the deposits. BRGM (1982) used the samples and lithologs got from these exploratory boreholes to delineate three target areas, namely, Agbaja-Mount Patti, Kotonkarifi and Bassa-Nge. Further lithological studies suggested three types of cyclotherm for the ironstone deposits; they are coarsening upward, fining upward and fining upward and downward (Adeleye and Badejoko, 1975). It was also observed that the ironstones were deposited in a fluvial dominated deltaic environment (Adeleye and Badejoko, 1975; BRGM, 1982; Astier et al., 1989).

Petrographic studies revealed two types of ferruginous facies; the fine interbedded oolites and the weathered oolites (Jones, 1953, 1958). Texturally the ironstone deposits were classified into their oolitic or pisolitic facies (Jones, 1965; Oresajo, 1979; BRGM, 1982; Agyingi, 1991). Earlier mineralogical studies revealed the prepondence of goethite and hematite as ooids with subordinate existence of iron silicate and carbonate minerals as matrix (Jones, 1955, 1958, 1965; BRGM, 1982; Uwadiale and Hall, 1985). Recent workers have confirmed the presence of the above mentioned ooids but believed that the

primary matrix material is dominantly kaolinite (Ladipo et al., 1988, 1993; Mucke, 1993; Haase, 1993).

The iron content of the Mount Patti ironstones was first estimated to be 50% with a reserve of about 2,000 million tons (Dunstan, 1911). This reserve was later found to be over-estimated (Jones, 1955). Detailed chemical study of the ironstone deposits revealed an assay of 43-45% Fe and that P_2O_5 increases with iron content (Jones, 1955; Adeleye and Badejoko, 1975). Later studies confirmed the range of the iron content and further ascertain that the ironstones are rich in phosphorus and alumina and low in silica and titania (Oresajo, 1979; Uwadiale and Hall, 1985; Astier et al., 1989; Mucke, 1993; Ladipo et al., 1993; Haase, 1993).

The presence of deleterious phosphorus and alumina in the deposits has been largely responsible for not using the ironstones in the steel industry. Bearing this in mind BRGM (1982) designed a selective oil agglomeration and magnetising reduction beneficiation technique for the removal of phosphorus contents of ironstone deposits. This technique was however modified to involve the addition of lime powder and injection of oxygen into the beneficiation scheme during sintering (Uwadiale and Hall, 1985; Astier et al., 1989; Uwadiale, 1991, 1992).

Models proposed for the origin of the ironstone deposits include, synsedimentary, lateritic and post-diagenetic models. Falconer (1911), Adeleye and Dessauvagie (1972), Adeleye (1973) and Oresajo (1979) suggested a synsedimentary origin for the ironstones because their depositional characteristics and relation-ship with other sediments of the basin show that the ooids were formed within a high energy domain. The lateritic model was postulated presumably due to the absence of fossils in the ironstone beds (Du Preez, 1956) and to the presence of iron oxide and hydroxide in of the ooids (Jones. 1955, 1958; Kogbe, 1978). Recently, a post-diagenetic iron enrichment model has been suggested for the ironstone deposits (Ladipo et al., 1988, 1993; Mucke, 1993; Haase, 1993; Mucke et al., 1994).

1.8   Review of Nomenclature

Iron formation is considered to be a stratigraphic unit consisting essentially of iron-rich chemical sedimentary rock. Generally they are rocks with more than 15% Fe (Kimberley, 1978). Several authors have used the terms, ironstone and iron formation, in restricted ways. For instance "ironstone" has been used to name non-cherty, oolitic rocks of Phanerozoic age while "iron-formation" has been used exclusively for cherty, banded

iron formations of Precambrian age (Gross, 1965; James 1966; Skinner, 1969; Dimroth, 1975; Guilbert and Park, 1986). However, these restrictions have been found by some authors to be inconsistent with the simplicity of the names (Dimroth and Chauvel, 1973; Hall and Goode, 1978; Kimberley, 1978; Trendall, 1983; Kimberley, 1980, 1989). It was also argued that the alternative usages of these terms have been sufficiently varied recently that none of the usages can be defended on the grounds of overwhelming support.

Thus by analogy with limestone, ironstone is simply an iron-rich chemical sedimentary rock. The word formation refers to a stratigraphic unit and so "iron formation" is applied to any stratigraphic unit which is composed predominantly of ironstone (Kimberley, 1989). The preposition that ironstone should be a lithological term, age notwithstanding was upheld during the Phanerozoic Ironstone Workshop (Young, 1989). The workshop however rejected the earlier classification scheme of oolitic iron-stone formation into "Minette" or "Clinton" type deposits. The complex mineralogy of most ironstone has made any petrographic nomenclature unwieldy. It is probably most important in these rocks to stress the textural information in the nomenclature and

add mineralogical information as the context requires. Dunham's (1962) style of classification, based on texture originally erected for carbonates was used as basis for the nomenclature of ironstones. The workshop proposed that in view of the common occurrence of ironstones and limestones in a single sequence, the use of "... stone" in the Dunham Classification should be replaced by "... ironstone" (e.g. mud-ironstone, ooidal pack-ironstone). It was further recommended that mineralogical and allochem qualifiers be used where appropriate. The basic nomenclature for the allochems within ironstones follows that of limestones (Table 2). For petrographic examination emphasis should be laid on the allochem and groundmass mineralogy. The workshop however agreed that the allochem and groundmass mineralogy should be expressed as noun and adjective, respectively. If no adjectival form is available then the noun may be used. In all cases the allochem mineralogy is given before the allochem type and the groundmass mineralogy before the textural term. Thus a berthierine-rich, matrix supported ironstone with 15% goethite ooids could be termed a "goethite ooidal berthierine wacke-ironstone".

TABLE 2: Recommended terminology of allochems in ironstones (modified after Young, 1989).

Concentrically structured grains	
<2mm	>2mm
grain	ooid	pisoid
adjective	ooidal	pisoidal
rock	oolite	pisolite

Plastically deformed concentrically structured grains

grain	spaslolith
adjective	spaslolithic

Grains without concentric structure

grain	peloid
adjective	peloidal

Petrographic terms whose use is not recommended

oolith
oolitoid
pisolith
pisoloid (+ pisoloid rock)

CHAPTER TWO

GEOLOGICAL SETTING OF THE NUPE BASIN

2.1 Regional Geology

2.1.1 Tectonic Setting

The Nupe Basin, also referred to as the Middle Niger Basin or the Bida Basin, is a NW-SE trending intracratonic basin adjacent to the main axis of the Benue Trough (Fig. 6). The basin is often regarded as a northwestern extension of the Anambra Basin to the southeast (Fig. 6), both of which were major depocenters during the second major sedimentary cycle of southern Nigeria in Upper Cretaceous (Murat, 1972).

Several authors have expressed their views as regards to the genesis of the Nupe Basin. King (1950), Kennedy (1965), Holmes (1975), Ojo and Ajakaiye (1976) and Whiteman (1982) support the idea that the Nupe Basin was formed as a post-Santonian event, except Agyingi (1991) who observed two possibilities of a pre-Santonian origin. Firstly, Agyingi (1991) suggested that as a result of tensional build-up in the Benue Basin during the separation of Africa from South America (Aptian-Albian), the adjacent area probably sagged along northwest-southeast oriented fracture to ease the tensional build-up and gave

Legend:
- ||||| Benue Trough
- ≡ Nupe Basin
- +++ Precambrian

Map labels: Sokoto, IULLEMEDEN BASIN, R. Niger, NUPE BASIN, Bida, Lokoja, R. Benue, ANAMBRA BASIN, Enugu, Lagos, Accra, NIGER DELTA, ATLANTIC OCEAN

15°N, 10°, 5°N, 0°E, 5°, 10°E

Km.0   100 Km.

26
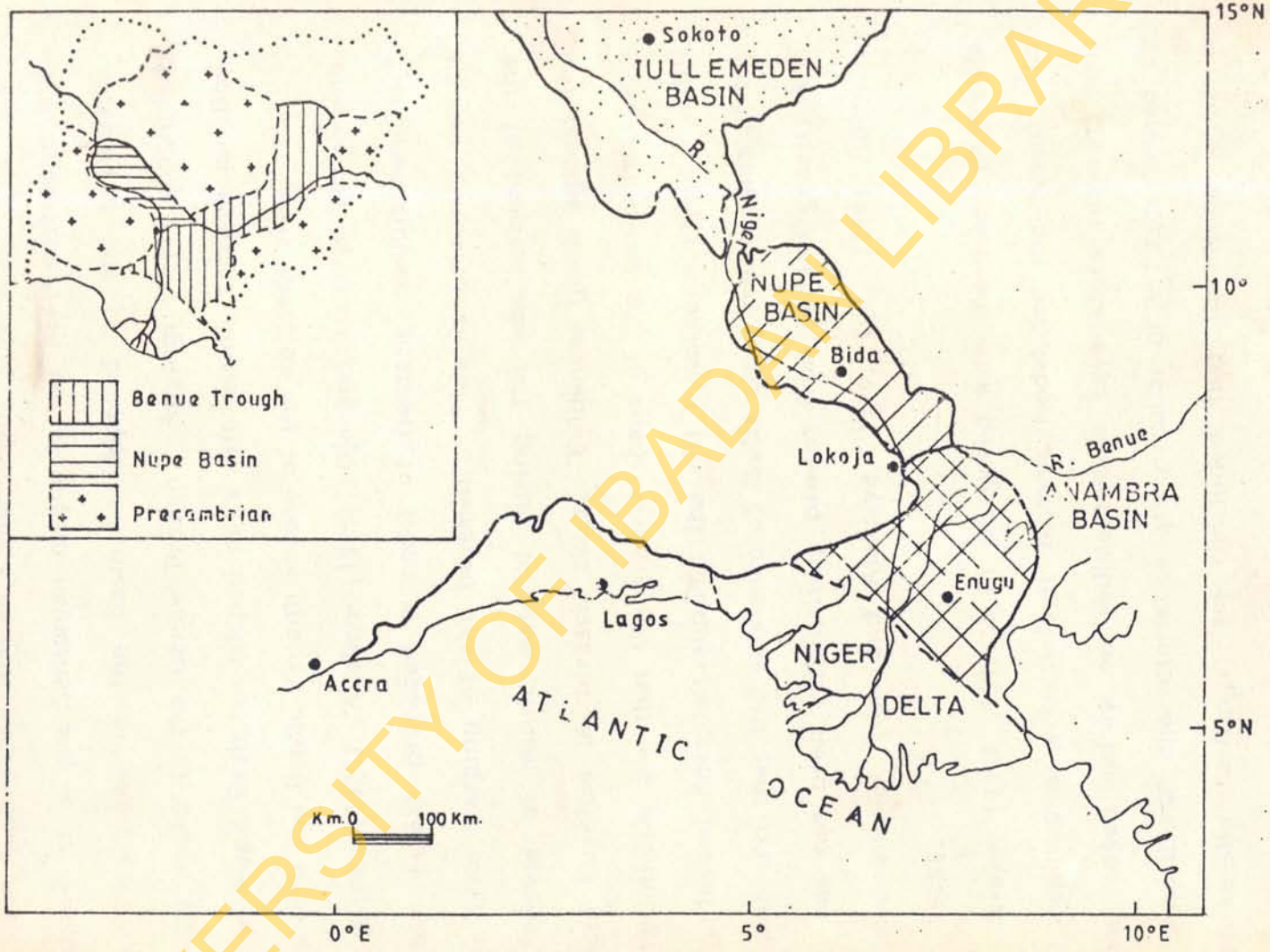
FIG. 6 : NUPE BASIN AND ITS ADJOINING UPPER CRETACEOUS AND TERTIARY SEDIMENTARY BASINS. (modified after Whiteman, 1982)

rise to the Nupe depression as a side basin. The other observation in support of a pre-Santonian origin is the northwest-southeast oriented fractures in the basin as opposed to the northeast-southwest trend in the Benue Trough. Agyingi (1991) concluded that the Nupe Basin developed as a rift within a triple junction system with the Benue Trough as one of the adjacent arms.

Holmes (1975), Adeleye (1975), Ojo and Ajakaiye (1976) and Whiteman (1982) proposed a model of isostatic readjustment and gentle down warping of the basement. This is primarily due to the removal of mantle material during the emplacement of the Younger Granites in Jurassic times. Evidences given against the rift hypothesis are that the general shape of the basin (maximum width, 160km) does not support the rift hypothesis (typical width 50±13km) and that the existence of faults along the margins of the basin has not been conclusively proven from ground gravity and magnetic studies (Ojo and Ajakaiye, 1976; Ojo, 1984; Adeniyi, 1985, 1986).

Braide (1990, 1992a,b,c) disagreed with these earlier models and proposed a wrench-fault tectonic model for the basin. His studies based mainly on sedimentologic parameters revealed that the depositional characteristics are peculiar of a basin formed by a strike-slip faulting. He concluded that the Nupe Basin is

structurally related to the wrench tectonics of the Benue Trough (Braide, 1990, 1992a,b,c). However, possible tectonic framework of the Nupe Basin is suggested in Chapter Three.

2.1.2   Stratigraphy

Rocks in the Middle Niger Basin can be divided into two major types, the basement complex and the sedimentary formations. The basement complex is from Precambrian to lower Paleozoic in age and it is undifferentiated in some areas. The sedimentary formations are flat-lying Campanian-Maestrichtian sediments. The ages of the beds is based on some identified Campanian-Maestrichtian palynomorphs (Adeleye, 1973; Agyingi, 1991).

Directly overlying the basement complex are poorly exposed basal beds of coarse conglomerate and cross stratified sandstone with angular pebbles (Adeleye and Halstead, 1972). Conformably overlying these basal beds are continental sediments comprising mainly sandstone, siltstone and claystone. These beds are known by various local names, Bida Sandstone around Bida and as Lokoja Sandstone around the rivers Niger/Benue confluence. The formation is made up of two members, the Doko Member and Jima Member (Adeleye, 1974).

Sandstones of the Doko Member are arokosic to quartose and poorly sorted with angular to sub-angular grains. The quartz

and feldpar grains are irregular to roughly tabular. Arkosic sandstones inter-beded with fine-grained feldspathic sandstone are poorly sorted and commonly medium to coarse-grained. Quartzose sandstones are poorly sorted and fine to coarse-grained. They grade into the basal arkose. Jima Member which overlies conformably the Doko Member consists dominantly of intercalations of cross-stratified quartzose sandstone, siltstone and claystones. Fossils found in this member are leaf impressions.

Bida sandstone is overlain by oolitic/pisolitic ironstones of the Sakpe Ironstone Formation which consists of the Wuya and Baro Members (Adeleye, 1973). Wuya Member consists of oolitic and pisolitic ironstones with intercalations of locally developed claystones. Baro Member is made up of oolitic ironstones with scattered nodules of pyrite. Irregular intercalations of ferruginous sandstone are found in this member. Occurrence of faunal, bivalves and fossil wood has shown that the Sakpe Ironstone Formation was deposited under marine conditions (Adeleye, 1971). The lateral equivalent of the Sakpe Ironstone Formation is however absent in the Lokoja area.

Regionally, overlying the Sakpe Ironstone are dominantly argillaceous beds with subsidiary fine grained sandstones and lignite. These argillaceous strata are known as the Enagi

Formation and Patti Formation around Bida and Lokoja, respectively. The Patti Formation consists of fine to medium grained sandstone, carbonaceous siltstone and shale with massive thin intercalations of coal. Abundant leaf impressions and rootlets are common within the formation (Adeleye, 1971). Adeleye (1973) suggested a Maestrichtian age for the formation and that the formation was deposited during the withdrawal of the Tethys northwards (Adeleye and Halstead, 1972).

Succeeding the argillaceous strata is another ironstone horizon dominated by goethitic ooids. This ironstone is referred to as the Batati Ironstone Formation around Bida and as Agbaja Formation around the Niger/Benue confluence. The ironstone beds form resistant cappings to the Campanian Maestrichtian sediments of the Nupe Basin. Found associated with the ironstone especially in the Bida area are ferruginous claystone, carbonaceous shaly beds and siltstone. Two ironstone members are recognised in the Bida area, namely, Edochigi Ironstone Member, dominantly made up of goethite ooids and the underlying Kutigi Member which is mainly goethite and kaolinitic ooids.

The entire Campanian-Maestrichtian strata are unfolded and show a northerly regional dip. However, the Cenozoic and later erosions have greatly affected the present day distribution of the

strata (Jones, 1955, 1958; Adeleye, 1971, 1973; Agyingi, 1991; Braide, 1992a,b,c). A generalised stratigraphical correlation chart can be made for the Campanian-Maestrichtian strata of the Middle Niger Basin stretching from Dekina in the south to Sokoto in the north (Fig. 5).

2.2   Local Geology

2.2.1   Structural Analysis of the Lokoja District

Three main geological boundaries were demarcated using the imageries (Fig. 7).

(i)   Alluvium, along the rivers Niger and Benue.

(ii)   Sedimentary rocks, between the river alluvium and the basement rocks.

(iii)   Basement rocks towards the south and north of the river Niger.

Lineaments in the study area can be subdivided into three major sets oriented in a N50 – 60°E, N130 – 140°E and N5 – 15°E direc-tions (Fig. 7). The northeastern sector (B2, Fig. 7) is highly sheared with abundant N-S trending lineaments, characteristics of Proterozoic schist belts. NE-SW and NW-SE fracture trends are common in all the rock types identified. These fractures cross-cut the N-S lineament, while the NW-SE fractures truncate the NE-SW. Relative age relationships of these fractures were confirmed from field observation and measurements in the Lokoja

area. It is worth mentioning that both rivers Niger and Benue are structurally controlled as their trends are related to the identified NW-SE and NE-SW trends, respectively. The major fracture sets established above also suggest that at least two important tectonic events occurred post-Precambrian in the Nupe Basin.

2.2.2   Lithostratigraphy of the Lokoja District

1.   LOKOJA SANDSTONE

The Lokoja Sandstone rests uncomformably on the basement complex and the contact is exposed around Lokoja town and at about 2 km to Lokoja along the Okene-Lokoja road. This forma-tion which extends from Filele to Kotonkarifi in the northeastern part of the study area is made up of conglomerates often overlain by sandstone units. The average overall thickness of the forma-tion is estimated at about 30m (Adeleye, 1973; Agyingi, 1991; Braide, 1992a).

Conglomerates are not present in all the localities but where present they occur as loosely stratified bodies overlying uncom-formably the basement rocks (Figs. 8 and 9). The conglomerates consist of well rounded quartz, feldspars and metamorphic/igneous rock pebbles and cobbles in a whitish kaolinitic to micaceous
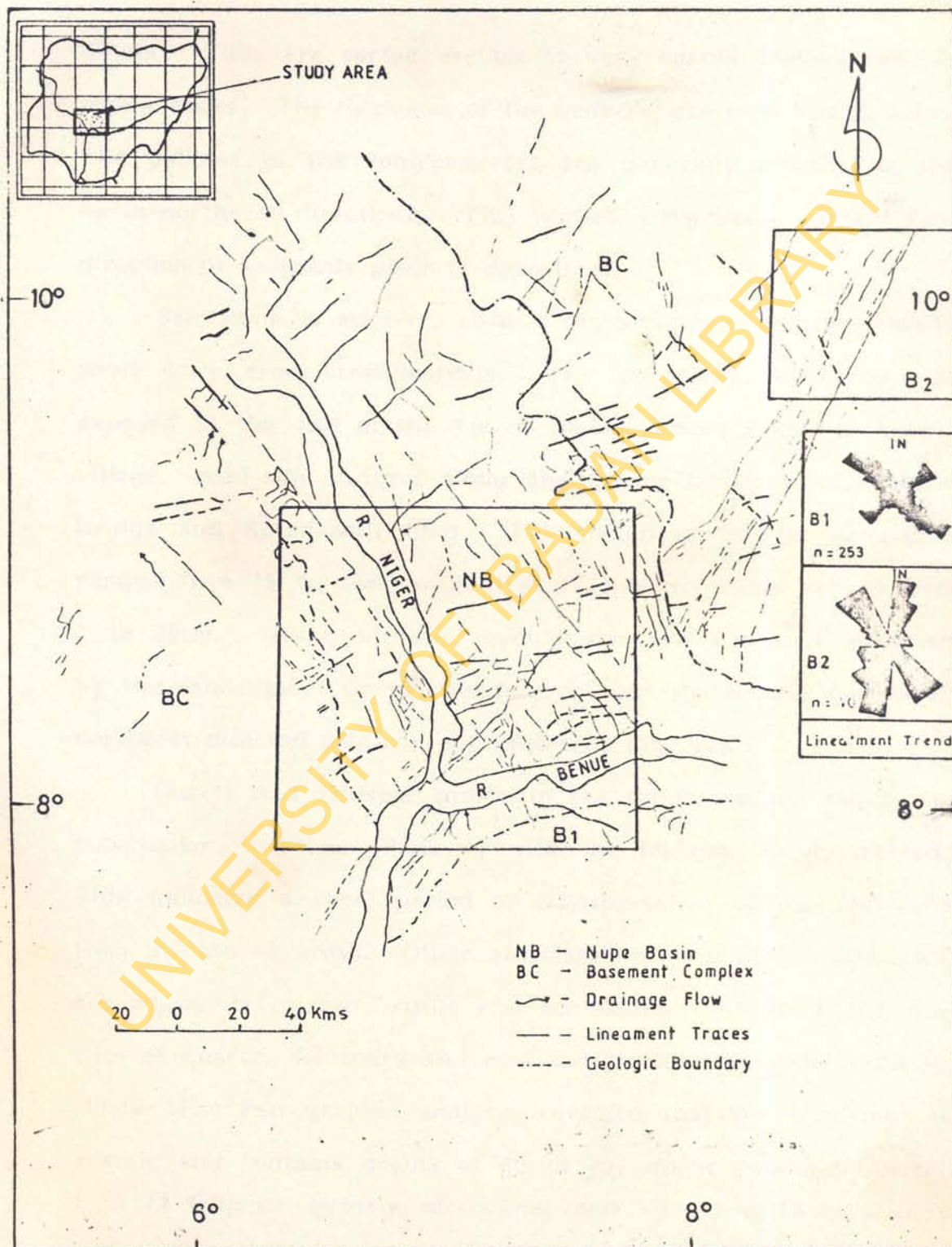
FIG. 7. LINEAMENT TRACES OF THE LOKOJA

NB — Nupe Basin
BC — Basement Complex
∿ — Drainage Flow
— — Lineament Traces
-·- — Geologic Boundary

20 0 20 40 Kms

matrix. They are sorted medium to very coarse grained reddish brown rocks. The thickness of the beds ranges from 5cm to 2.5m. The pebbles in the conglomerates are generally oriented in the north-northeast directions. This implies a northeast current flow direction of sediments prior to deposition.

Sandstone is massive, medium to coarse grained and exhibits small scale cross-stratifications. The sandstone units are well exposed at the foot of the Agbaja plateau about 3 kms to Agbaja village, road-side cutting along the Lokoja-Jamata road, Jamata bridge and Kotonkarifi town. The thickness for the sandstone ranges from 15 to 30m, while that of the cross-sets ranges from 2 to 30cm. Fining upward cyclotherms are also well exhibited by the sandstone. Cross-stratification azimuths show a dominantly northeast directed paleocurrent (Table 3, Fig. 10).

Quartz and feldspar grains in the sandstone are angular to subangular in shape (Plate 1) with the feldspar rarely altered. This indicates a short period of transportation of the sediments from the source areas. Other associated mineral of the sandstone are muscovite, zircon, rutile and tourmaline. Kaolinite and fine silts of quartz, feldspars and mica constitute the matrix materials (Plate 1). Petrographic analysis revealed that the sandstone is arkosic and contains grains of 60 t0 80% monocrystalline quartz, 1 to 7% feldspar (mostly microcline) and less than 1% crystalline rock fragments, in a matrix of about 15%.
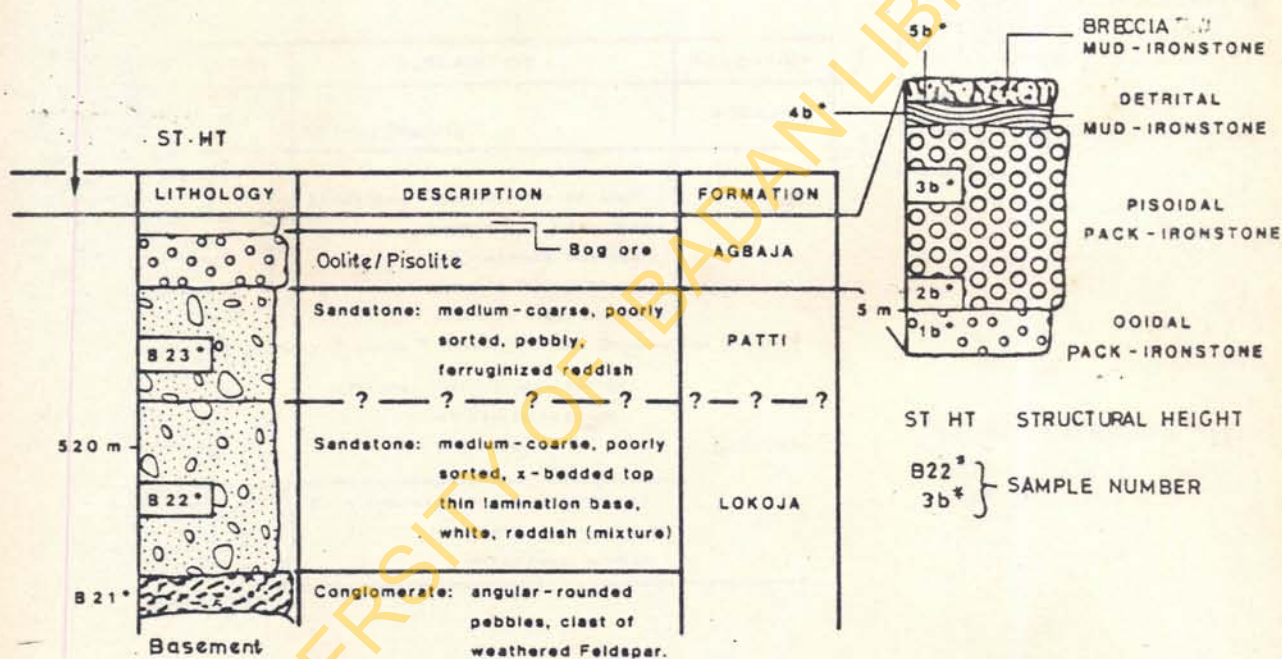
Fig. 8 : Lithologic section of Agbaja plateau locality AG / B
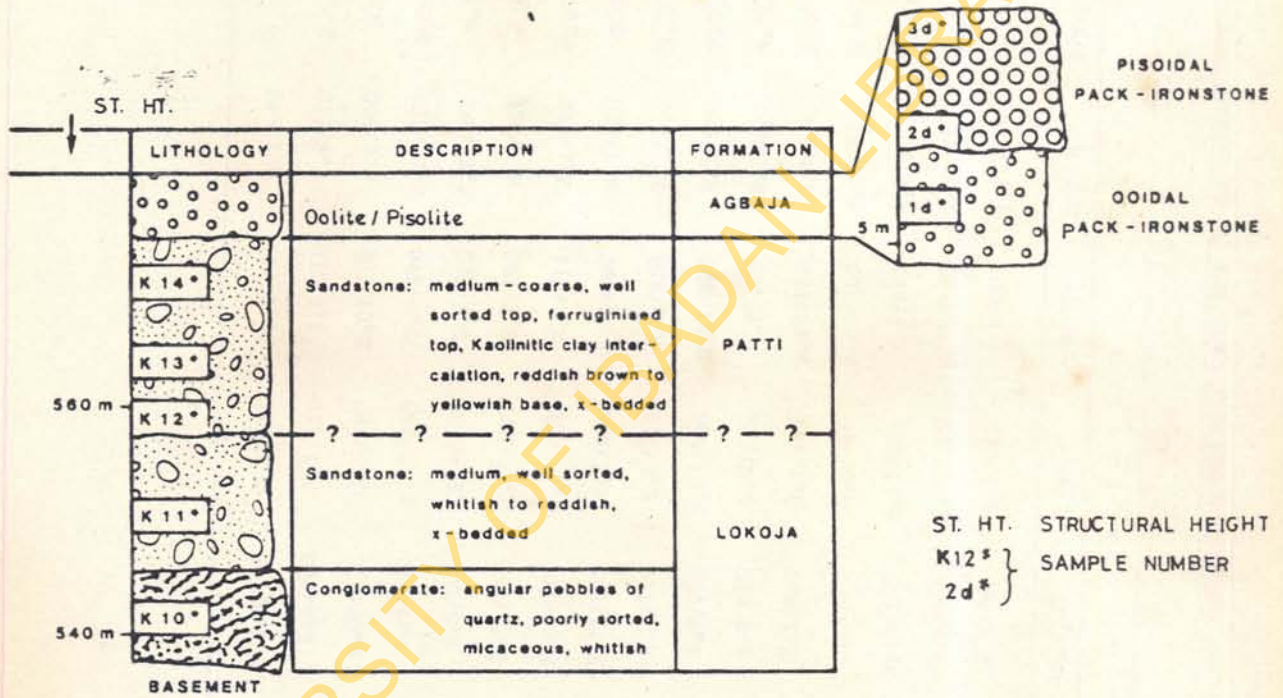
Fig. 9: Lithologic section of Agbaja Plateau, locality AG /K

Table 3:   AZIMUTH DIRECTIONS OF THE SANDSTONE CROSS BEDDINGS FOR LOKOJA AND PATTI FORMATIONS

				LOCATION					
KP/C/58	KP/C/68	KP/A/5	AG/K/M	AG/B/22	AG/A/77	KP/B/55	AG/A/20	AG/A/20	AG/B/22
007/3°E	007/21°E	013/3°E	022/18°E	043/7°E	022/4°W	046/8°E	042/12°E	302/5°E	038/18°E
005/10°E	014/18°E	065/18°E	063/15°E	072/11°E	037/11°E	028/5°E	006/21°E	021/8°E	051/17°E
318/8°E	025/14°E	007/4°W	065/12°E	035/6°E	015/13°W	021/14°E	006/21°E	033/4°E	045/3°E
017/15°E	037/20°E	013/14°W	024/23°W	038/12°E	020/9°E	025/180°E	047/8°E	034/5°E	328/4°E
079/12°E	030/5°E	019/10°E	007/1°E	024/24°E	064/4°E	048/6°E	042/10°E	055/4°E	339/15°E
038/12°E	109/3°E	026/24°W	008/2°W	021/8°E	331/8°E	027/8°E	030/12°W	347/3°E	042/10°E
027/11°E	056/3°E	035/22°W	011/6°W	008/13°E	006/13°E	005/6°E	338/9°E	022/10°E	051/4°E
018/16°E	023/4°E	038/13°E	021/1°E	016/4°N	118/5°E	001/7°E	018/5°E	017/8°E	075/7°E
024/14°E	013/5°E	051/5°E	024/1°E	349/10°E	014/7°E	018/21°E	026/11°E	021/12°E	357/10°E
056/6°E	358/11°W	021/10°W	015/7°E	115/2°N	009/12°E	341/19°W	014/2°E	054/4°E	035/12°E
029/8°E	346/9°E	014/6°W	351/8°W	088/2°E	025/14°E	352/10°E	028/2°E	038/3°E	048/6°E
042/15°E	338/9°W	048/4°W	020/15°E	075/7°E	033/6°E	002/5°W	021/7°E	041/10°E	057/3°E
048/14°E	067/17°W	058/16°E	028/10°E	045/6°E	068/20°E	052/4°W	016/13°E	046/5°E	065/3°E
015/12°E	114/4°E	004/6°E	006/2°W	021/10°E	084/14°E	015/10°W	014/6°E	042/12°W	035/7°E
308/5°E	322/19°E	018/15°E	017/5°E	011/8°E	015/3°E	074/8°E	024/15°E	310/8°E	041/16°E
354/7°E	018/15°E	026/25°E	025/3°E	017/18°E	039/3°E	003/4°E	047/1°N	336/8°E.	

37
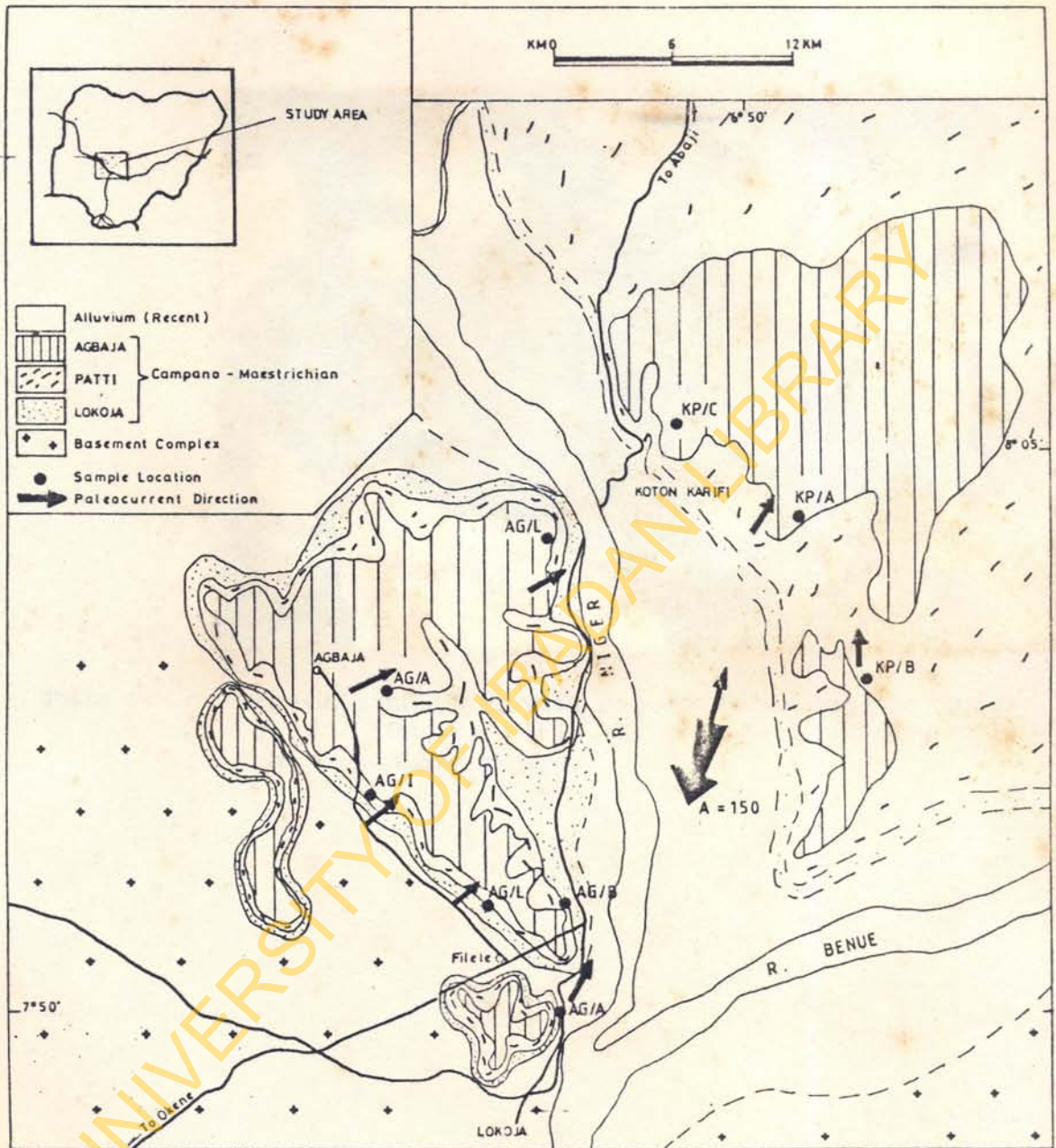
Fig. 10 : Geological Map of the Lokoja Area, Central Nigeria.
(modified after June, 1955)

Plate 1: Arkosic sandstone, with angular to subangular quartz (Q) and feldspar (F) CP x 4.5mm. Transmitted light CP = Cross polars.

II.   PATTI FORMATION

Patti Formation rests conformably on the underlying Lokoja Sandstone.   Generally, the formation is made up of intercalations of sandstone, siltstone and carbonaceous mudstone units, usually with no defined stratigraphic sequence. However, in few localities intra-formational conglomerate consisting dominantly of loosely packed rounded quartz pebbles are seen directly overlying the Lokoja Sandstone.   The conglomerate unit rarely exceeds 50cm in thickness and is commonly not stratified.   The rocks of this formation are well exposed towards the northern edge of the study area, along the Kotonkarifi-Abuja road cutting.   Maximum thickness of the formation is estimated at about 100m (Figs. 11 to 17).

Three sandstone facies were recognised, based on their level in the stratigraphic sequence of the Patti Formation.   The lower unit which commonly overlies the conglomerate is massive, medium to coarse grained and contains whitish clay matrix.   Middle sandstone facies that displays both planar and trough cross-stratification (Plate 2) are randomly found overlying or underlying the mudstone.   Cross-stratified beds are fairly consolidated, poorly sorted and medium to coarse grained.   Paleocurrent data revealed a northeast directional flow for the sediment.   Fining upward sequence is characteristic of the sandstone facies.
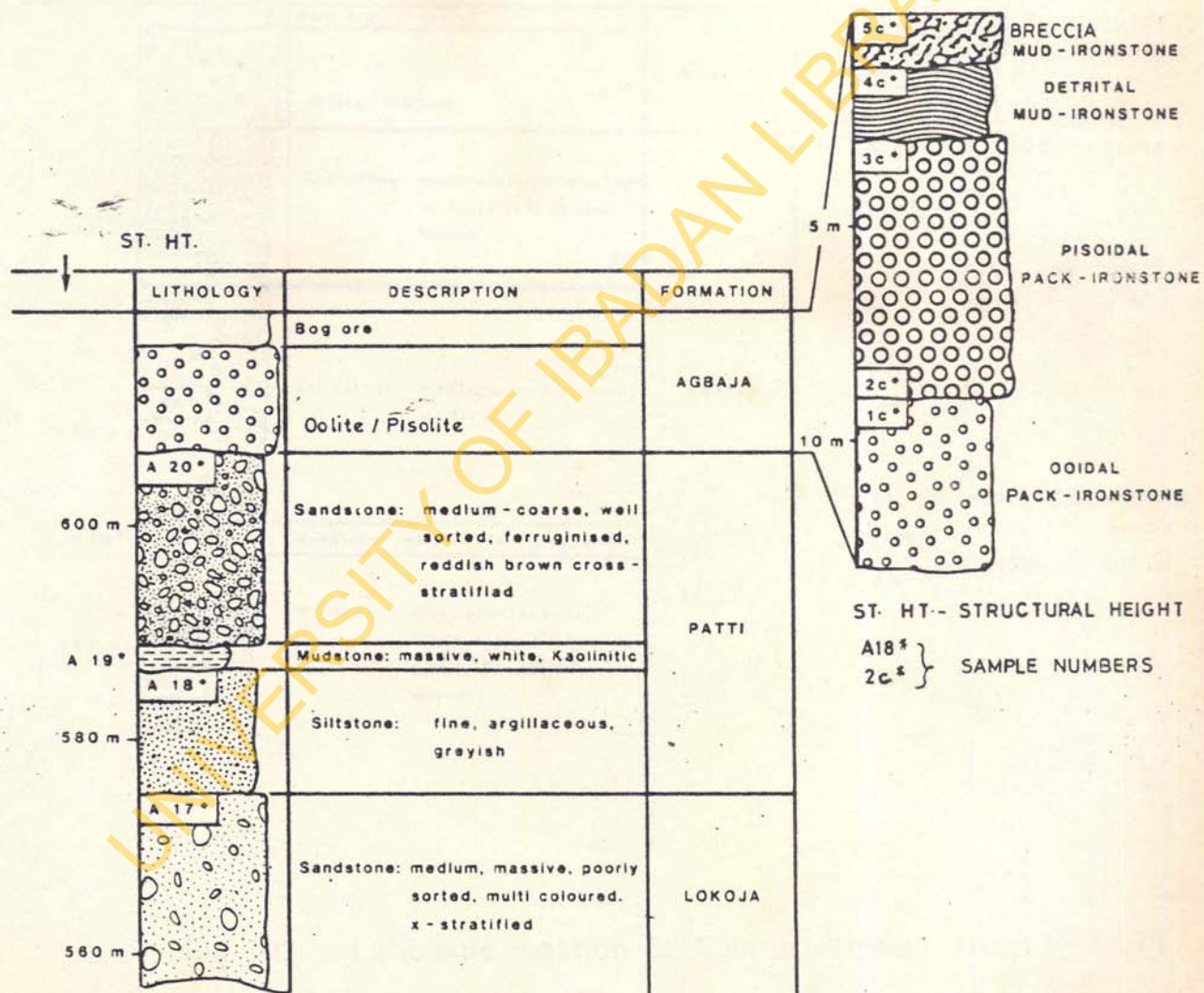
Fig. 11: Lithologic section of Agbaja Plateau locality AG/A
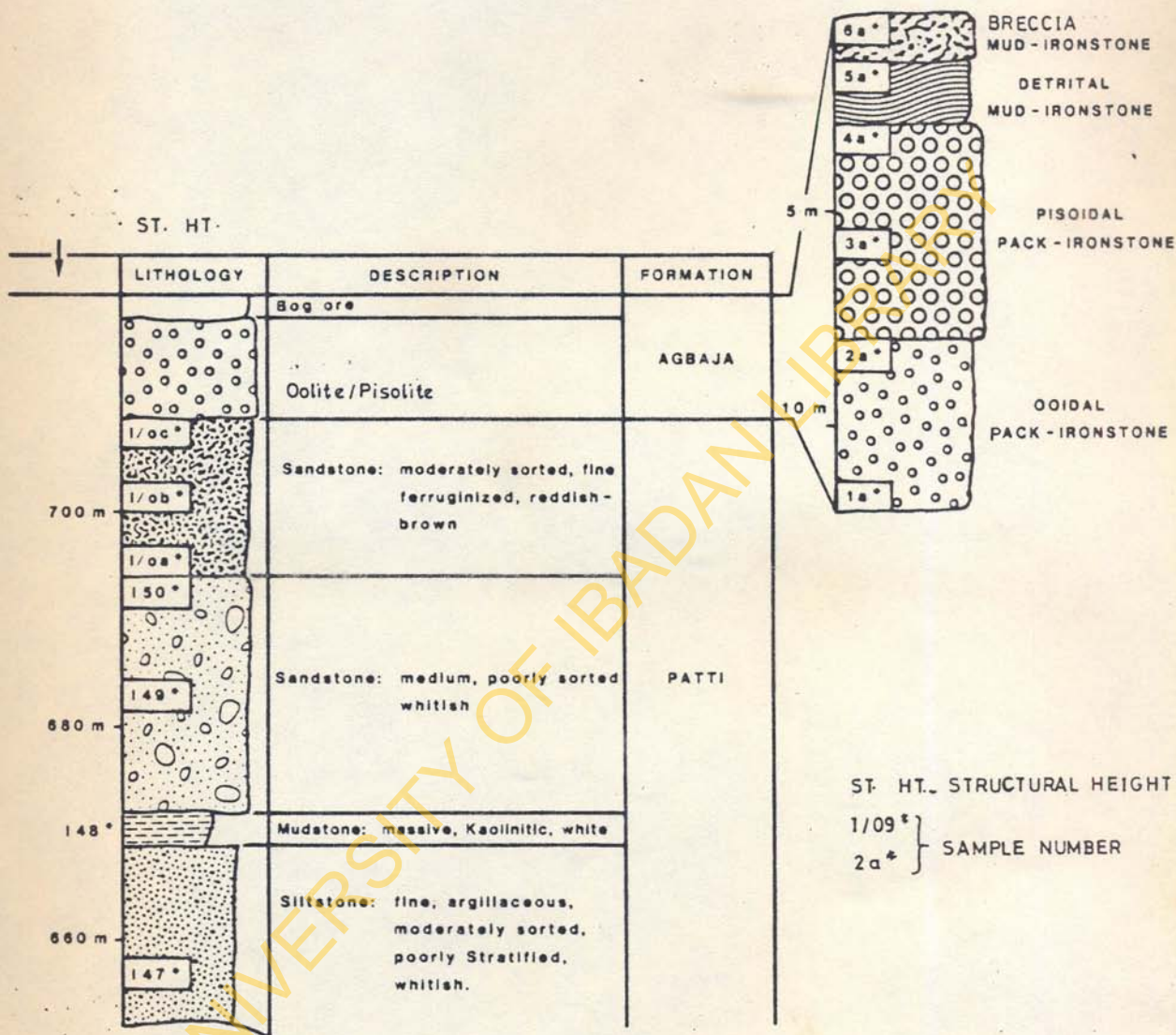
Fig. 12: Lithologic section of Agbaja Plateau locality AG/I
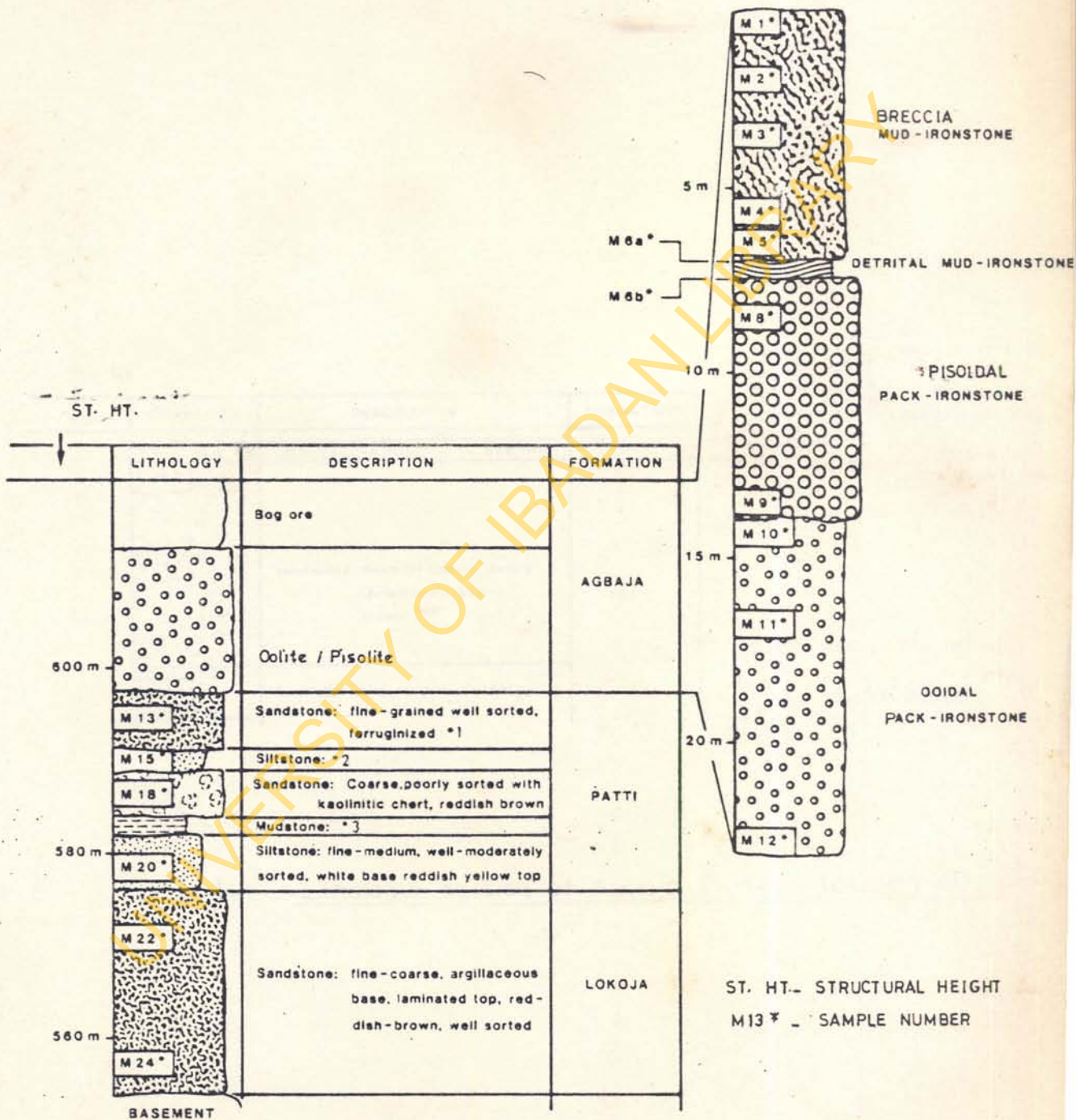
Fig·13 : Lithologic section of Agbaja Plateau, locality AG /M
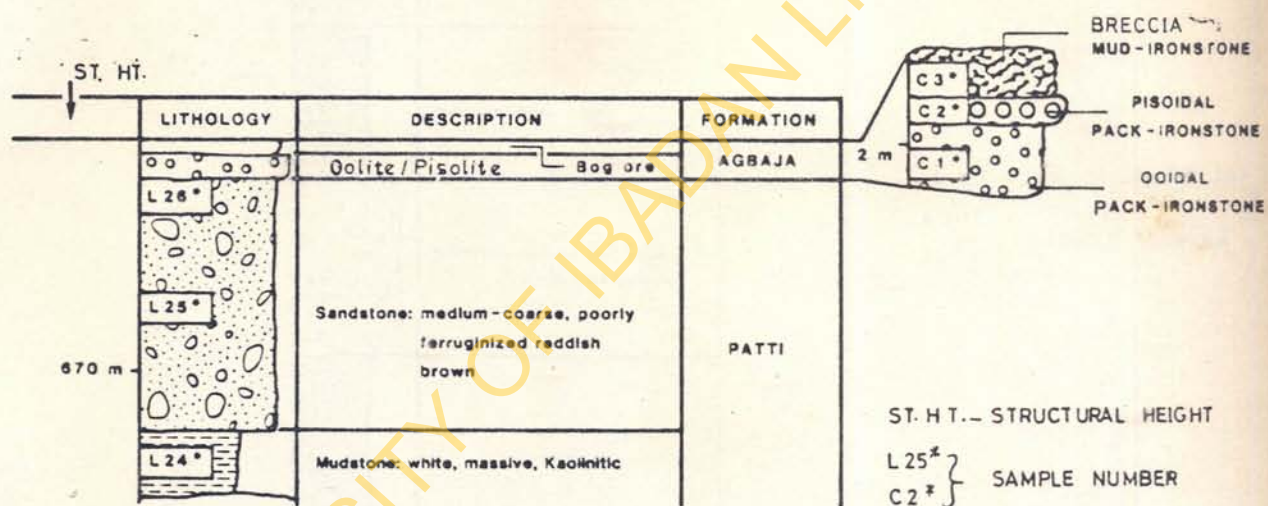
Fig. 14: Lithologic section of Agbaja . Plateau locality AG/L
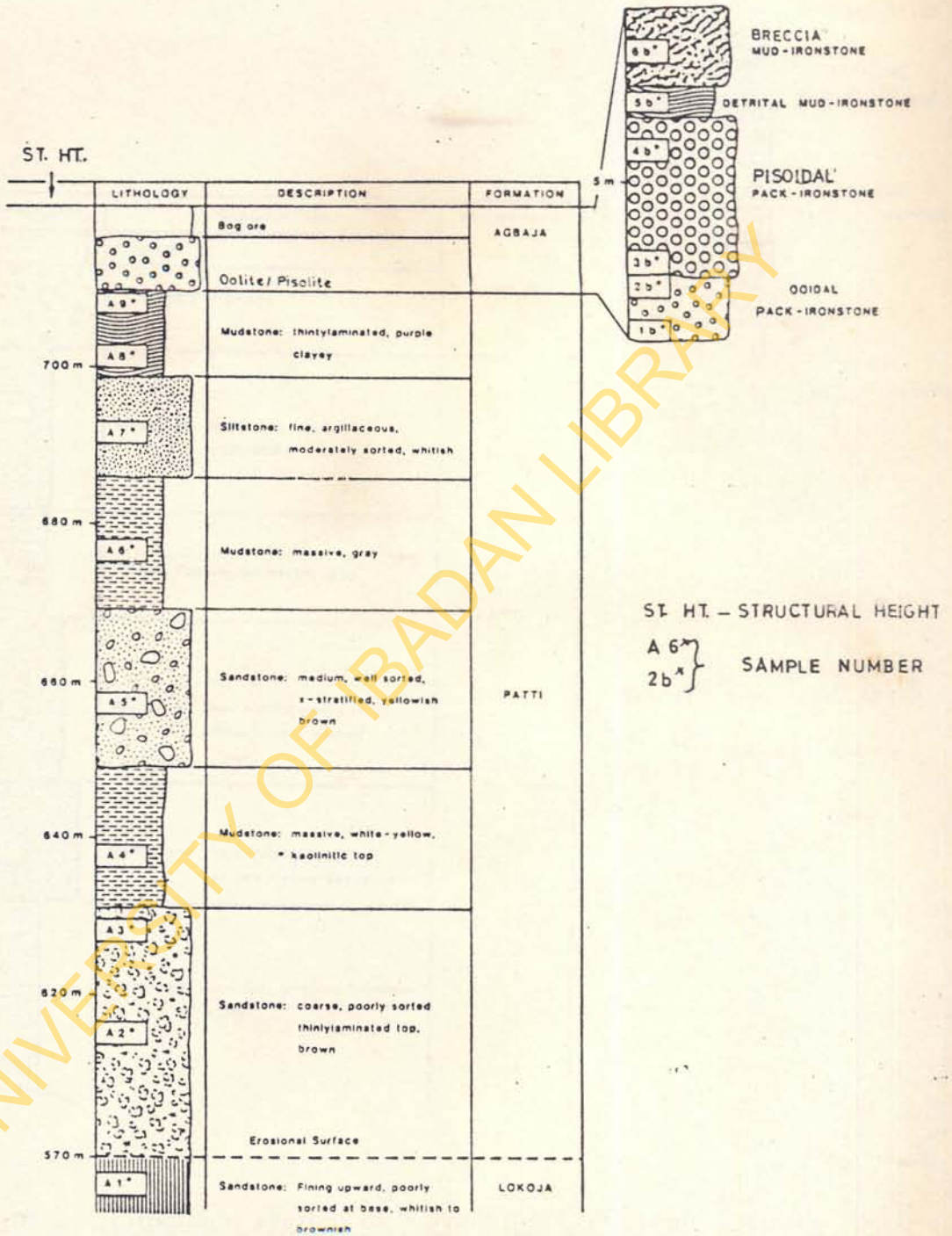
Fig. 15: Lithologic section of Kotonkarifi Plateau locality KP/C
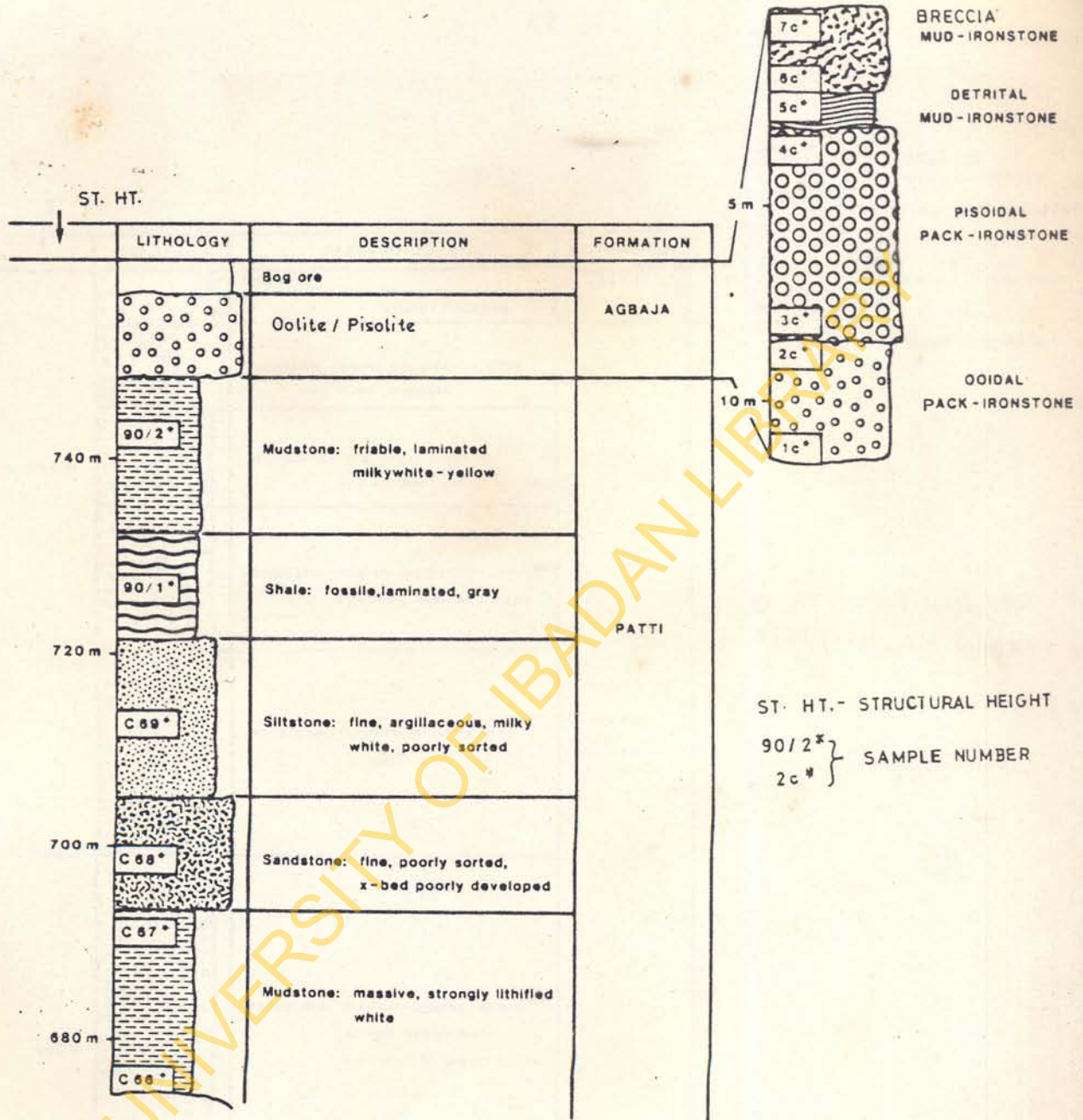
Fig.16 : Lithologic section of Kotonkarifi Plateau locality KP/C
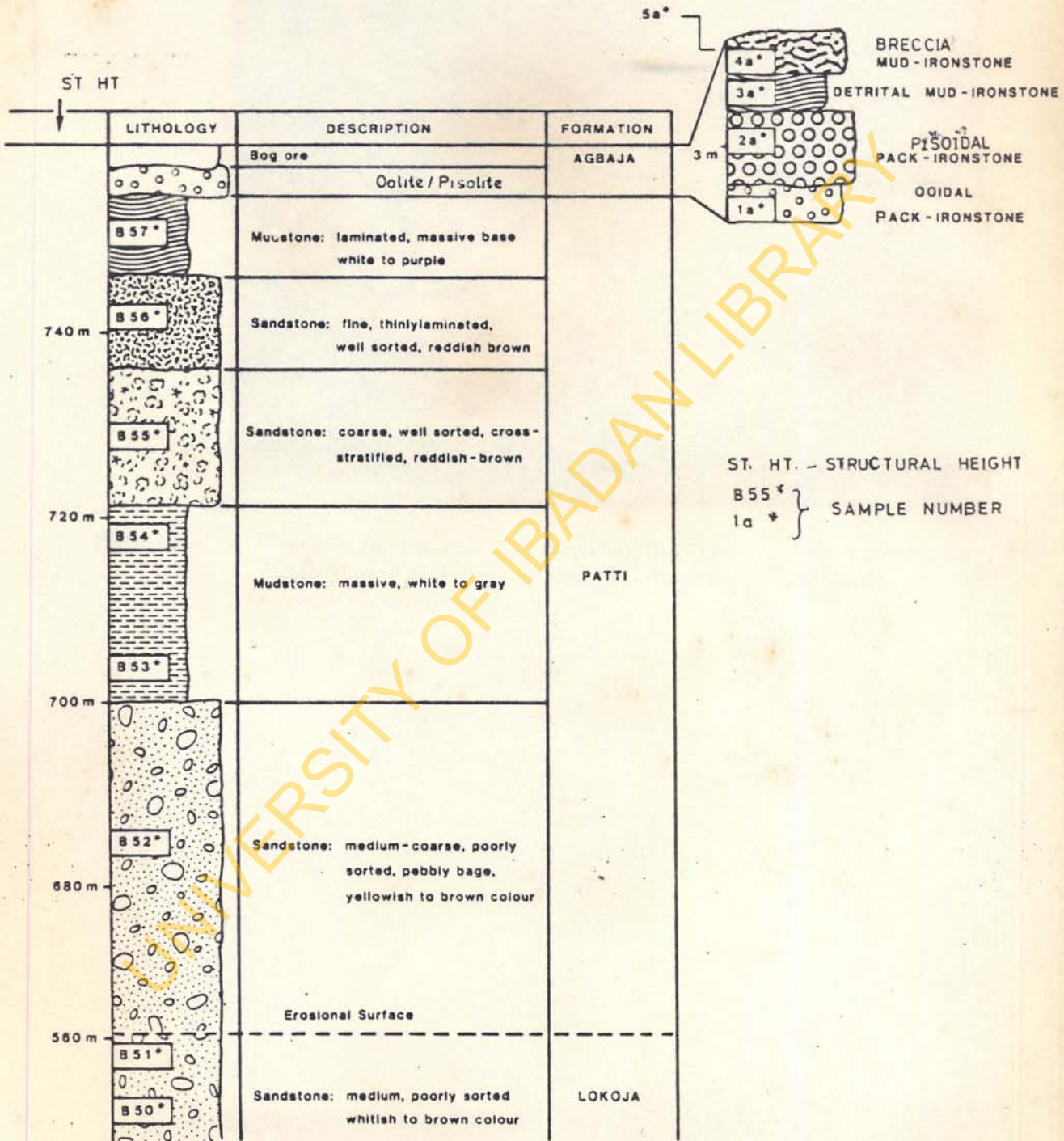
Fig. 17 : Lithologic section of Kotonkariff Plateau, locality KP/B

Plate 2: Planar to trough cross-stratification of the sandstone bodies of Patti Formation, at Kotonkarifi plateau.

Ferruginous sandstones, reddish brown in colour overlain by the oolitic ironstone formation constitute the third sandstone facies. They are usually fine to medium grained, well sorted, massive and show parallel laminations.

These sandstone facies are dominantly made up of quartz grains which are angular to subrounded in shape (Plate 3). The quartz content which averages about 86% is set in a kaolinitic matrix of about 13%. Thus, these sandstone facies can be referred to as quartz arenite. The petrographic descriptions given above are also true of ferruginous sandstone except that the cement is goethite and hematite (Plate 4). These iron minerals usually replace the kaolinitic matrix of the sandstone (Plate 4). Replaced matrix is characterised by colloidal texture (Plate 5).

Siltstone, a fine-grained, carbonaceous, friable, poorly sorted rock, is found as intercalations within the various sandstone facies (Figs. 11 to 17). It is commonly grey white to brown and show parallel laminated beds. In lithologic sequence, it exhibits graded bedding with sandy base and clay-silt tops. Siltstones are highly bioturbated with iron stains. Constituent minerals are clay, quartz and feldspar. Subangular to rounded grains of quartz and feldspar constitute about 95% embedded in a whitist kaolinitic matrix.

Plate 3: Quartz arenite, angular quartz (Q) grain with poorly sorted fabric, CP x 4.5mm. Transmitted light.

Plate 4: Ferruginized sandstone: cement is goethite (G) and hematite (H) replacing kaolinite (K) OM x 450 μm. Reflected light. C - cross polars, OM - oil immersion.

Plate 5: Ferruginized sandstone. Colloidal texture exhibited by the cement. Clast of leucoxene (L) enveloped by the cement. OM x 450μm. Reflected light. OM – oil immersion.

Mudstone beds occur as intercalations within the sandstone and siltstone facies outcropping on Mount Patti and at Kotonkarifi and Gegu. They are well laminated, fissile, sometimes friable and whitish to yellowish in colour. The laminated structures are distinctly shown by the repetition of thin beds with varying colours along the vertical sequence. However, in Gegu and the northern half of the study area, the mudstone is shaly, black and highly carbonaceous. Another distinct feature of the mudstone is the presence of plant debris, pyrite and wood fragments.

XRD studies of the mudstone revealed a rock made up of kaolinite and quartz (Fig. 18). Its coarse fractions are commonly quartz and iron minerals (mainly ilmenite).

III.   AGBAJA IRONSTONE FORMATION

Agbaja Ironstone Formation which conformably overlies the Patti Formation varies considerably in colour and grain size along the vertical profile. Field evidence and borehole logs have shown that the Agbaja ironstone is coarsening upward (Figs. 19 and 20) and that ore thickness decreases from the west to the east in the Agbaja area while the reverse is the case in the Kotonkarifi area (Fig. 21). However, the maximum thickness of the formation averages about 15m. Furthermore, three lithofacies were

Fig. 18. : XRD analysis of mudstone.(K = kaolinite Q = quartz)

Intensity

S N S

AG/A AG/B AG/K AG/I AG/M AG/L KP/C KP/A KP/B

54

1 m

0

0   5 km

BRECCIA   MUD-IRONSTONE

DETRITAL MUD-IRONSTONE

PISOIDAL PACK-IRONSTONE

OOIDAL PACK-IRONSTONE
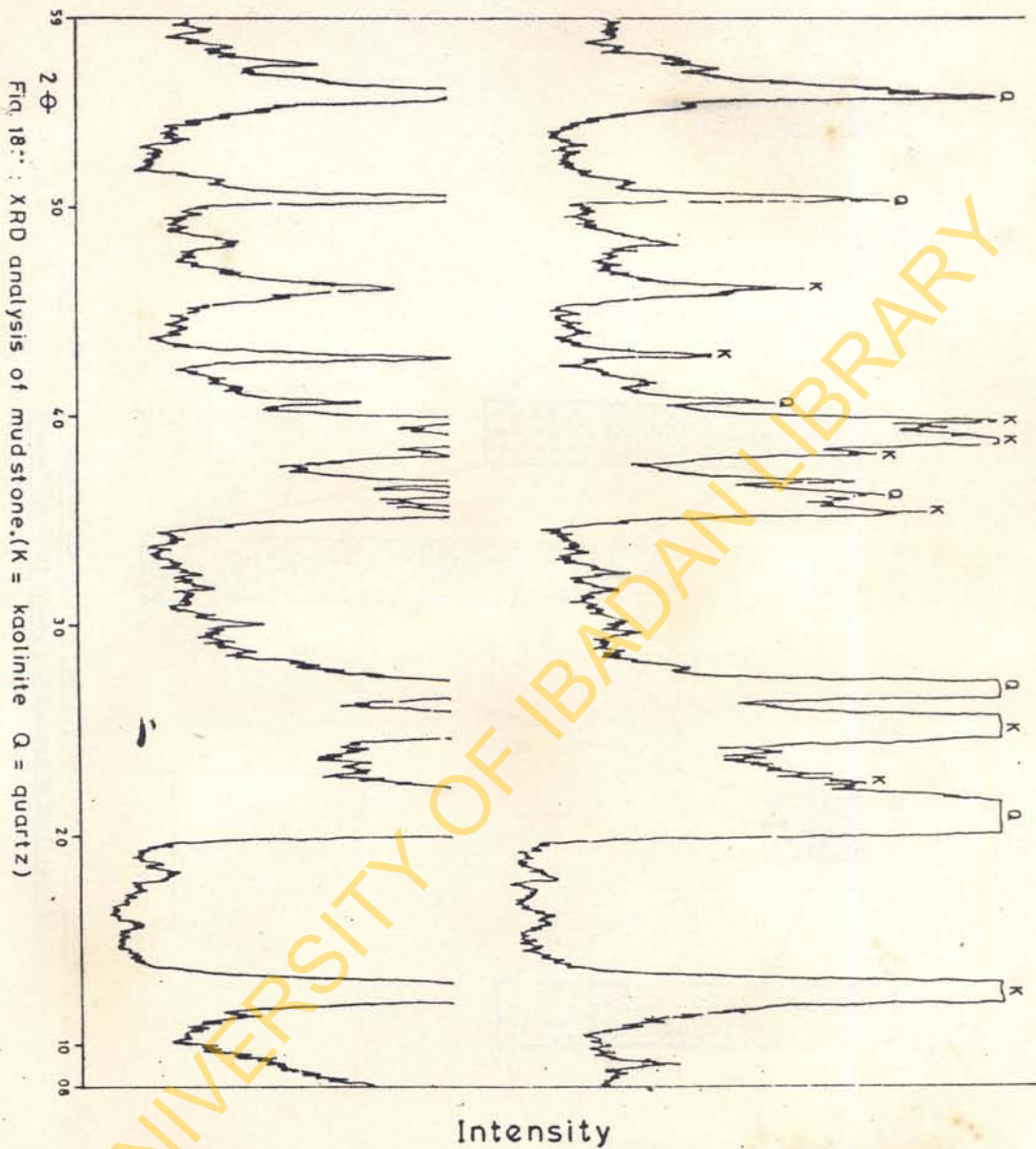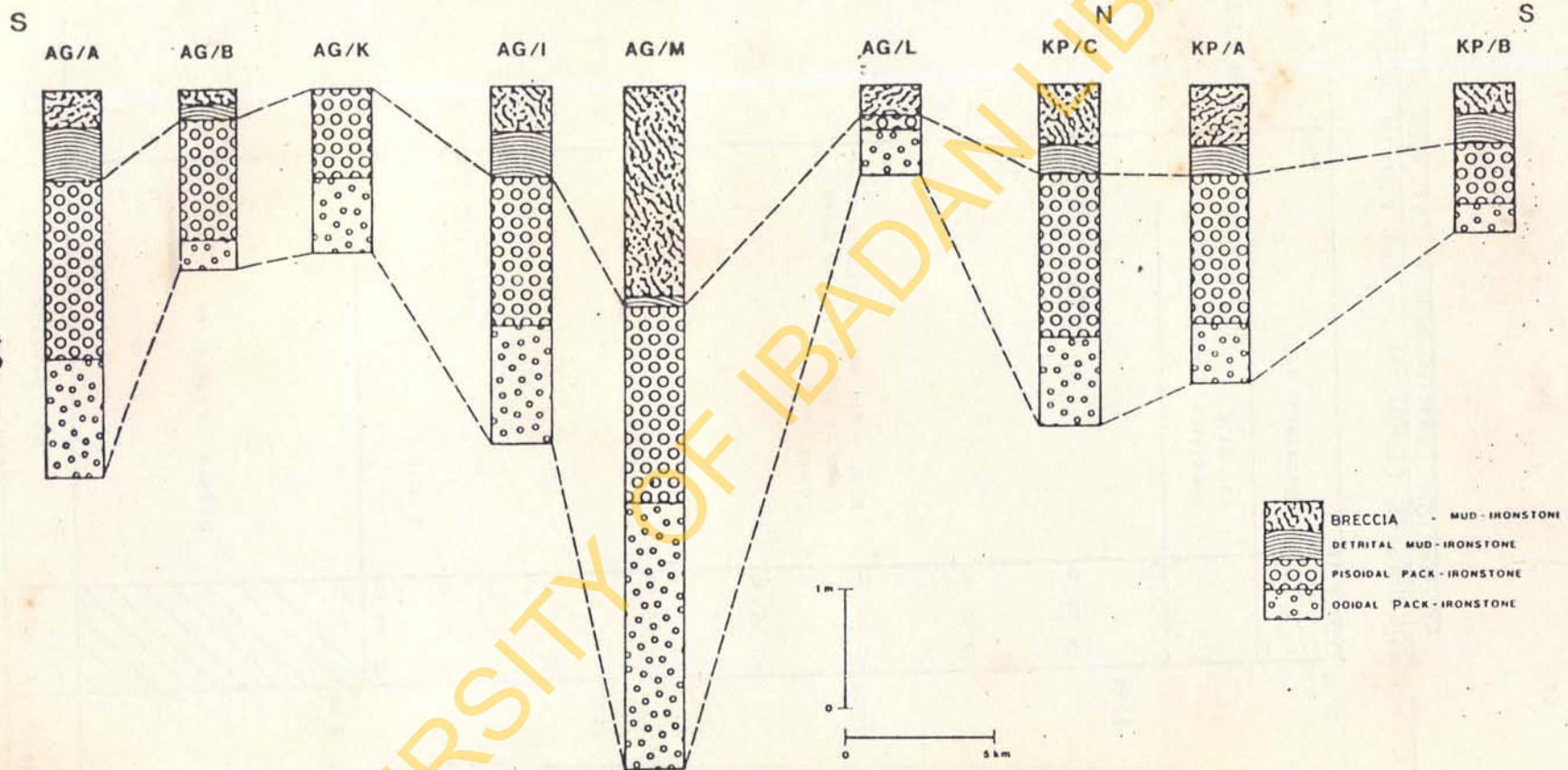
Fig. 19.   Lithologic correlation of the petrographic varieties of the Agbaja
Ironstone Formation, compared with figure 10

DEPTH (m)	LITHO-LOGY	DESCRIPTION	FORMATION
0		Bogore , Concretion	
5.00			
		Oolite	
10.00			AGBAJA
15.00		Oolite brownish top , yellowish brown base, white void, ferruginious	
20.00			
		Sandstone , gray – brown , fine red grit	PATTI
24.00		Mudstone, gray	
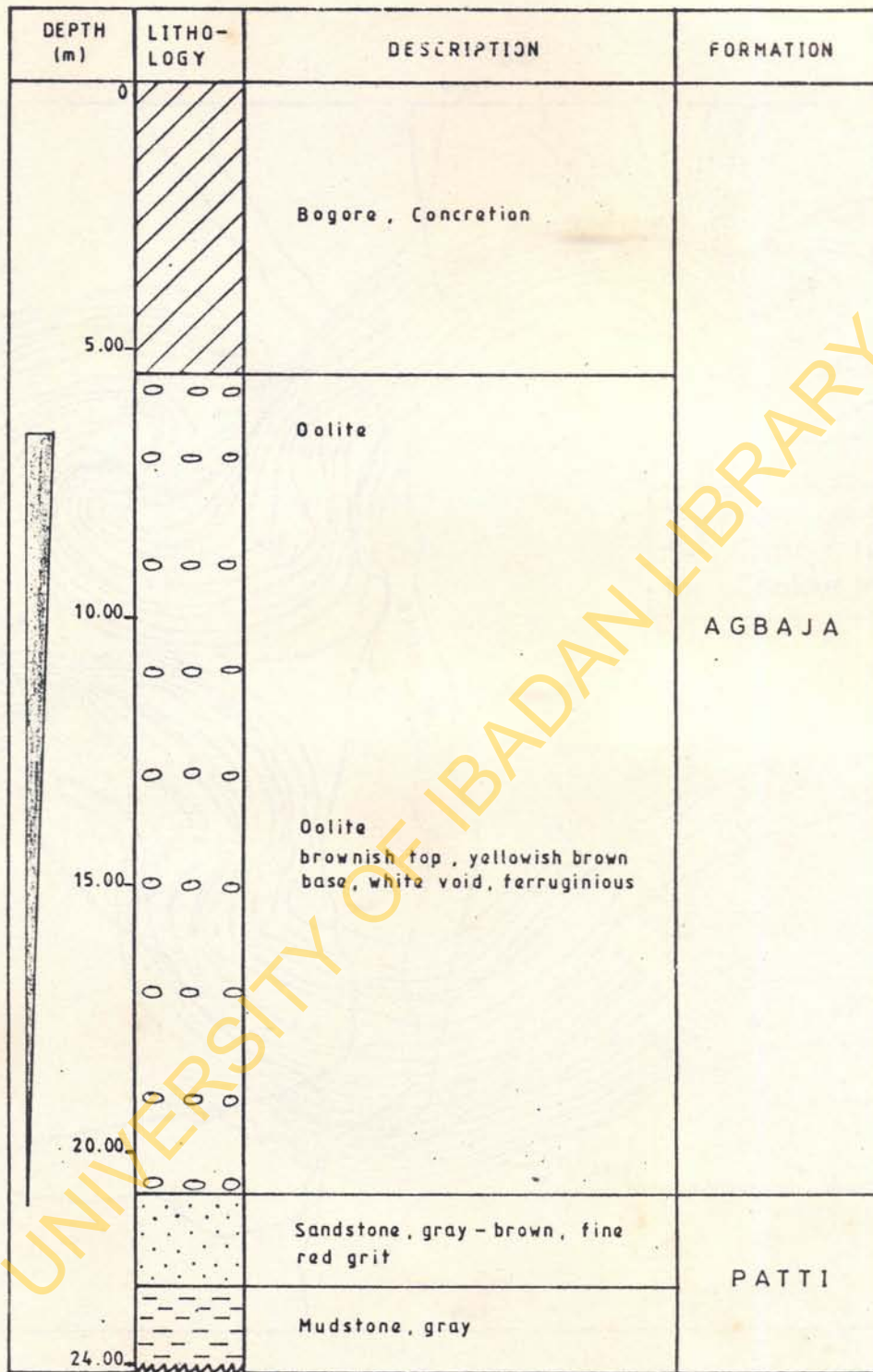
FIG.20 : SUBSURFACE LITHOLOGY OF THE AGBAJA IRONSTONE
FORMATION (Representative C.S. 22, BRGM 1982)

56
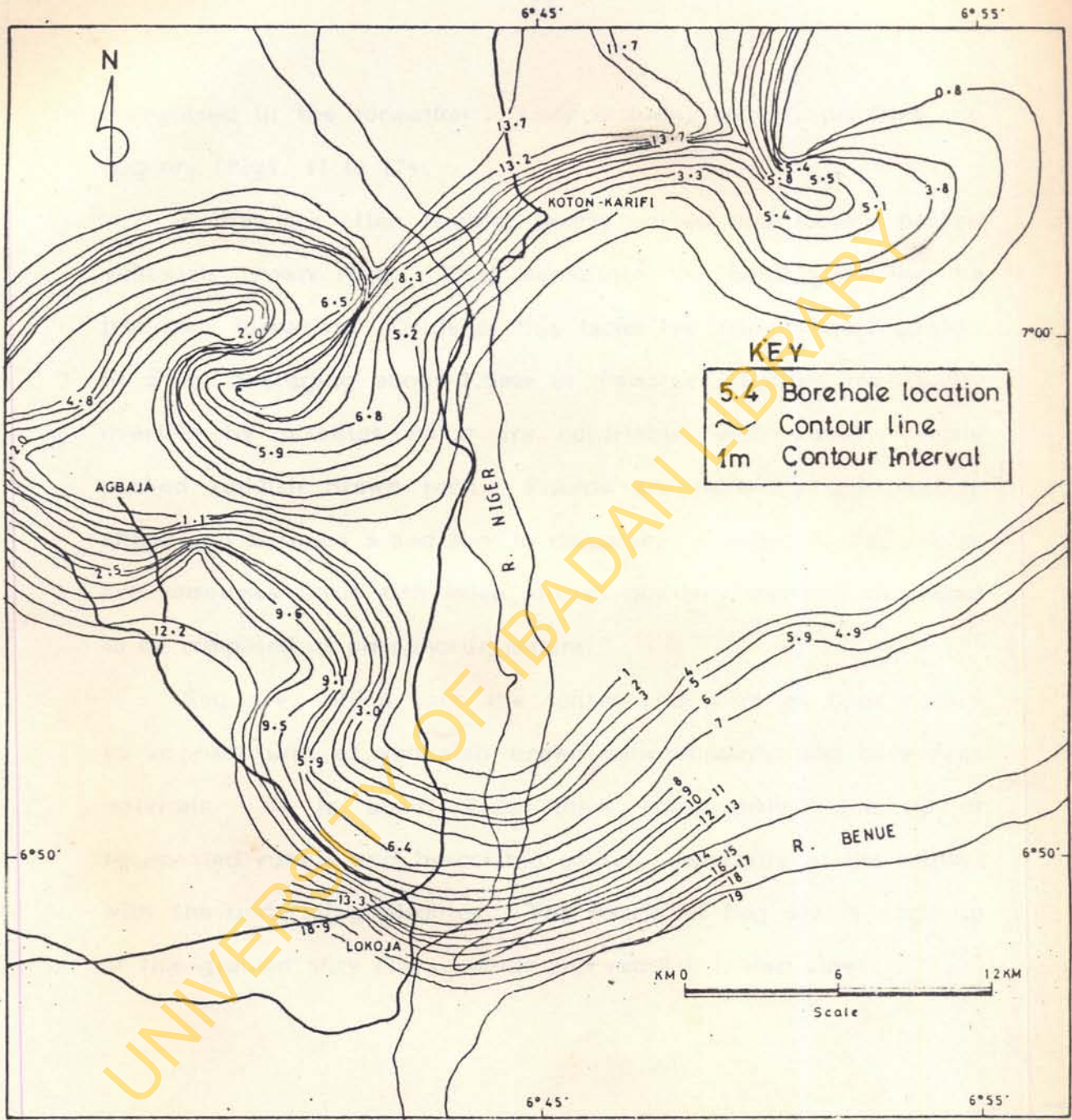
Fig 21 : ISOPACH MAP OF THE AGBAJA IRONSTONE - FORMATION. MIDDLE
NIGER VALLEY

recognised in the formation. They include, oolites, pisolites and bog ore (Figs. 11 to 17).

Oolites are often friable, poorly sorted and loosely packed yellowish brown rock. They constitute the basal part for the ironstone formation. Ooids of this facies are usually subspheroidal in shape averaging about 1.5mm in diameter. Oolites are usually overlain by pisolites which are nonfriable, well sorted, closely packed reddish brown rock. Pisoids are perfectly spherical in shape and between 5 and 8mm in diameter. Cavities in the pisoids are sometimes filled with loose whitish powdery material suspected to be composed of phosphorus mineral.

Bog ore, which caps the oolites and pisolites beds occurs as compact unit of yellowish brown concretionary and cavernous materials. It is about 1.2m thick, dominantly made up of recemented rubble and brecciated oolites, especially at the contact with the underlying pisolites. The matrix of bog ore is made up of fine-grained silty clays, sands and reddish brown clays.

CHAPTER THREE

TECTONIC FRAMEWORK AND DEPOSITIONAL ENVIRONMENT
OF THE LOKOJA DISTRICT

Petrological and sedimentological characteristics of the sediments were used in determining the environment of deposition for the study area. Apart from the identified sedimentary structures during field mapping, grain size analysis, heavy mineral analysis and thin section examination of the sandstone were used in deducing the source area and type of source for the sediments of the Nupe Basin. However, the tectonic framework for the district was proposed based on the earlier discussed structural elements and views of previous workers on the Nigerian sedimentary basins.

3.1   Tectonic Framework of the Lokoja District

The imageries studied coupled with geophysical evidences (Ojo and Ajakaiye, 1976; Ojo, 1984; Adeniyi, 1985, 1986) show that some tectonic activities took place in the Nupe Basin. Hence, the tensional stresses generated at the time of basin formation caused the disturbance of the Moho (Adeniyi, 1986), and subsequent fracturing in the crust. From these studies it is apparent

that the basin floor is irregular and could not have resulted from a simple crustal sagging or rifting. This irregularity in the basin floor can only be model for fault reactivation of pre-existing mega-structures in the Precambrian basement complex (Benkhelil, 1982; Steel et al., 1985; Ractcliffe and Burton, 1985; Ajakaiye et al., 1986; Abimbola, 1987; Braide, 1990). Based on the structural and deformational mechanism, a geodynamic synthesis of the Lokoja district is proposed.

After the Pan-African thermotectonic event the emplacement of the Younger Granites and the formation of the Benue Trough occurred. The Younger Granites is said to be related to anorogenic event. However, tectonism may have played a role as manifested by a special arrangement of the Younger Granite massifs as a sigmoidal-shaped lens suggesting a NE-SW sinistral shear (Benkhelil, 1986). Aeromagnetic studies of Ajakaiye et al. (1986) also linked the emplacement of these anorogenic granites with the probable reactivation of a transform fault (Romanche). This activity marks the beginning of a large scale fracturing in the continental crust and the initial stage of continental separation of Africa from South America (Benkhelil, 1982; Benkhelil, 1986; Ajakaiye et al., 1986; Benkhelil, 1987). Subsequent reactivation of two parallel transform faults (Chain and Charcot) (Ajakaiye et

al., 1986) by an extensional force (Benkhelil, 1989) generated an asymmetrical depression, now known as the Benue Trough. This deformational mechanism proposed for the Benue Trough occurred between Aptian and early Cenomanian.

NW-SE fracture systems which are the second important fracture trend may constitute the conjugate trend for the NE-SW trend. Field evidences confirm that this trend is younger because it is seen usually perpendicular and often truncating the NE-SW fracture systems. Since conjugate fractures are developed to release the stress built-up (Ramsay, 1980), hence, the NW-SE trends may have been formed to release the tensional build-up generated during the initial reactivation of the transform faults. These fracture trends commonly occur in both basement and sedimentary environments of Nigeria. However, the NW-SE fracture trends were fully reactivated during Santonian. As appraised, it became difficult to believe a rift or cratonic sagging models for the development of the basin. It is also pertinent to mention that a pre-Santonian origin for the basin as suggested by Agyingi (1991) is unrealistic. But a pre-Santonian development of the NW-SE fractures could be accepted. As recorded in other sedimentary environments of Nigeria, the only deformational episode that took place after the continental separation of Africa from South America

was in Santonian. Also, the absence of pre-Santonian sediments in the Lokoja area supports the post-Santonian origin for the Nupe Basin.

It is proposed that a reactivation of possibly two parallel conjugate NW-SE basement fractures during Santonian, resulted in block faulting and formation of series of hidden horst and graben structures beneath the present Nupe Basin. Subsequently these horsts and grabens were sealed up with Campanian-Maestrichtian sediments. Asymmetrical nature of the basin floor supports to some extent the extensional tectonic model of Mitchell and Reading (1978). Absence of intra-formational unconformities and minimal syndepositional folds in the Lokoja area does not support a possible compressional setting model for the basin. Thus the sediments of the Nupe Basin were therefore interpreted to have been deposited in a strike slip basin, as earlier proposed for the adjacent Benue Trough (Benkhelil, 1982, 1986; Ajakaiye et al., 1986; Abimbola, 1987).

3.2   Depositional Environment of the Lokoja District

3.2.1   Depositional Characteristics

Sediments of the study area consist of five distinct litho-facies; namely, conglomerates, sandstone, siltstone, mudstone and

ironstone. These facies are also characterised by a fining upward cyclotherm which indicates a decreasing energy as deposition progresses (Allen, 1970). Field evidences also revealed the presence of sedimentary structures within this lithofacies, which include bioturbation, graded bedding, concretionary structures as well as parallel and cross-stratifications. Parallel, thin laminations are well displayed by siltstone and mudstone, while carbonaceous shale exhibit thick laminations. Planar cross-stratification pre-dominates over trough cross-stratification in cross-stratified sandstone (Plate 2).

Paleocurrent directions within the area reflect sediment in-filling from the basin margins and longitudinal transport across the basin axis towards the northeast (Fig. 10). Paleocurrent pattern and depositional facies indicate that the main source of the materials was located to the southwestern portion of the basin.

Particle size distribution for the clastic sediments of both Lokoja and Patti Formations is unimodal. Sorting for both forma-tions is poor to moderate with the Lokoja Sandstone being often poor (Tables 4 and 5). This lateral variation in the degree of sorting indicates that the Lokoja Sandstone is nearer to the source. Its medium to coarse grained texture also confirms this (Table 4) while that of Patti Formation is fine to medium grained (Table 5).

Other textural studies show a very finely to very coarsely skewed mesokurtic sands for Lokoja Sandstone (Table 4) and leptokurtic for Patti Formation (Table 5). These characteristics confirm fluviatile sediments deposited under low energy conditions and short transportation.

Opaque minerals, mostly ilmenite, constitute about 60-88% abundance of the heavy mineral assemblages of both formations. Common heavy minerals in the order of their relative abundances include, zircon, tourmaline, staurolite, rutile, garnet and hornblende. Ziron grains are dominantly subangular to angular with inclusions of opaques and gas bubbles. Blue, pink and green varieties of tourmaline occur as angular, prismatic to irregular grains (Plates 6 and 7). Rutile, reddish in colour, is subangular to angular in shape. Angular nature of these minerals shows the textural immaturity of the sandstones of both formations.

ZTR index which ranges from 61 to 89% for the Lokoja Sandstone and from 83 to 95% for the Patti Formation (Table 6), indicates the abundance of ultrastable heavy minerals over the metastable ones in the Lokoja area. Higher ZTR index value for Patti Formation clastic sediments indicates their relative higher mineralogical maturity over the Lokoja Sandstone (Fig. 22). Heavy

Table 4: TEXTURAL PARAMETERS FROM GRAIN SIZE ANALYSES OF SANDSTONE OF THE LOKOJA SANDSTONE

Sample No.	Mean	Skewness	Sorting	Kurtosis	Formation	Sample No.	Mean	Skewness	Sorting	Kurtosis	Formation
KP/B/51a	1.20	0.27	1.26	0.92		KP/B/51	Medium	Coarse	Poor	Leptokurtic	
KP/B/51c	0.62	0.31	1.53	0.95		KP/B/51c	Coarse	V. Coarse	Poor	Leptokurtic	
KP/B/50	1.12	0.20	1.48	1.14		KP/B/50	Medium	Coarse	Poor	Leptokurtic	
KP/A/1	0.42	0.89	0.74	0.59		KP/A/1	Coarse	V. Coarse	Moderate	Very-Platy-kurtic	
AG/A/17	0.50	-0.07	1.52	1.06		AG/A/17	Coarse	Near Symmetrical	Poor	Leptokurtic	
AG/K/11c	0.93	0.52	1.27	1.00	LOKOJA	AG/K/11c	Coarse	Coarse	Poor	Leptokurtic	LOKOJA
AG/B/23e	0.81	0.09	1.49	1.11		AG/B/23e	V. Coarse	V. Coarse	Poor	Leptokurtic	
AG/B/23a	0.42	0.56	1.40	1.81		AG/B/23	Coarse	V. Coarse	Moderate	Leptokurtic	
AG/B/22a	0.52	0.48	1.56	1.46		AG/B/22a	V. Coarse	V. Coarse	Poor	Leptokurtic	
AG/B/22b	1.41	0.30	1.04	1.08		AG/B/22b	Medium	V. Coarse	Poor	Leptokurtic	
AG/B/22e	0.97	0.33	1.71	1.01		AG/B/22c	Coarse	V. Coarse	Poor	Leptokurtic	

64

Table 5   TEXTURAL PARAMETERS FROM GRAIN SIZE ANALYSES OF SANDSTONE AND SILTSTONE OF THE PATTI FORMATION

Sample No.	Mean	Skew-ness	Sort-ing	Kurto-sis	Forma-tion	Sample No.	Mean	Skewness	Sorting	Kurtosis	Formation
AG/K/12a	1.25	0.31	1.37	1.22		AG/K/12	Medium	V. coarse	Poor	Leptokurtic	
AG/K/12c	1.19	0.29	1.28	1.13		AG/K/12	Medium	Coarse	Poor	Leptokurtic	
AG/I/06	0.43	0.35	0.92	1.79		AG/I/06	Coarse	V. Coarse	Moderate	Very Leptokurtic	
AG/B/24c	2.73	-0.62	1.39	1.19		AG/B/24	Fine	V. Fine	Poorly	Leptokurtic	
AG/B/24e	2.00	-0.52	1.41	1.12		AG/B/24e	Medium	V. Fine	Poorly	Leptokurtic	
AG/A/20a	2.92	0.64	0.86	1.12	PATTI	AG/A/20	Fine	V. Coarse	Moderate	Leptokurtic	PATTI
AG/A/20b	2.52	0.35	0.93	1.62		AG/A/20b	Fine	V. Coarse	Moderate	Very- Leptokurtic	
KP/C/68a	0.97	0.19	0.95	1.53		KP/C/68	Coarse	Coarse	Moderate	Leptokurtic	
KP/C/68d	0.81	0.15	0.95	1.46		KP/C/68d	Coarse	Coarse	Moderate	Leptokurtic	
KP/B/56	2.73	-0.47	1.40	1.22		KP/B/56	Medium	V. Fine	Poor	Leptokurtic	
KP/B/55a	1.49	0.36	0.82	1.39		KP/B/55	Medium	V. Coarse	Moderate	Very- Leptokurtic	
KP/B/55c	1.51	0.37	0.83	1.52		KP/B/55c	Medium	V. Coarse	Moderate	Leptokurtic	
KP/A/5	1.34	-0.14	0.95	0.58		KP/A/5	Medium	Fine	Moderate	Leptokurtic	

65

mineral assemblages show a basement source for both formations, but with more contribution from igneous minerals (Fig. 22).

The presence of two types of optically distinctive quartz grains (undulose extinction and perfect extinction) also suggest a basement source for the clastic sediments of both formations. Also, the absence of feldspar in the sandstone of Patti Formation might be related to the effect of weathering during the course of transportation to a slightly distant depocenter. Increase in round-ness of quartz grains, decrease in grain size and increase in maturity levels from Lokoja Sandstone to Patti Formation may suggest the reworking of older beds. Decrease in grain size also explains the presence of kaolinite, not only as matrix but as the major clay mineral of the mudstone, as the feldspar has been decomposed into kaolinite.

3.2.2 Paleoenvironment

Depositional characteristics of the Lokoja area resemble those of modern fluvial deposits which evolved into two distinct facies: aluvial fans and flood basin (Fig. 23).

Sedimentation in the Lokoja area started in Campanian-Maestrichtian times (Adeleye, 1974; Jan du Chen et al., 1978; Ladipo, 1986, 1988; Agyingi, 1991) with the immature sediments of the Lokoja Sandstone deposited marginally along the flanks of

Plate 6: Tourmaline (T), prismatic, associated with angular grains of staurolite (S). PP x 4.5mm. Transmitted light.
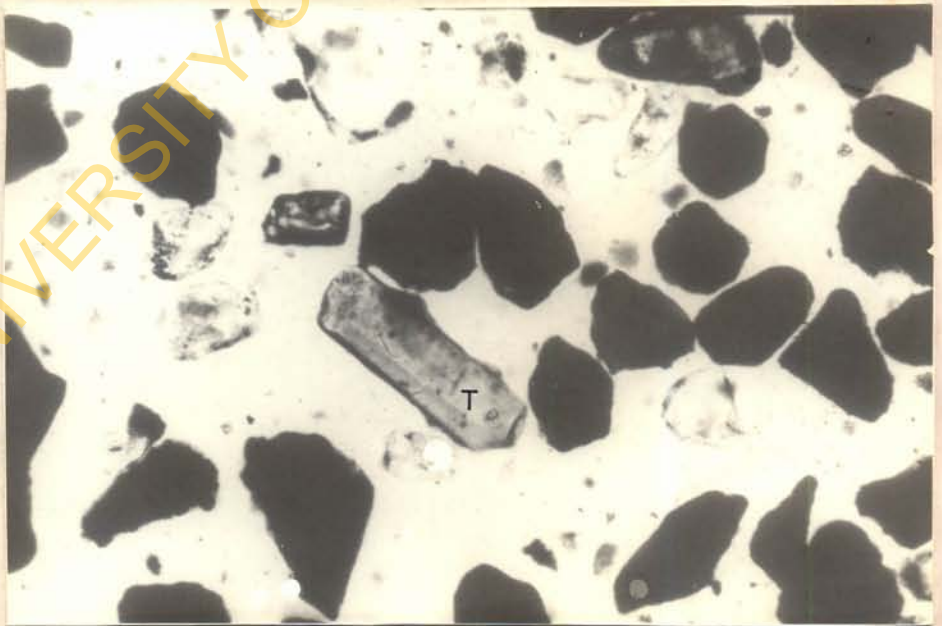
Plate 7: Tourmaline (T) with opaques, mostly ilmenite. PP x 4.5mm. Transmitted light. PP – Plane polarized light.

Table 6:   RELATIVE ABUNDANCE (%) AND ZTR INDEX VALUE OF THE HEAVY MINERAL POPULATION OF SANDSTONE UNITS OF BOTH LOKOJA AND PATTI FORMATIONS

SAMPLE NO	AMOUNT OF MINERAL PER NON - OPAQUE						SAMPLE OPAQUE IRON OXIDE	Z T R INDEX (%)	TOTAL NO OF Z(%)	TOTAL NO OF T+R (%)	TOTAL NO OF S+G (%)	TOTAL NO OF Z+T+R+S+G	GEOLOGIC FORMATION
	Z	R	T	S	G	H							
KP/A5	8	2	2	1	1	-	36	85.7	8 (57.1)	4 (28.6)	2 (14.3)	14	PATTI
KP/B55a	11	1	3	1	-	-	40	93.8	11 (68.8)	4 (25.0)	1 (6.3)	16	
KP/B55c	16	2	3	1	-	-	44	95.55	16 (72.7)	5 (22.7)	1 (4.5)	22	
KP/B56	5	6	4	2	-	-	27	88.2	5 (29.4)	10 (58.8)	2 (11.8)	17	
KP/C68b	6	2	3	1	1	-	25	84.6	6 (46.2)	5 (38.5)	2 (15.3)	13	
KP/C68d	11	6	3	4	-	-	37	83.3	11 (45.8)	9 (37.5)	4 (16.7)	24	
AG/A20a	11	3	4	1	1	-	31	90.0	11 (55.0)	7 (35.0)	2 (10.0)	20	
AG/A20b	8	2	2	1	-	-	28	92.3	8 (61.5)	4 (30.8)	1 (1.7)	13	
AG/B24c	9	3	7	2	-	-	34	90.5	9 (42.9)	10 (47.6)	2 (9.5)	21	
AG/B24e	6	4	2	2	-	-	30	85.7	6 (42.9)	6 (42.9)	2 (14.3)	14	
AG/I/0b	3	2	1	2	-	-	60	85.7	3 (37.5)	3 (37.8)	2 (25.0)	8	
AG/K12a	13	1	1	-	1	-	93	93.8	13 (81.3)	2 (12.5)	1 (6.3)	16	
AG/K12c	15	2	3	1	-	-	33	95.2	15 (71.4)	5 (28.8)	1 (4.8)	21	
KP/A1	6	3	5	3	1	1	31	73.7	6 (33.3)	8 (44.4)	4 (22.2)	18	LOKOJA
KP/B50	4	6	4	2	2	-	27	77.8	4 (22.2)	10 (55.5)	4 (22.2)	18	
KP/B51a	3	7	2	1	-	1	28	85.7	3 (23.1)	9 (69.2)	1 (7.7)	13	
KP/B51c	5	5	2	2	2	-	30	75.0	5 (31.3)	7 (43.8)	4 (25.0)	16	
AG/A17	8	4	7	4	1	-	36	79.2	8 (33.3)	11 (45.8)	5 (20.8)	24	
AG/B22a	2	5	1	3	2	-	21	61.5	2 (15.4)	6 (46.2)	5 (38.5)	13	
AG/B22b	10	6	3	4	-	-	36	82.6	10 (43.5)	9 (39.1)	4 (17.4)	23	
AG/B72c	5	6	4	2	2	-	40	78.9	5 (26.3)	10 (52.6)	4 (21.1)	19	
AG/B23a	7	4	5	1	1	-	27	88.8	7 (38.9)	9 (50.0)	2 (11.1)	18	
AG/B23e	3	8	1	2	1	-	33	80.0	3 (20.0)	9 (60.0)	3 (20.0)	15	
AG/K11b	8	3	4	4	-	-	30	75.0	8 (42.1)	7 (36.8)	4 (21.1)	19	
AG/K11c	6	4	4	2	1	-	42	82.4	6 (35.3)	8 (47.1)	3 (17.6)	17	

Z = Zircon,   R = Rutile,   T = Tourmaline,   S = Staurolite,   G = Garnet,   H = Hornblade
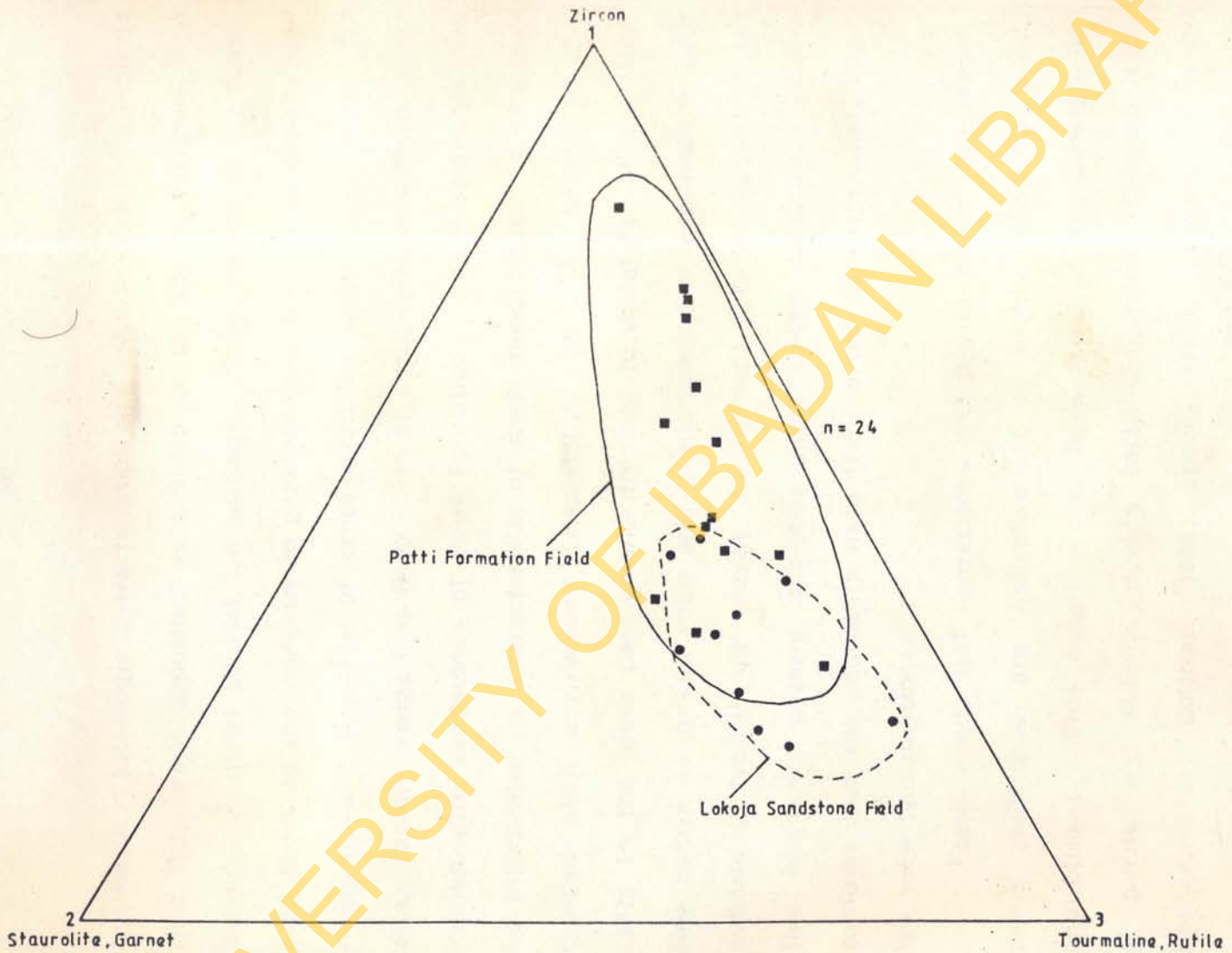
FIG.22 : RELATIVE ABUNDANCE OF IGNEOUS (1), METAMORPHIC (2), AND METAMORPHIC AND / OR IGNEOUS (3)
MINERAL SPECIES (■ Patti Formation, ● Lokoja Sandstone)

the basin. Lithologic characteristics and azimuth directions indicate that they were deposited as braided or meandering streams in a marginal to distal alluvial fan settings. Conglomerate of the Lokoja area forms in the marginal to proximal fans and passes distally into fining-upward sequence of cross-stratified sandstones. Distal fan areas rapidly wedge into flood basin of argillaceous sediments inter-calated with sandstones of Patti Formation. These sediments may be interpreted as characteristic of sheet flood typical of extensive braided plain environment (Haszeldine, 1983; McPherson et al., 1987) in the lower part of the proximal to distal fan areas. High fine matrix to grains ratio and predominance of argillaceous beds indicate a typical low energy environment. Great volume of the fine sediments present suggests high stream capacity. It also confirms that the sediments were transported as suspension, under low velocity conditions.

Fossil wood, leaf impressions and pyrite within the carbona-ceous mudstones are indicative of a highly reducing swamp environment. This condition may have favoured the precipitation of pyrite and siderite during early diagenesis (Coleman 1966; Berner, 1981; Coleman, 1985; Spear, 1989). Parallel laminated siltstone intercalated with sandstone are extensively bioturbated and highly stained with iron oxides. The presence of bioturbation
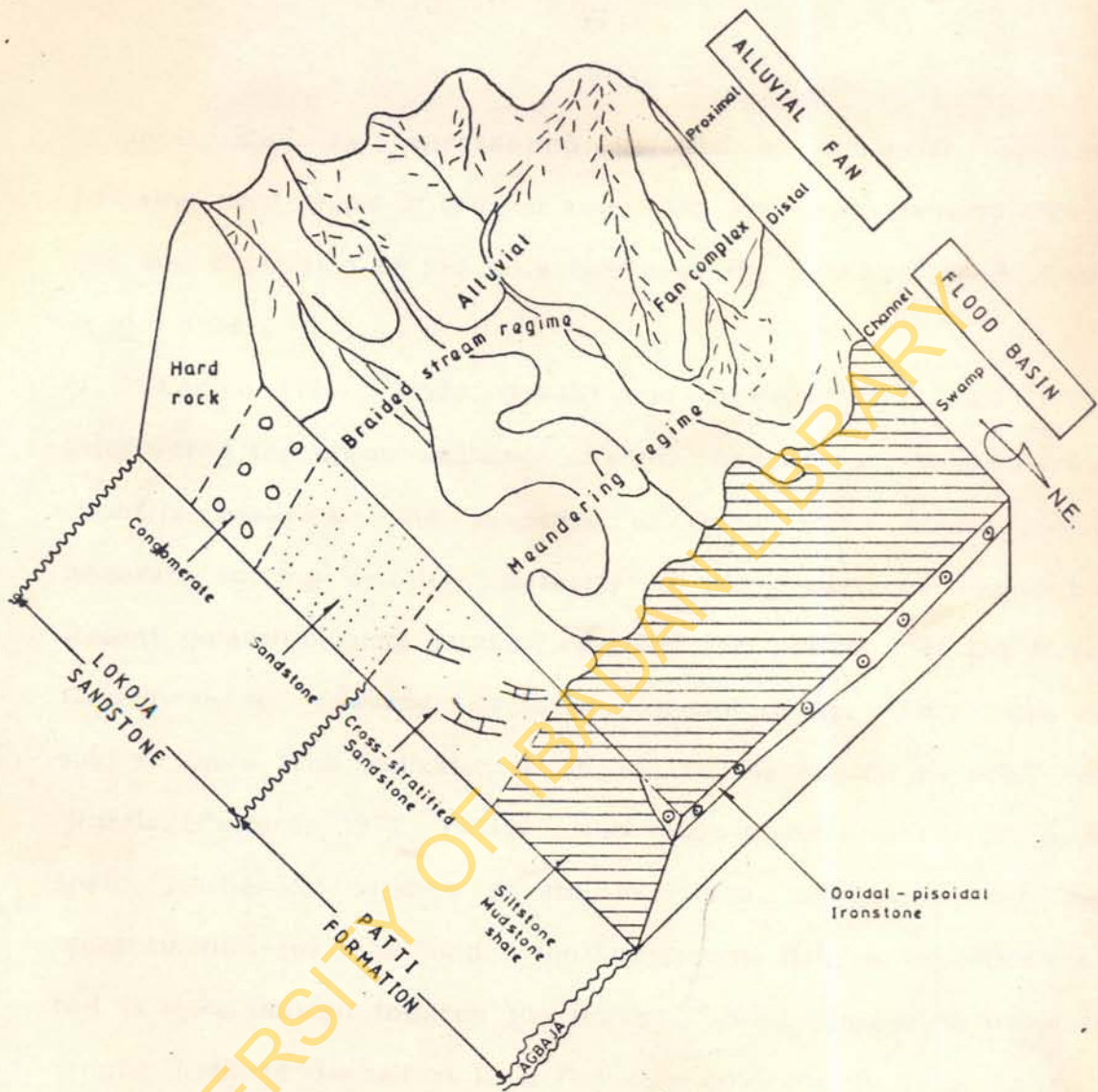
Fig 23 : Schematic illustration of paleoenvironment of the Lokoja sub-basin.

is interpreted as representing periods of subaerial exposure following each phase of erosion associated with transgressing shoreline and deposition of the silty bed over the swamps (Jan du Chen et al., 1978).

Ladipo (1986, 1988a, 1988b) and Ladipo et al., (1988, 1993) interpreted the upper sequence of Patti Formation as shallow marine deposits based on the presence of Ophiomorpha trace fossils, moderate sorting and maturity of the arenaceous sediments. Recent palaeontological studies revealed the presence of the foram Gavelinella sp. (Bassey, personal communication). This foram is said to be a true indicator of shallow marine habitat especially in Nigeria (Petters, 1978, 1980). Also, Idowu and Enu (1992), from their geochemical studies of the mudstone, suggested that the epicontinental sea that flooded the Lokoja area has marine influence, but is more noticed towards the north. Thus, the sedimentological studies indicate deposition in a fluviatile environment (Fig. 23) but with probable influx of marine water into the swampy floodplain. Sedimentological characteristics, such as the lithofacies present and the regional fining upward cyclotherm, suggest an active uplift of the source area and subsequent development of an asymmetrically subsided basin.

CHAPTER FOUR

PETROGRAPHIC STUDIES OF THE AGBAJA
IRONSTONE FORMATION

4.1   Sampling and Sample Preparation

Over sixty samples of the Agbaja Ironstone Formation were cut and prepared for petrographic analysis. Petrographic studies were carried out on thin and polished sections of these samples. Besides mineralogical identification, microscopic studies further show the textural attributes of the ironstone. Using their allochem types and textural characteristics four petrographic varieties were identi-fied for the ironstone. They are the ooidal pack-ironstone, pisoidal pack-ironstone, detrital mud-ironstone and breccia mud-ironstone (Figs. 11 to 17). The first two varieties correspond to the oolites and pisolites while the later two correspond to the bog ore (Figs. 11 to 17).

To complement the microscopic studies, X-ray diffraction studies, using a model Philips PW 1710 BASIS of the Mineralogisch-Petrologisches Institut der Universitat Gottingen was also used in identifying minerals present in each variety. The instrument setting are as stated below:

Graphite monochromator, Cu anode

Voltage/current - 40KV, 55mA

Recording/Scanning rate - $5°/2\theta/cm/min$

Mineral identification was made by comparison of computed d-values with diffraction data of Berry (1974) and Chen (1977).

4.2   Description of the Petrographic Varieties

4.2.1   Ooidal Pack-Ironstone

Ooidal pack-ironstone is characterised by spherical, oblong and fragmented ooids (Plate 8), well sorted and loosely packed within a kaolinitic matrix (Plate 9). The mineral assemblage of the concentric laminae and the core is used in naming the ooids. Types of ooids found in the ooidal pack-ironstone are kaolinite, kaolinite-goethite and hematite ooids.

Kaolinite ooids, averaging about 1.5mm in diameter have perfect concentric laminae symmetrically arranged about their nucleus (Plate 10). Their cores are rarely made up of quartz. Cortex of kaolinite-goethite ooids is predominantly composed of goethite or goethite-hematite with relics of kaolinite. Their structures are often very smooth, subspherical to ooid. The ooids have laminae of variable thickness, that cover any irregularities of the core. Concentric laminae of kaolinite-goethite ooids may form
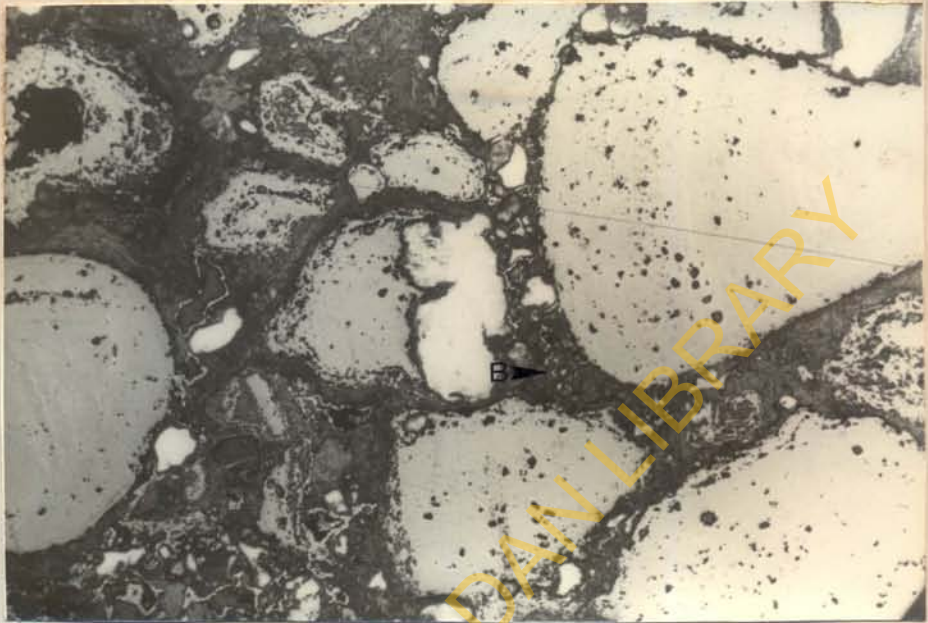
Plate 8: Fragmented ooids. Note the angular to oblong shape of the fragments. Dissemination of Bolivarite (B) within the matrix.
PP x 3.2mm. Reflected light.
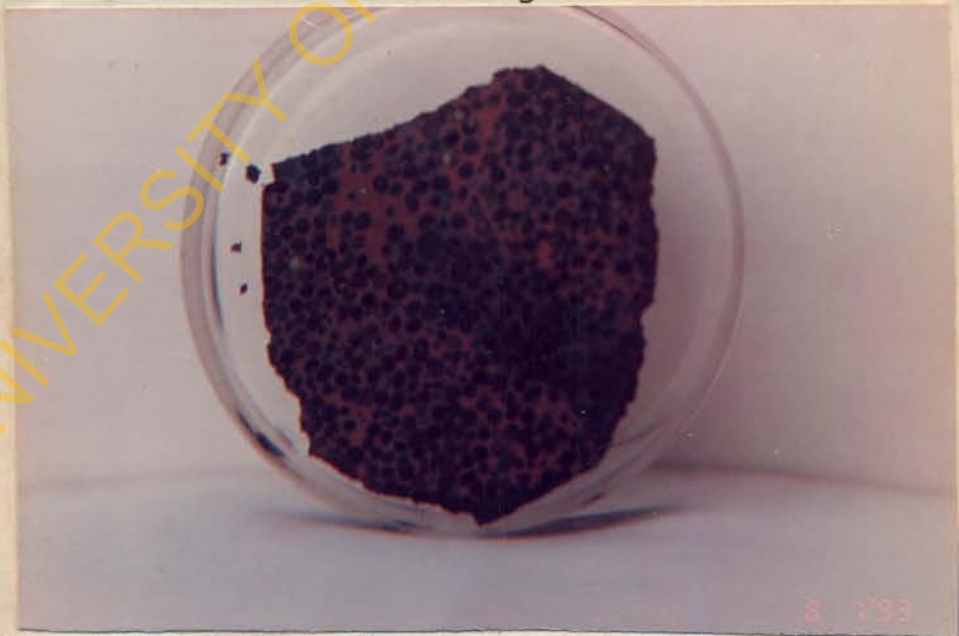
Plate 9: Polished slab of ooidal pack-ironstone, well sorted, loosely packed oolite.
PP - Plane polarized light.

Plate 10: Kaolinite ooids with concentric laminae disposed symmetrically about a kaolinite (K) nucleus. PP x 3.2mm. Reflected light.

several discrete zones of goethite, suggesting iron enrichment zones with stacked vermicules (ghosts) of kaolinite (Plate 11). Laminae of hematite are sometimes associated with this kaolinite-goethite ooids. Each lamina is between 2 and 15μm in thickness forming cortex of about 120μm in depth. Mostly the concentric outline of the ooids passes inwards into a core of kaolinite or pseudomorphs of goethite after pyrite (Plate 12). Hematite ooids are characterised by the occurrence of pseudomorphs of hematite after pyrite in their cores (Plate 13) or as framboids (organic matter) incorporated into their concentric rings (Plate 14).

Reddish kaolinite (iron stained) constitutes the dominant matrix for the various ooids. Mineral constituents of the matrix also include detrital grains of quartz, mica and heavy minerals, such as ilmenite, rutile, pseudorutile, leucoxene, zircon and staurolite. Also found in the matrix are need-like crystals of pseudomorphs of goethite after siderite (Plates 15 and 16).

Two modes of iron enrichment are manifested in the Agbaja Ironstone Formation, they are the replacing and open-space mechanisms (ferruginization). The mode of iron enrichment in the ooidal pack-ironstone is the replacing type, which usually advanced through the permeable kaolinite. In the kaolinite ooids, replacement starts from the core to the cortex and progressively advances
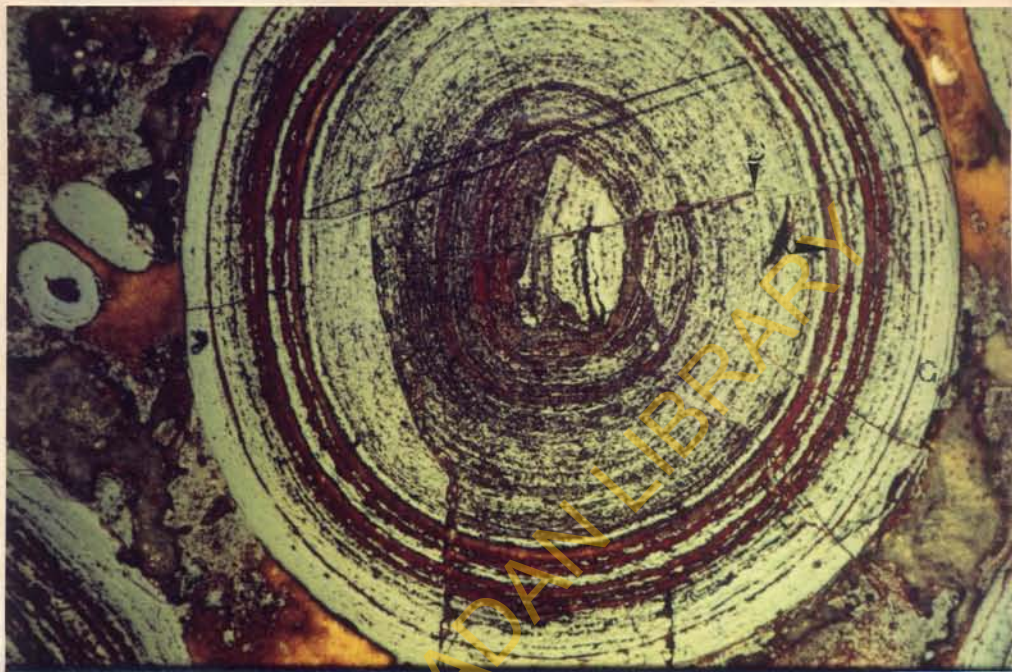
Plate 11: Goethite-kaolinite ooid, subspherical in shape with discrete rings of goethite (G), kaolinite (K) and irregularly distributed desiccation cracks (D). CP x 3.2mm. Reflected light.
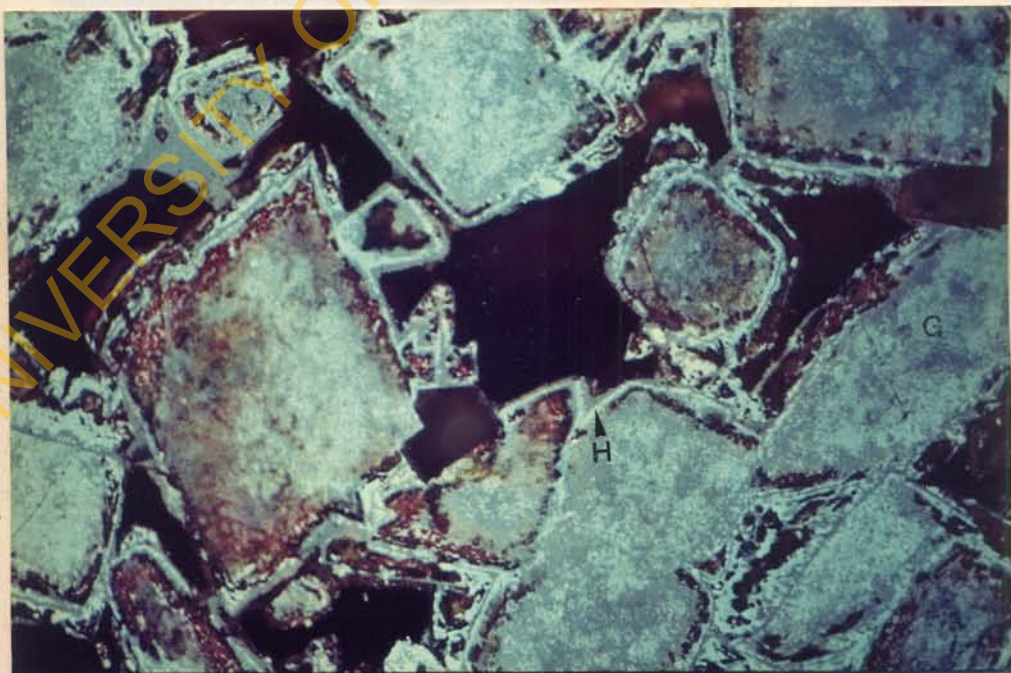
Plate 12: Pseudomorphs of goethite (G) and hematite (H) after pyrite in the core of an ooid. The pseudomorphs exhibit the rhombohedral shape of pyrite. OM x 450 μm. Reflected light.
CP - Cross polars, OM - Oil immersion.

Plate 13: Hematite ooid characterised by pseudomorphs of hematite after pyrite at the core. CP x 3.2mm. Reflected light.

Plate 14: Framboid texture, incorporation of pyrite pseudomorphs (hematitized) into the concentric rings of the ooid. OM x 450μm. Reflected light.
CP - Cross polars, OM - Oil immersion.

Plate 15: Need-like to dog-tooth crystals of pseudomorphs of goethite (G) and hematite (H) after siderite in a kaolinitic matrix. OM x 450 μm. Reflected light.
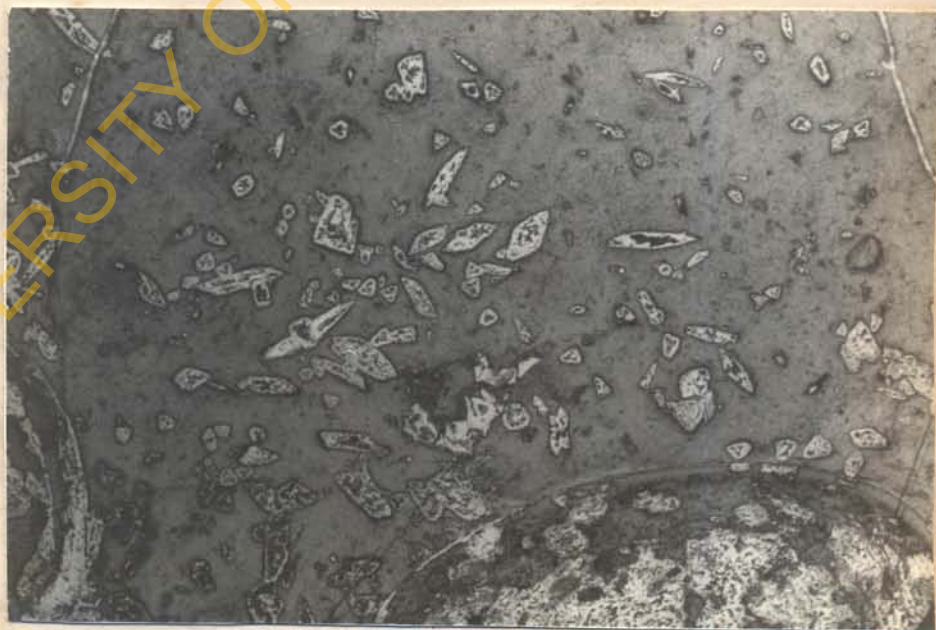
Plate 16: Crystals of pseudomorphs of goethite after siderite in a kaolinitic matrix. CP x 3.2mm. Reflected light. CP - Cross polars, OM - Oil immersion.

into the kaolinitic matrix. The cracks which occur as irregular to regular desiccation cracks in the ooidal pack-ironstone are not mineralized (Plate 11).

Major mineral constituents of ooidal pack-ironstone are kaolinite, goethite and hematite with minor amounts of quartz, mica and ilmenite (Fig. 24).

4.2.2 Pisoidal Pack-Ironstone

Pisoids of the pisoidal pack-ironstone are elliptical, oval, subspherical and fragmentary (Plate 17) in shape and are composite in nature. Pisoidal pack-ironstone consists of poorly sorted, loosely packed pisolites (Plate 18), with pisoids or peloids exhibiting tangential grain contact (Plate 19). Pisoids are characterised by the presence of concentric rings and fragmentary cores, while peloids lack concentric rings and are dominantly composed of goethite with an outer rim of hematite (Plate 19).

Pisoids are made up of goethite and hematite, symmetrically arranged as mosaic of concentric rings about a composite core. Composite cores are commonly made up of goethite and ooidal fragments (Plates 20 and 21). The thickness of the cortex is about 250μm and that of the constituent laminae averages 5μm (Plate 22). The concentric rings consist of predominantly goethite and minor hematite and relics of yellowish kaolinite.
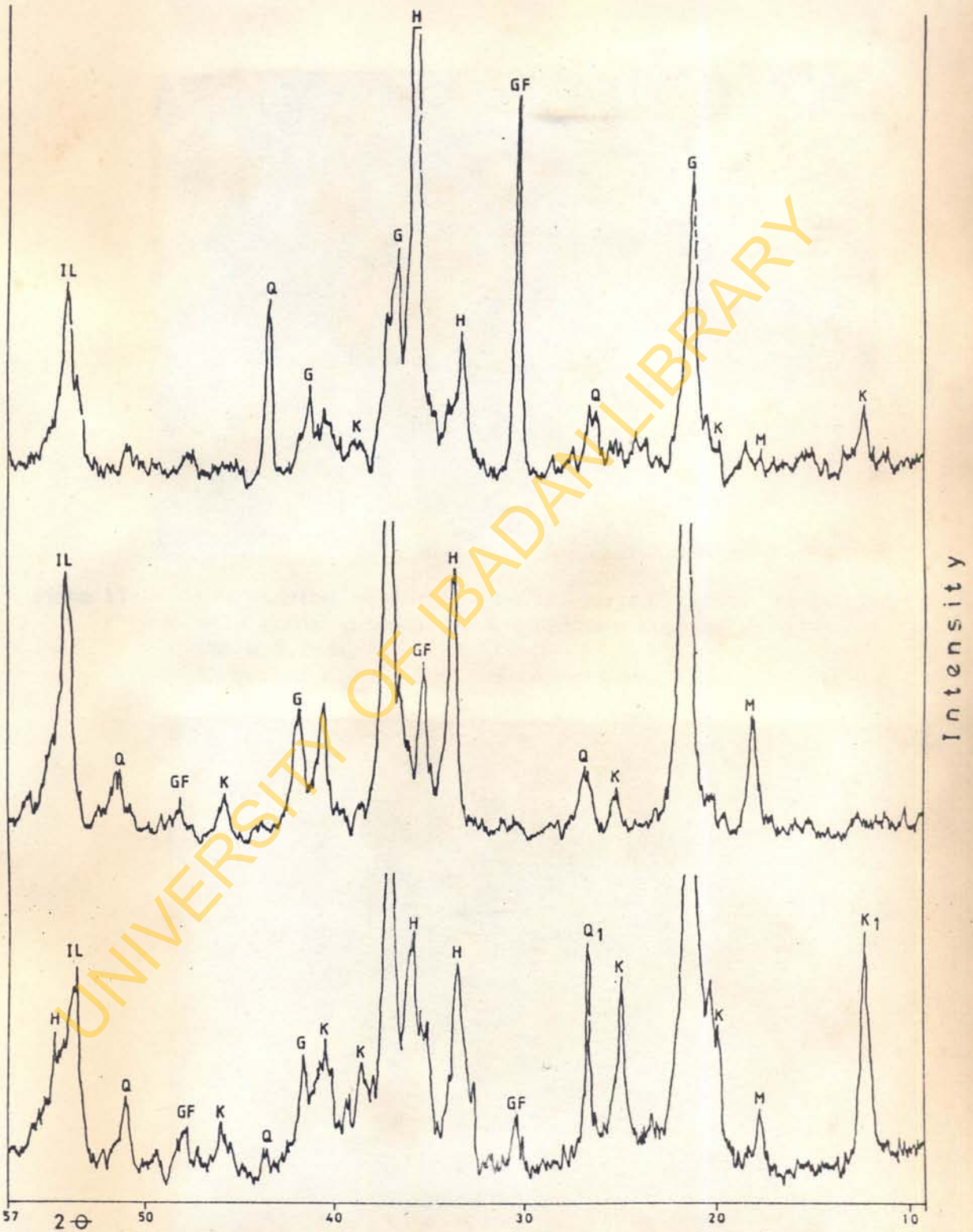
Fig. 24. XRD analysis of Ooidal pack - ironstone.(Q = quartz , G = goethite GF = Goyazite -Crandallite, H =hematite, M= mica , K= kaolinite and IL = ilmenite)

Plate 17: Fragmented peloids, poorly sorted fabric associated with ooidal-pisoidal pack-ironstone boundary.
OM x 3.2mm.
Reflected light. OM – oil immersion.
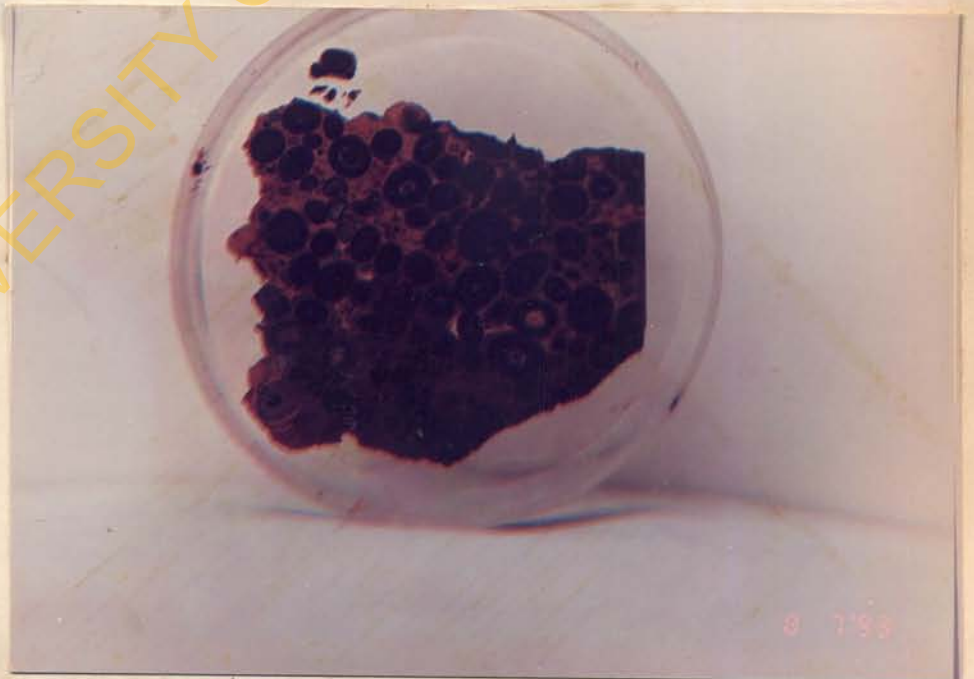
Plate 18: Polished slab of pisoidal pack-ironstone, poorly sorted, loosely packed pisolite.

Plate 19: Peloidal pack-ironstone with tangential peloid-peloid contact arrangement. CP x 3.2mm. Reflected light. CP – Cross polars.

Matrix of the basal part of the pisoidal pack-ironstone is kaolinite (yellow) (Plate 23), but it is being replaced by goethite especially at the uppermost part of the ironstone. In this matrix detrital grains are rarely present.

Replacing and open space ferruginization are common iron enrichment mechanisms in the pisoidal pack-ironstone. Iron enrichment of the kaolinitic matrix occur when goethite advances through the permeable kaolinite to fill its pore spaces. Open space ferruginization is initiated by the in-filling of desiccation cracks, firstly by permeable kaolinite which is later replaced by goethite advancing through the permeable kaolinite (Plate 24). Irregular cavities within the matrix exhibit colloidal texture (Plate 25) while those created in the peloids are sometimes filled with a milky white material (Plate 26), suspected to be a phosphorus mineral. However, microscopic studies further show that the in-filling of open-space by geothite also initiated the replacement of the permeable kaolinitic matrix by goethite.

The pisoidal pack-ironstone is dominantly composed of goethite, with minor amounts of hematite and kaolinite. Other minor mineals indicated by X-ray diffraction studies are goyazite-crandallite, mica, quartz and ilmenite (Fig. 25).

Plate 20: Composite pisoid with goethite (G) fragment core and kaolinite (K) relics in the infilled desiccation cracks. OM x 450μm. Reflected light.
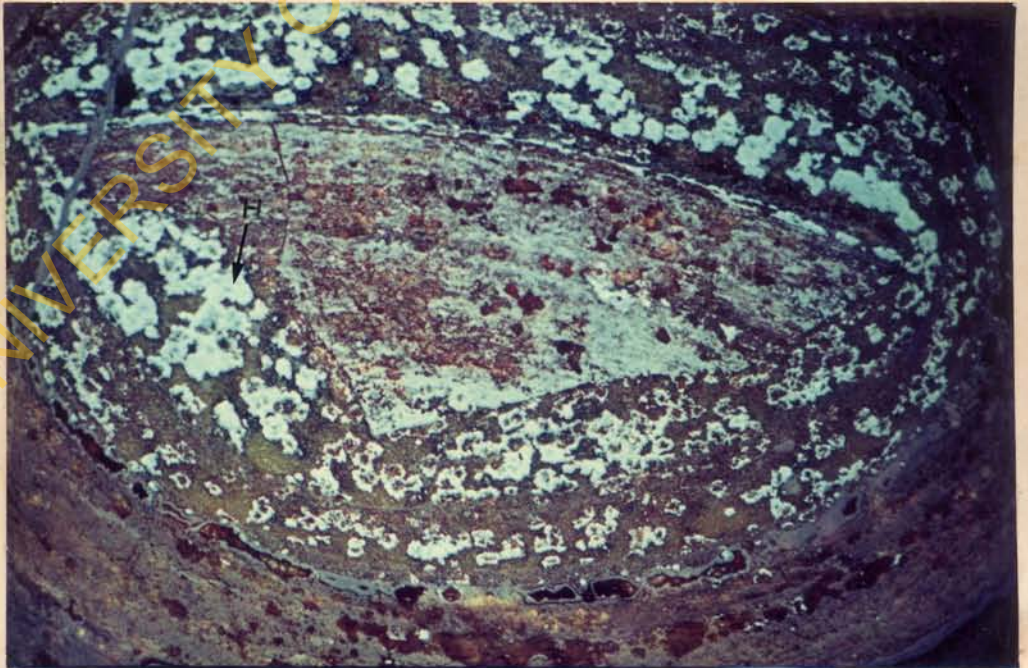
Plate 21: Composite pisoid with fragmented goethite ooid as composite core. The pisoid also exhibits framboids of hematite (H). OM x 450μm. Reflected light.
OM - Oil immersion.

Plate 22: Concentric lamina of a pisoid. Symmetrically arranged goethite (G) with faint rings of hematite (H). OM x 450μm. Reflected light.
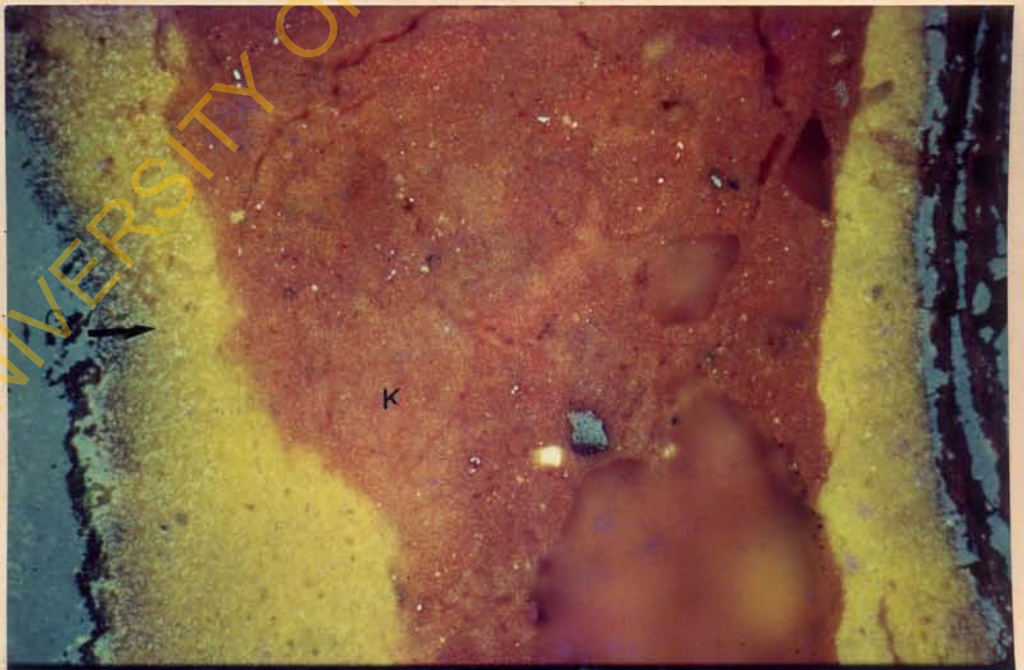
Plate 23: Kaolinitic matrix, yellow, detritus-free kaolinite (K) and the reddish brown detritus kaolinite (kb). Arrow shows the direction of active replacement of the yellow kaolinite by goethite (G). OM x 450μm. Reflected light.
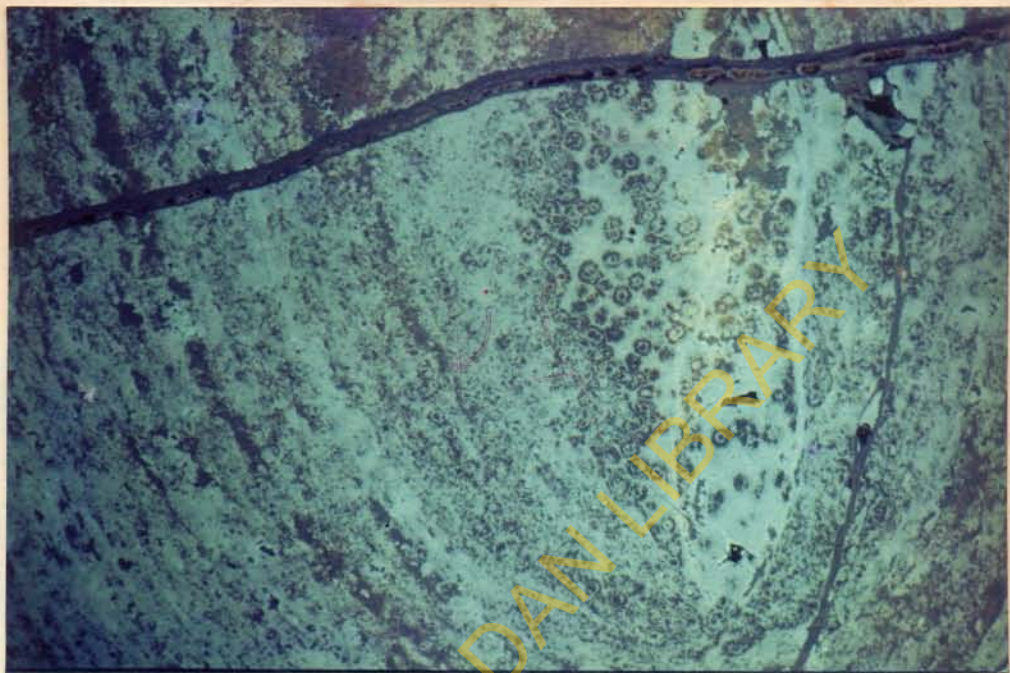
Plate 24: Peloid with cavity infilling and framboids at the core. OM x 450μm. Reflected light.
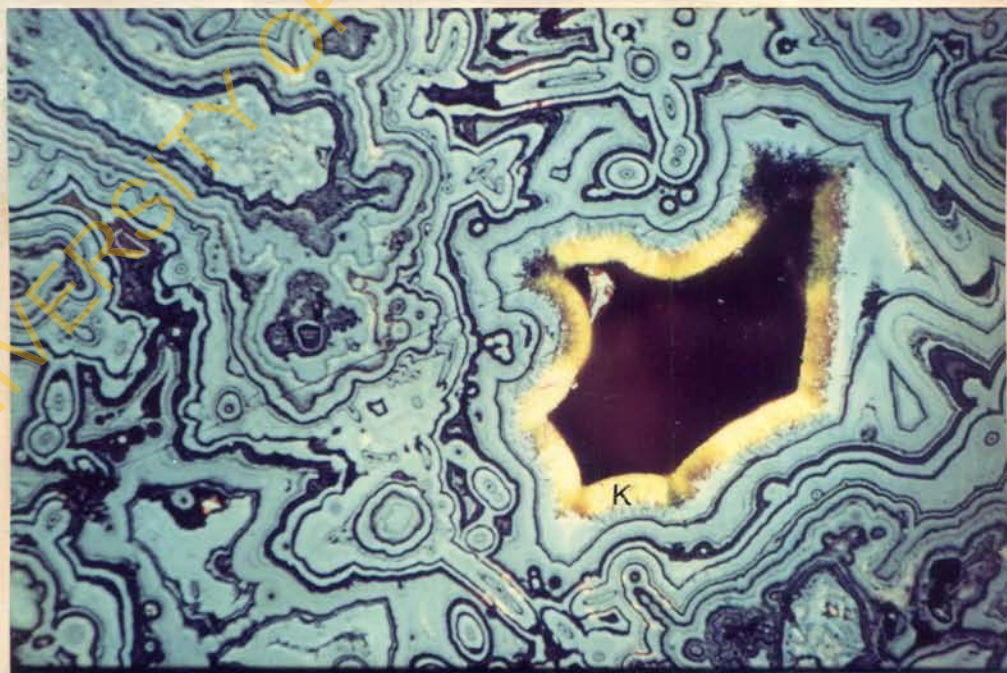
Plate 25: Colloidal texture. Note the yellow crystalline kaolinite (K). OM x 450μm. Reflected light.
OM – Oil immersion.
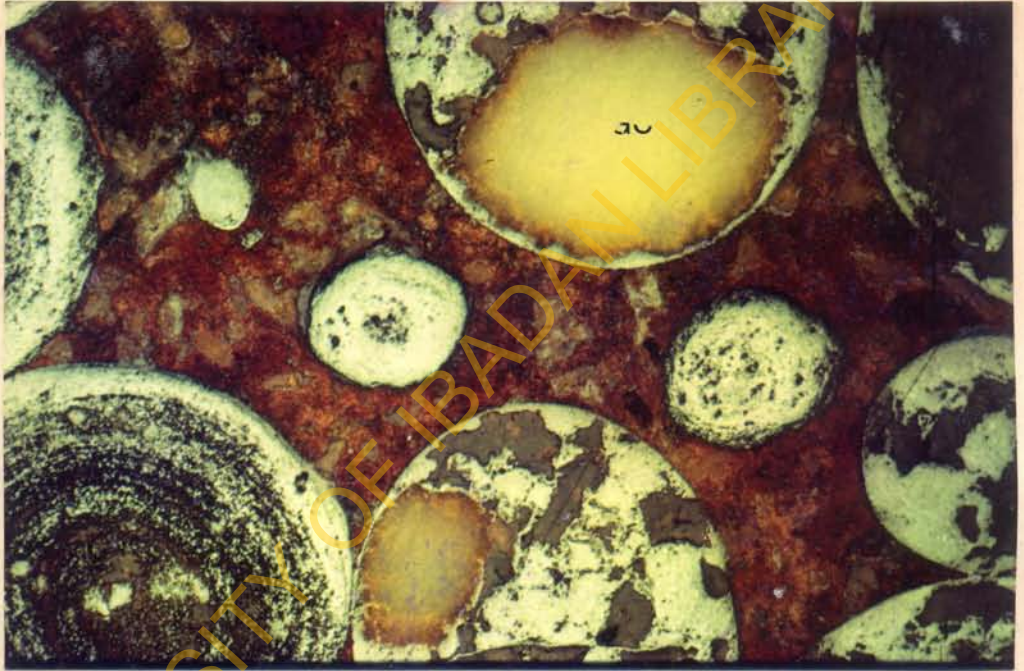
Plate 26: Peloidal pack-ironstone with exsolved of goyazite-crandallite (GC). PP x 3.2mm. Reflected light.
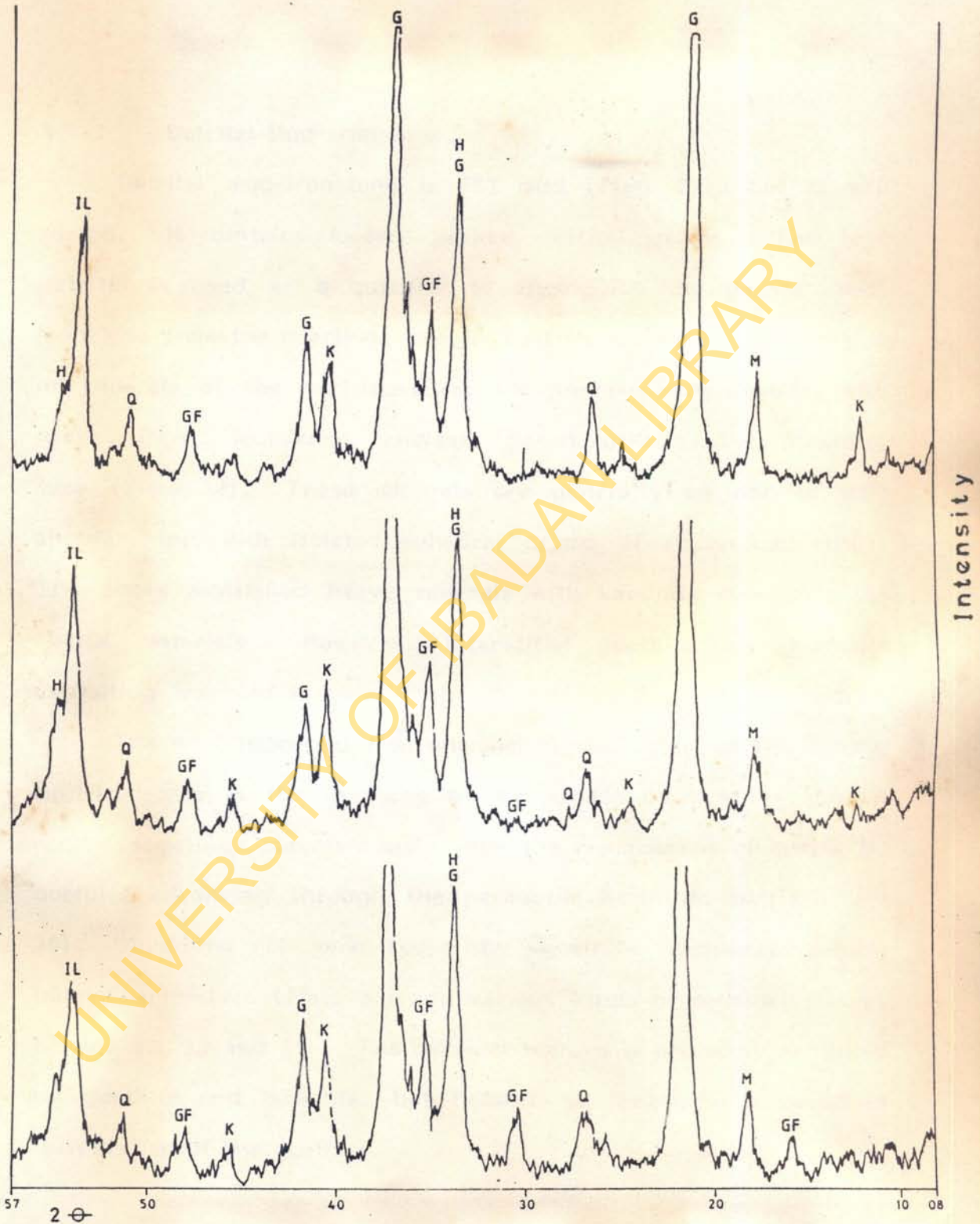
Fig 25 : XRD analysis for Pisoidal pack - ironstone.(Q = quartz, G= goethite,
GF = Goyazite - Crandallite, H =hematite, M= mica, K = Kaolinite and IL = ilmenite)

4.2.3   Detrital Mud-Ironstone

Detrital mud-ironstone is 95% mud (Plate 27), but is well sorted. It contains loosely packed detrital grains. The term detrital is used as a qualifier to distinguish the detrital mud-ironstone from the overlying breccia mud-ironstone. Detrital grains or minerals of the mud-ironstone are predominantly quartz, with minor zircon, leucoxene, anatase, pseudorutile, rutile, ilmenite, mica (Plate 28). These minerals are generally angular to sub-angular, but with isolated euhedral grains of zircon and rutile. The above mentioned heavy minerals with kaolinite constitute the matrix materials. However, interstitial goethite and hematite exhibiting framboid texture (Plate 29) are also found in the matrix.

The most important iron enrichment mechanism in the detrital mud-ironstone is the in-filling of open-space by goethite, but it occurs sometimes simultaneously with the replacement of matrix by goethite advancing through the permeable kaolinitic matrix (Plate 30). In-filling of open-space by goethite commonly exhibit botryoidal texture (Plate 31) and various kinds of colloidal texture (Plates 32, 33 and 34). The colloidal texture is commonly exhibited by goethite and hematite, but hematite is formed as a result of dehydration of the goethite.

Plate 27: Polished slab of detrital mud–ironstone exhibiting a dendritic pattern of mineralised stringers.
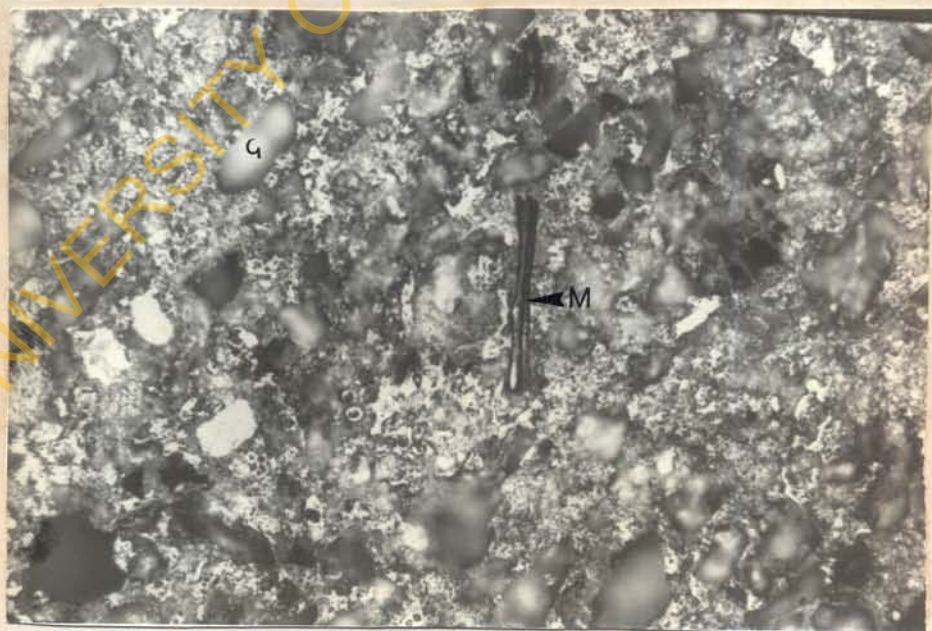
Plate 28: Detrital mud–ironstone. Angular grains of quartz (q), mica (M) in a kaolinitic matrix. OM x 450μm. Reflected light. OM – Oil immersion.
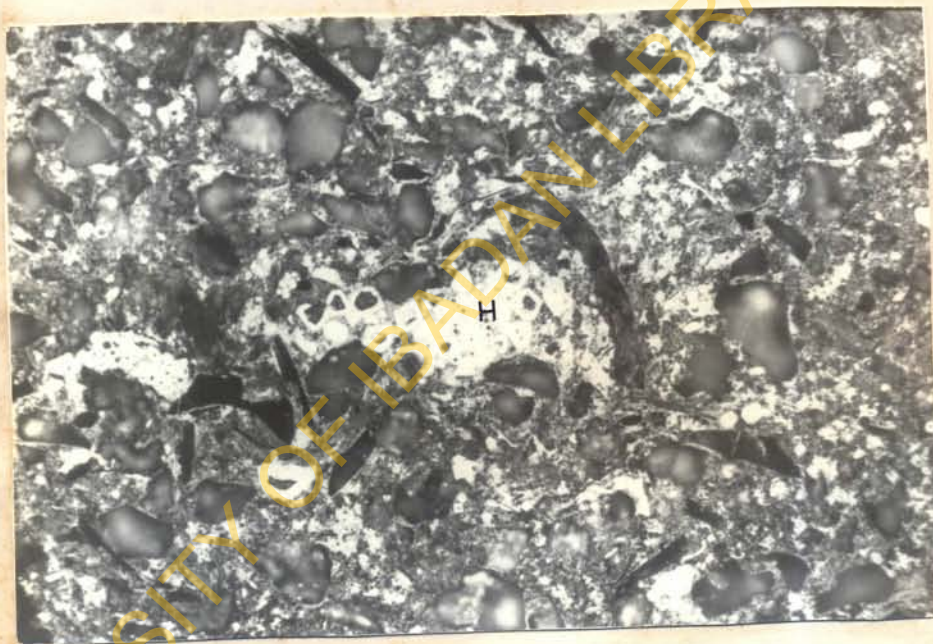
Plate 29: Detrital mud-ironstone with clusters of framboids and pseudomorphs of hematite (H) after pyrite. OM x 450 μm. Reflected light.
OM - Oil immersion.
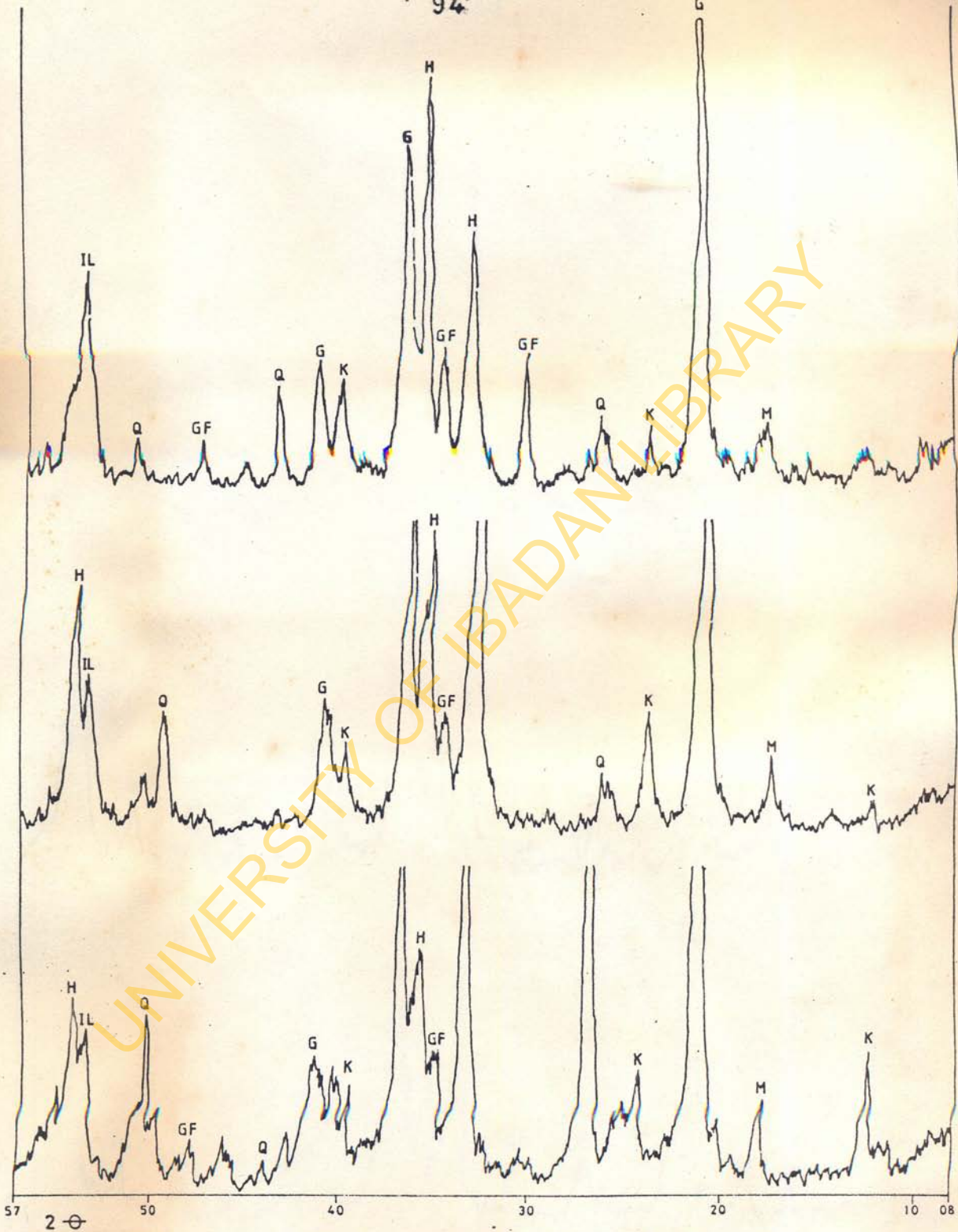
Fig. 26 : : XRD analysis of Detrital mud - ironstone.(Q = quartz , G = goethite , GF = Goyazite - Crandallite, H = hematite, M = mica , K = kaolinite and IL = ilmenite)
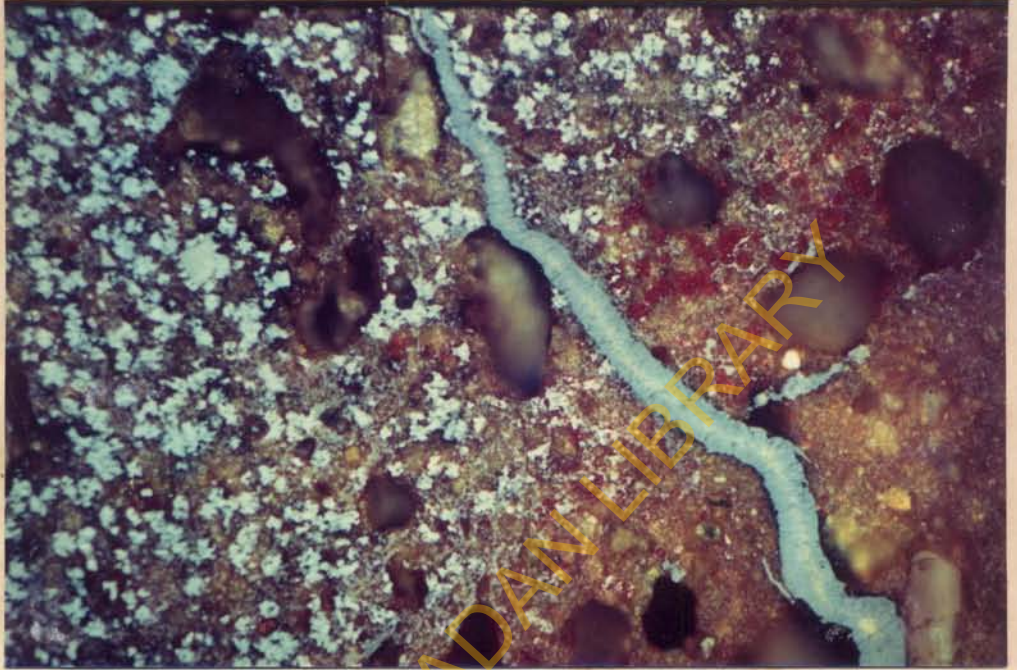
Plate 30:   Detrital mud-ironstone. Replacement and in-filling of open space by goethite (G). Kaolinitic matrix (K) is replaced by goethite (G). OM x 450μm. Reflected light.
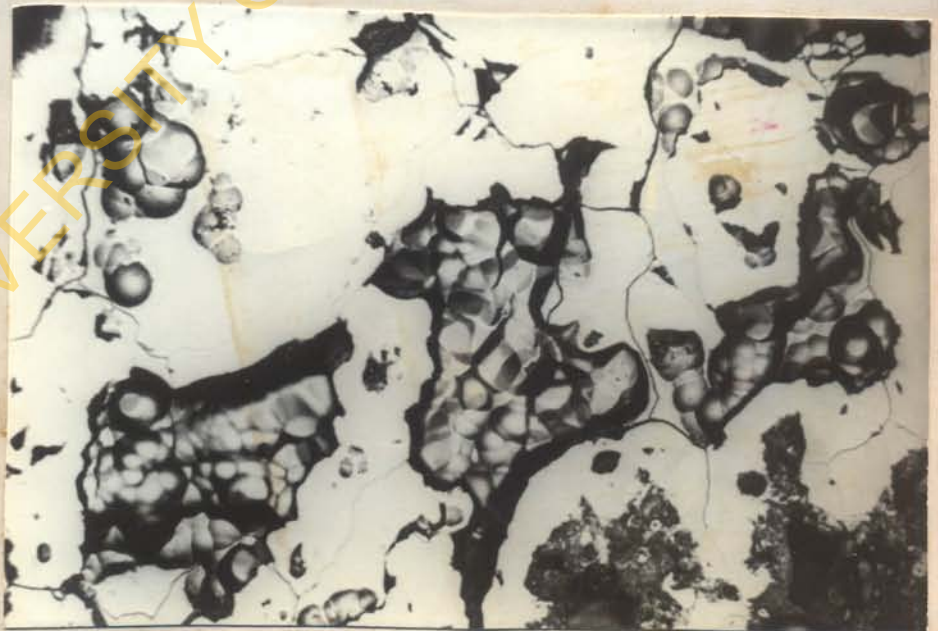
Plate 31:   Botyroidal texture, exhibited by goethite in-filling of cavities. OM x 450μm. Reflected light. OM - Oil immersion.
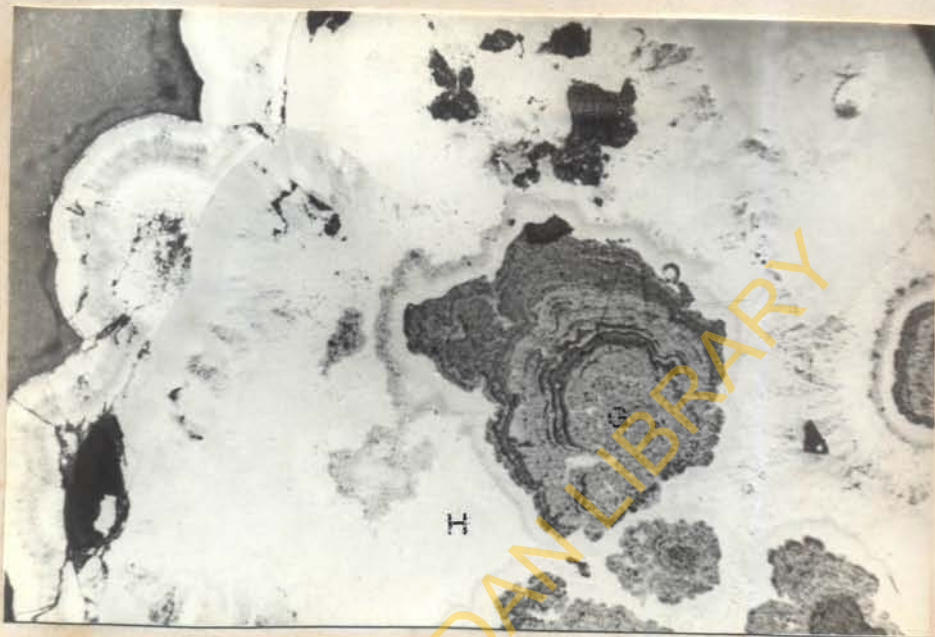
Plate 32: Detrital mud–ironstone. Colloidal texture showing different zones of goethite (G) and hematite (H). OM x 450μm. Reflected light. Colloidal goethite replaced by colloidal hematite during dehydration.
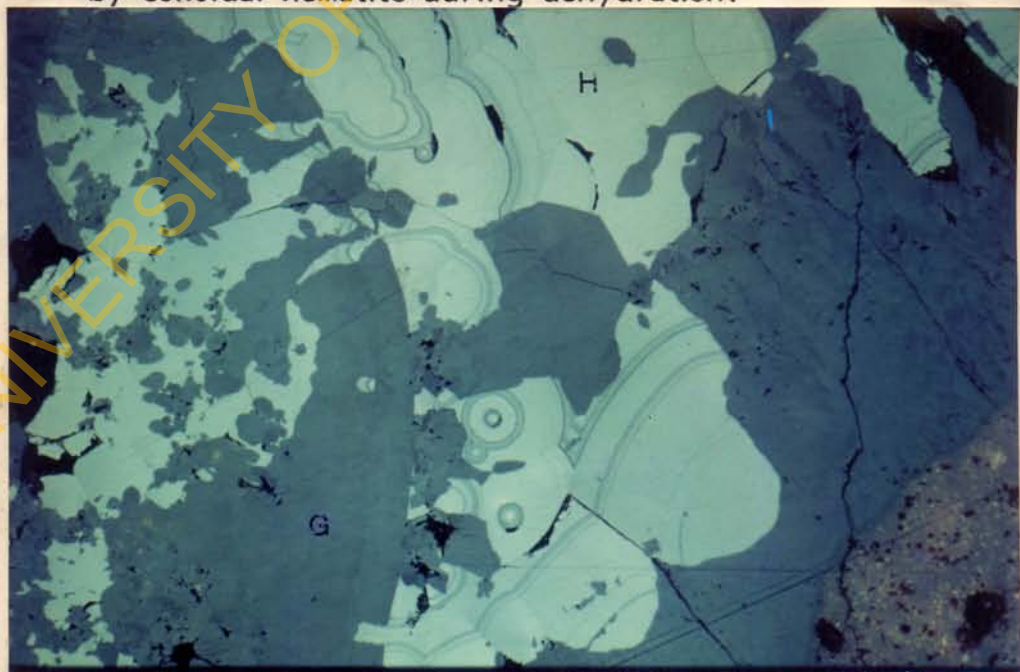
Plate 33: Detrital mud–ironstone. Colloidal texture exhibited by goethite (G) and hematite (H). OM x 450μm. Reflected light. Colloidal goethite replaced by colloidal hematite during dehydration.
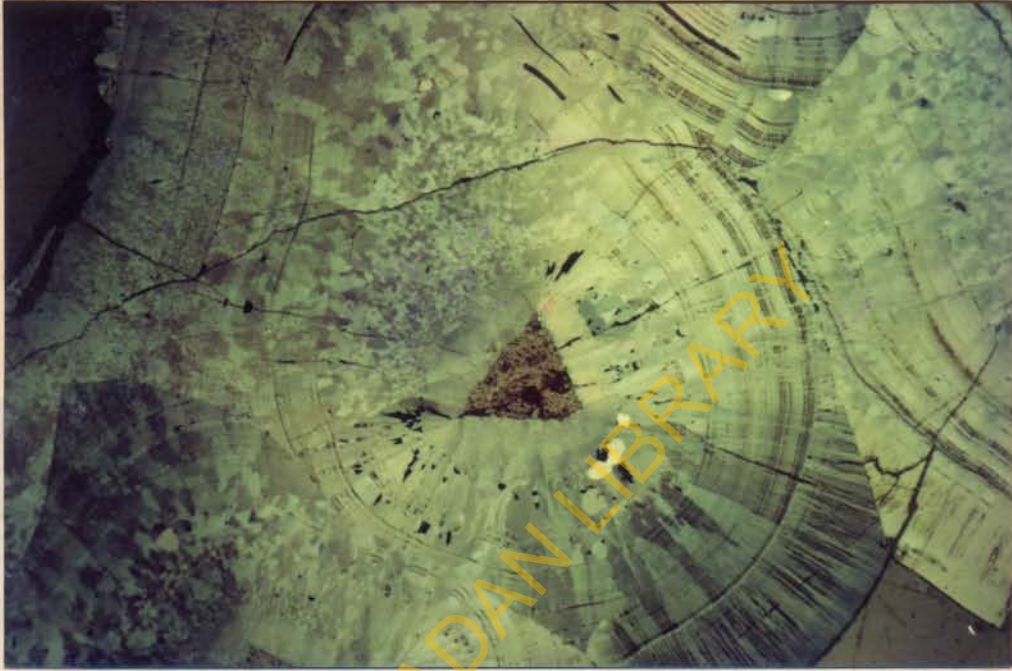
Plate 34: Detrital mud-ironstone. Colloidal texture showing circular rims and fibrous and graphic arrangements exhibited by goethite (G). PP x 3.22mm. Reflected light. PP - Plane polarized light.

Plate 35: Polished slab of breccia mud-ironstone, poorly sorted clasts (C) of isolated breccias in reddish brown kaolinitic (K) matrix.
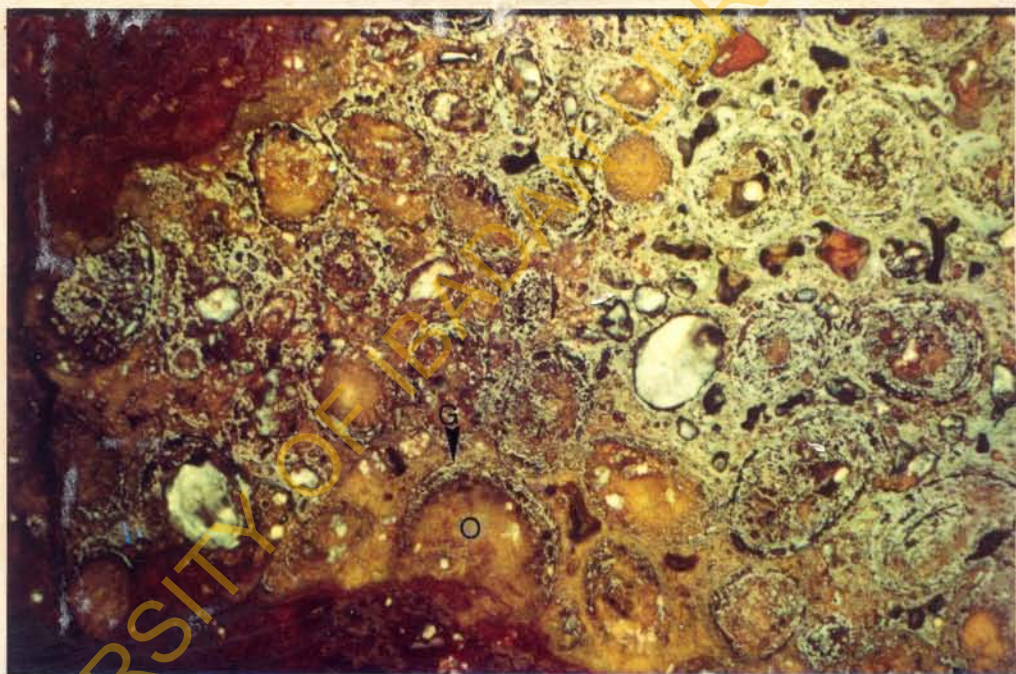
Plate 36:   Kaolinite oomolds (O) with goethite (G) rings. PP
x 3.2mm. Goethite (G) replaces the kaolinite oomolds
(O). Reflected light. PP – Plane polarized light.
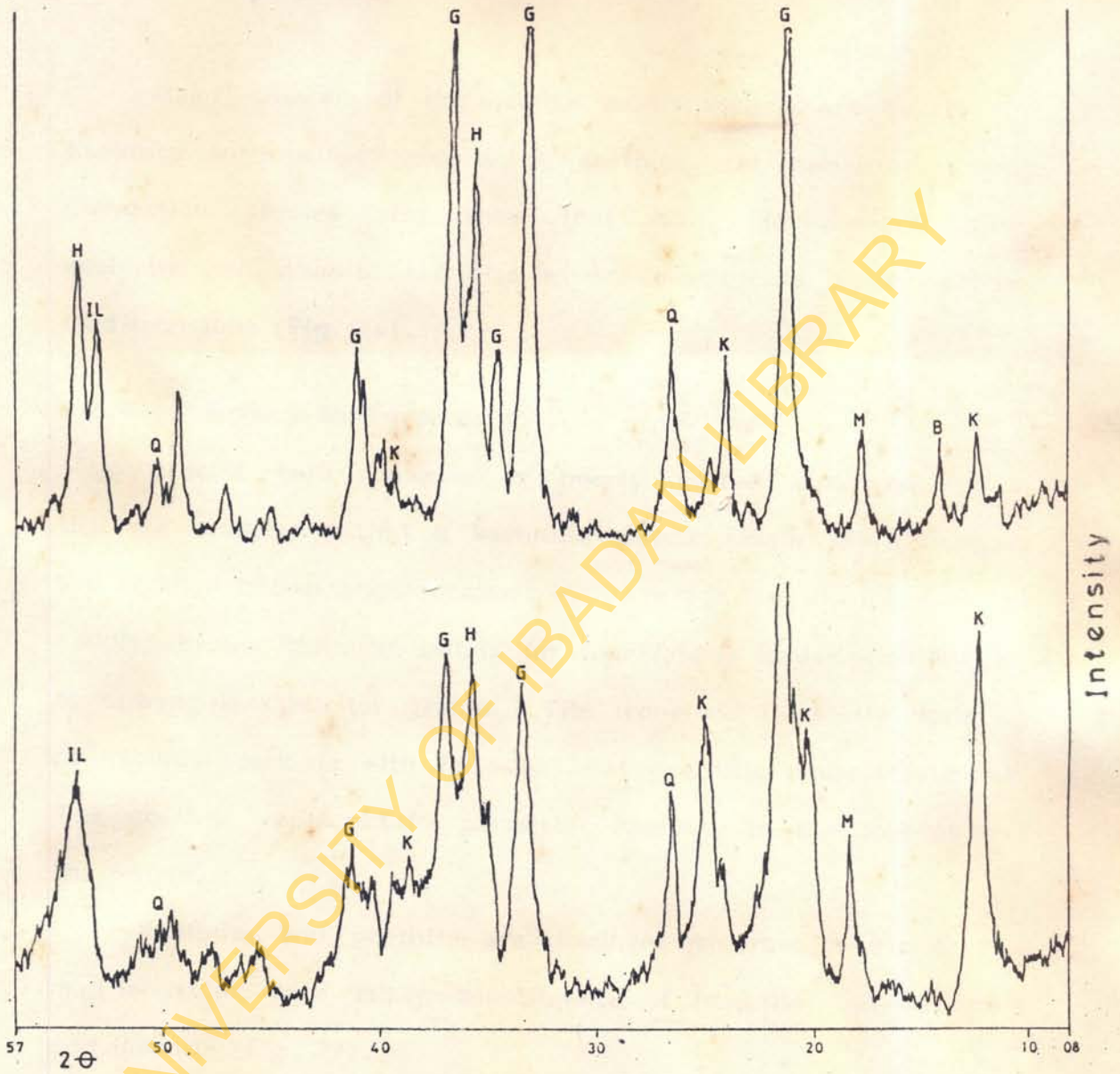
Fig 27: XRD analysis of Breccia mud – ironstone.(Q = quartz, G = goethite, H = hematite, K = kaolinite, B = boehmite, M = mica and IL = ilmenite)

Major minerals of the detrital mud-ironstone are quartz and kaolinite with minor amount of goethite and hematite. X-ray diffraction studies also show that mica, goyazite-crandallite, boehmite and ilmenite are also minor constituents of the detrital mud-ironstone (Fig. 26).

4.2.4 Breccia Mud-Ironstone

Breccia mud-ironstone is poorly sorted and consists of discrete breccias within a kaolinitic matrix (Plate 35). Breccias are reddish brown angular clasts with average length of 5mm. The reddish brown kaolinitic matrix for the clast is loaded with angular to subangular detrital grains. The ironstone is mostly made up of kaolinite oomolds with false to faint goethitic rings (Plate 36). The goethite replaces the permeable kaolinite in the oomolds and the matrix.

Kaolinite and goethite are dominant minerals of the breccia mud-ironstone with minor constituents of hematite, quartz, mica and ilmenite (Fig. 27).

4.3 Mineralogy of the Ironstone

Microscopic characteristics of the minerals present in the ironstone were studied using a light reflecting microscope. Minerals identified from ore microscopy are kaolinite, goethite, hematite and goyazite-crandallite.

Kaolinite, a major constituent of the ooids, oomolds and matrix, is reddish brown, cryptocrystalline and commonly found associated with detrital grains (Plate 23). A second generation kaolinite is yellow, crystalline, fibrous when bordering cavities (Plate 25) and completely devoid of detrital grains. X-ray diffraction chart reveals that kaolinite shows prominent reflection between 7.18 - 7.21 Å in all the petrographic varieties. (Figs. 24 to 27).

Goethite as observed under reflected light is dull grey to bright grey in colour, often with bluish tint (Plate 20) and reddish brown internal reflection. It occurs in close association with hematite to form colloidal texture (Plate 25).

Hematite under reflected light is white cryptocrystalline mineral which is characterised by deep red internal reflection under crossed polars. It is formed by dehydration of goethite, thus its colloidal texture when in close association with goethite. It occurs as pseudomorphs after pyrite and framboids in both ooids and matrix of all the petrographic varieties (Plates 21 and 29).

Milky white crystalline grains, earlier suspected to be a phosphorus mineral, which fills cavities created by fragmented ooids (Plate 26) was shown as goyazite-crandallite from X-ray diffraction studies (Figs. 24 to 27) and chemical data (Table 7). First order peaks of between 2.95 and 2.96 Å indicate the phosphorus series

in the diffractograms (Fig. 26). Crystalline grains of goyazite-crandallite are however restricted to cavities in the pisoidal pack-ironstone. Bolivarite, an amorphous phosphorus mineral disseminated mostly within goethitic matrix and veins of ooidal pack-ironstone, pisoidal pack-ironstone and detrital mud-ironstone, was calculated from chemical data (Table 7). These phosphorous minerals are rich in aluminium with minor amount of calcium. In addition, goyazite-crandallite is rich in BaO and SrO while bolivarite is rich in iron (Table 7).

Highly cleave ferruginized mica (Plate 28), zircon, ilmenite, rutile, pseudorutile and leucoxene occur as angular to subangular grains within the kaolinitic matrix. Angular grains of quartz sometimes occur as nuclei to ooids and as part of the kaolinitic matrix (Plate 28). The presence of such grains points to a primary source very close to the site of deposition.

Pyrite and siderite occur as pseudomorphs and framboids of goethite and hematite.

Table 7: CHEMICAL ANALYSES OF THE PHOSPHORUS MINERALS. 1a, 2a and 3a are COMPOSTIONS OF MINERALS CALCULATED IN MOL. PERCENT. 1 and 2 ARE CHEMICAL ANALYSES FOR GOYAZITE-CRANDALLITE SERIES WHILE 3 IS FOR BOLIVARITE

OXIDES	1	2	3
SiO_2	-	-	2.78
Al_2O_3	33.79	34.07	26.69
Fe_2O_3	0.76	0.91	6.54
CaO	8.57	9.05	1.36
MgO	-	-	0.26
BaO	7.25	7.14	-
SrO	2.49	1.76	-
P_2O_5	31.82	32.17	19.14
H_2O+ calc.	14.12	14.28	8.57
H_2O- calc.	-	-	34.27
Total	98.80	99.64	99.61

	1a		2a		3a	
Al	2.957)		2.949)		1.650)	
Fe 3+	0.042)		0.050)		0.258)	
Mg	-)	2.999	-)	2.999	0.020)	1.999
Ca	-)		-)		0.077)	
Si	-)		-)		0.146)	
Ca	0.682)		0.712)	1.000	-	
Ba	0.211)		0.213)		-	
Sr	0.107)		0.075)		-	
P	2.000		2.000		0.850	
OH	6.000		6.000		3.000	
O,OH	1.000		1.000		5.000	

FORMULAE

1. $(Ca_{0.682} Ba_{0.211} Sr_{0.107})_{1.000} (Al_{2.957} Fe^{3+}_{0.042})_{2.999} (PO_4)_2 (OH)_6$

2. $(Ca_{0.712} Ba_{0.213} Sr_{0.075})_{1.000} (Al_{2.949} Fe^{3+}_{0.050})_{2.999} (PO_4)_2 (OH)_6$

3. $(Al_{1.650} Fe^{3+}_{0.258} Ca_{0.077} Mg_{0.020})_{2.005} (P_{0.850} S:_{0.146})_{0.996} O_4 (OH_3) 6H_2\theta$

4.4   Paragenesis of the Ironstone

A mineral paragenetic sequence is proposed based on the intergrowth relationships between the minerals and the textural characteristics of all the petrographic varieties of the ironstone.

1.   In this study four petrographic varieties of the ironstone were described for the Agbaja Ironstone Formation. The ironstone varieties can be assigned to three different local events of deposition of the Agbaja Ironstone Formation.

2.   The constituent mineral of the ooids is kaolinite. The core and cortex of these ooids are made up of framboids and pseudomorphs of goethite and hematite after pyrite (Plates 13 and 14). It confirms the presence of pyrite before the formation of the kaolinite ooids.

3.   The matrix to the ooids is dominantly kaolinite with minor detrital quartz, mica and heavy minerals. Also of importance is the presence of pseudomorphs of goethite after siderite only in this matrix (Plate 15). The siderite is slightly later than pyrite and kaolinite in age. It is also formed after the formation of ooids, thus its presence only in the matrix

4.   Pure kaolinite ooids were observed (Plate 10) and their wholly or partially replaced equivalents were also identified (Plate 37). The kaolinite ooids are replaced by goethite, which is

subsequently dehydrated to hematite (Plate 37). During the dehydration of goethite to hematite, irregular desiccation cracks (unmineralised) and fragmented ooids were developed. This is the first stage of deposition of the Agbaja ironstone, that is formation of ooidal pack-ironstone.

5. Fragmented ooids developed in the first stage of deposition of ironstone form the nuclei to goethite pisoids of the pisoidal pack-ironstone. Also some earlier formed goethite ooids were redeposited and transformed to peloids after their cortex have been replaced by goethite. Yellow kaolinite, crystalline and detrital-free serve as the matrix for the pisoidal/peloidal pack-ironstone before its subsequent replacement by goethite (Plates 23 and 24). This kaolinite is formed later than the ooids, pisoids, peloids and matrix described earlier in items 2 to 5 above, and commonly replaces the reddish brown kaolinite (Plate 23).

6. Iron enrichment of the pisoids, peloids and matrix of the pisoidal pack-ironstone was initiated by in-filling of open-space created during dehydration of the coidal pack-ironstone. This shows that iron enrichment in pisoidal pack-ironstone is relatively later than the redeposition of fragmented ooids and formation of composite pisoids. This also confirms

Plate 37: Kaolinite ooid, showing rim replacement of concentric rings by goethite (G) through cavity in-filling. OM x 450μm. Reflected light. OM – Oil immersion.

another event of deposition in the Agbaja ironstone. The minerals which accompany the iron enrichment of the second stage of deposition of the ironstone are, goethite, goyazite-crandallite and bolivariate. The presence of these minerals in cavities and veins suggests that they are of the same age.

7.   The formation of kaolinitic matrix with detritals started the third stage of deposition of ironstone, and subsequent deposition of detrital mud-ironstone and breccia mud-ironstone. The detrital minerals are quartz, mica, zircon, nilite, ilmenite, pseudorutile and leucoxene (Table 8). The presence of framboids (Plate 30) in the mud-ironstone, especially in the detrital mud-ironstone linked their formation to a source rich in organic matter. Ferruginization through in-filling of open-space are only peculiar to the detrital mud-ironstone. Replacement of the matrix of detrital mud-ironstone occurs when the framboids are dehydrated to hematite. A common feature noticed in the detrital mud-ironstone is that its goethite veins cut across into pisoidal pack-ironstone. This confirms that the detrital mud-ironstone and pisoidal pack-ironstone were ferruginized at the same time.

Table 8: CHEMICAL ANALYSES OF ILMENITE, PSEUDORUTILE AND LEUCOXENE IN THE MUD-IRONSTONE

	(I)	(II)	(III)	(IV)
FeO	43.64	34.95	31.81	1.40
MnO	0.43	0.34	2.29	0.10
MgO	2.57	1.58	-	0.72
TiO_2	44.98	54.05	55.94	102.76
Al_2O_3	-	0.78	0.75	1.68
SiO_2	-	0.25	0.19	-
P_2O_5	-	0.20	0.21	-
$Fe^{2+} = Fe^{3+}$	7.43	6.95	8.37	-
	99.10	99.10	99.56	106.66
Fe^{2+}	0.875	0.861	0.029	-.045
Fe^{3+}	-	1.296	1.870	0.045
Mn	0.012	0.021	0.137	0.003
Mg	0.113	0.174	-	0.042
O	3.000	9.000	9.000	3.225
OH	-	-	-	5.775

(I)   Calculated on the basis of 0=3.00 while (II), (III) and (IV are calculated based on Ti = 3.000.

(I)   Ilmenite, (II) and (III) Pseudorutile, (IV) Leucoxene.

109

8. The three stages of deposition proposed for the ironstone was only affected by two events of iron enrichment. The first iron enrichment affected the kaolinite ooids of ooidal pack-ironstone before being redeposited as composite goethite pisoids. The second enrichment affected the pisoidal pack-ironstone and detrital mud-ironstone. Dehydration also takes place during the two periods of enrichment. First dehydration period associated with ooidal pack-ironstone led to the formation of passive desiccation cracks and conversion of goethite to hematite. Second period is marked by the conversion of colloform goethite to colloform hematite both in the detrital mud-ironstone and pisoidal pack-ironstone.

9. In summary, minerals such as pyrite, siderite, kaolinite quartz, mica and heavy minerals are associated with the initial or early formation of each of the ironstone petrographic varieties. While goethite, goyazite-crandallite, bolivarite and hematite are iron enrichment or ferruginization minerals in the various ironstone varieties (Fig. 28).

Fig.28 : Mineral paragenesis of the Agbaja Ironstone — Formation

CHAPTER FIVE

GEOCHEMISTRY OF THE AGBAJA IRONSTONE FORMATION

5.1   Analytical Techniques

Ten representative polished samples of the petrographic varieties were selected for microprobe analyses. Determinations were made for FeO, SiO_2, Al_2O_3, CaO, MgO, MnO, K_2O, Na_2O, P_2O_5, TiO_2, SrO and BaO. H_2O was calculated from the analytical data.

Microprobe, ARL-Type SEMQ with six spectrometry (2 x LiF 1 x PET, 2 x ADP, 1 x Tap) of Geochemischen Institut der Universitat Gottingen was used for the determination of the elements in all the ironstone petrographic varieties. Determination of the apparent concentration of the elements were obtained by comparison with known natural standards, i.e.

KAERSUTITE   -   Na, K, Ca, Mg, Al, Si

ILMENITE   -   Mn, Fe, Ti

APATITE   -   P

BARITE   -   Ba

STRONTIANITE -   Sr

and later corrected for using computer programme PRG. MAGIC
IV. The chemistry of the minerals of the ironstone petrographic
varieties was later calculated from the analytical results (Tables
9 to 14). The procedures for calculation of these data are
enumerated in Appendix V.

The chemical characteristics of the ironstone are discussed
in relation to the chemistry of the minerals and concentrations of
elements in the ferruginized and unferruginized constituents of
the various petrographic varieties. The unferruginized (UF)
constituents are those which the kaolinite contents are between
95.82 and 50.13%, while in the ferruginized (FG) constituents
kaolinite contents range from 49.00% to 0.55% (Tables 9 to 14).

5.2   Chemical Characteristics of the Ironstone

The concentrations of the major elements in the allochem
(ooids and pisoids) and the matrix of all the petrographic varieties
are presented in Tables 9 to 14.

SiO_2, Al_2O_3 and Fe_2O_3 account for between 81 and 90% in
the ironstone. SiO_2 content ranges from 23.71 to 51.41% and
Al_2O_3 from 22.01 to 36.54% in all the unferruginized constituents
of the ironstone (Tables 9 to 14). These oxides (SiO_2 and Al_2O_3)
can be as low as 0.22% in the ferruginized equivalent (Tables 9

Table 9: CHEMICAL ANALYSES OF OOIDS OF THE OOIDAL PACK-IRONSTONE

Sample No.	AG/M11														AG/A 1c													
	UNFERRUGINIZED					FERRUGINIZED									FERRUGINIZED													
	1	2	3	4	5	6	7	8	9	10	11	12	13	14	15	16	17	18	19	20	21	22	23	24	25	26	27	28
SiO_2	39.35	35.51	35.11	30.83	28.53	3.67	4.09	3.03	1.83	2.32	1.31	0.86	0.50	0.46	.28	21.12	17.31	0.98	2.65	2.58	3.12	2.38	0.74	0.55	1.58	0.37	2.49	2.10
TiO_2	0.25	0.13	-	0.16	-	-	0.10	0.10	-	-	0.98	-	0.12	0.14	-	-	0.47	-	-	-	-	-	-	-	0.16	0.11	-	0.15
Al_2O_3	34.24	32.65	32.00	29.37	28.75	10.66	13.53	13.40	8.36	8.27	10.35	1.11	4.96	5.25	1.83	22.67	18.61	0.93	5.91	4.55	3.12	4.60	2.03	1.94	2.87	1.64	0.96	5.56
Fe_2O_3	12.57	18.00	19.08	26.00	31.44	70.67	70.14	70.62	75.30	75.86	75.94	95.34	90.80	91.47	93.59	40.74	50.21	76.45	80.74	81.41	82.49	81.16	94.03	94.88	94.11	95.87	96.74	89.58
CaO	-	-	-	0.10	-	0.39	-	0.10	-	0.11	-	0.11	0.11	-	0.19	-	0.11	-	0.10	-	-	-	0.11	0.11	-	-	0.10	-
MgO	-	-	-	-	-	0.10	0.10	0.21	0.16	0.20	-	0.13	-	-	0.12	-	0.26	-	-	0.16	0.14	0.11	-	-	-	0.12	-	0.10
MnO	-	-	-	-	-	-	-	-	-	-	-	-	-	-	-	-	-	-	-	-	-	-	-	-	-	-	-	-
Na_2O	-	-	-	-	-	-	0.10	-	0.12	-	-	-	-	-	-	-	-	-	-	-	-	-	-	-	-	-	-	-
K_2O	-	-	-	-	-	-	-	-	-	-	-	-	-	-	-	0.11	-	-	-	-	-	-	-	-	-	-	-	-
P_2O_5	0.63	0.80	0.58	0.76	1.44	4.06	2.38	2.30	2.60	2.44	1.85	1.82	1.51	1.43	3.51	1.48	1.44	1.58	1.28	0.56	0.29	0.89	2.10	2.41	1.25	1.08	1.74	1.05
H_2O^+	13.35	13.10	13.06	12.72	12.36	10.40	10.26	10.30	11.01	11.03	10.58	0.43	1.66	1.55	0.38	12.95	11.74	11.82	10.55	10.62	10.53	11.18	0.63	0.57	1.68	0.50	0.26	1.20
Total	100.39	100.19	99.83	99.34	99.52	99.95	100.70	100.06	99.38	100.23	101.01	99.80	99.66	100.30	99.90	99.15	99.68	100.23	100.33	99.96	99.69	100.32	99.64	100.46	101.57	99.69	100.30	99.84
Kaolinite	85.52	79.23	78.01	70.00	63.09	7.88	8.78	6.50	3.92	4.99	2.81	1.85	1.08	0.99	0.60	45.54	37.17	2.11	5.69	5.53	6.69	5.11	1.59	1.19	3.40	0.79	1.05	4.51
Goethite	13.99	20.03	21.24	28.92	34.99	78.64	78.04	78.58	83.78	84.40	84.50	-	-	-	-	45.33	55.86	85.07	89.83	90.60	91.79	90.31	-	-	-	-	-	-
Hematite	-	-	-	-	-	-	-	-	-	-	-	95.34	90.80	91.47	93.59	-	-	-	-	-	-	-	94.03	94.88	94.11	95.87	96.74	89.58
Boehmite	-	-	-	-	-	8.88	11.20	12.27	8.80	8.09	10.87	0.78	6.04	6.27	1.89	6.70	4.48	11.00	3.43	3.11	0.78	3.90	1.81	1.87	2.65	1.72	0.67	4.45
SiO_2/Al_2O_3	1.15	1.09	1.10	1.05	1.11	0.34	0.30	0.23	0.22	0.28	0.13	0.77	0.10	0.10	0.15	0.93	0.93	0.11	0.53	0.57	1.00	0.52	0.36	0.28	0.55	0.23	0.51	0.38

Table 10: CHEMICAL ANALYSES OF THE CEMENT OF OOIDAL PACK-IRONSTONE

| Sample No. | AG/M11 | | | | | | | | | | | | | | AG/A 1c | | | | | | | | | | | |
| | UNFERRUGINISED | | | | | FERRUGINIZED | | | | | | | | UNFERRUGINIZED | | | | | FERRUGINIZED | | | | | | | |
	1	2	3	4	5	6	7	8	9	10	11	12	13	14	15	16	17	18	19	20	21	22	23	24	25	26
SiO_2	44.76	37.14	36.00	30.13	23.31	18.14	17.72	1.92	0.70	2.65	1.21	2.01	2.39	2.03	45.96	33.18	28.44	21.12	18.85	17.43	16.93	0.81	1.69	2.11	2.62	2.26
TiO_2	-	0.27	-	-	-	0.17	-	0.13	0.21	-	-	-	-	-	-	0.10	0.18	-	0.23	0.12	-	0.15	-	-	-	0.29
Al_2O_3	36.01	33.14	28.37	25.13	21.15	20.70	19.21	11.99	9.80	10.59	5.69	4.14	2.07	2.00	36.54	31.83	26.96	22.67	20.89	20.14	18.95	11.13	11.09	7.35	4.64	2.30
Fe_2O_3	4.18	14.78	21.53	30.18	41.60	45.82	48.08	69.69	74.34	75.35	79.40	81.10	83.29	84.49	4.68	20.56	29.19	40.74	45.34	47.72	49.12	72.86	72.94	77.30	79.82	83.19
CaO	0.17	0.15	-	-	-	-	-	-	-	0.11	0.11	0.11	-	-	0.10	-	0.11	-	-	-	-	-	-	0.11	0.11	-
MgO	0.18	-	-	-	-	0.18	0.12	0.14	-	0.25	0.15	0.36	0.34	0.26	0.22	0.11	0.13	-	0.15	0.14	0.11	-	-	0.15	0.21	0.32
MnO	-	-	-	-	-	-	-	-	-	0.10	0.17	0.36	0.37	0.30	-	-	-	-	-	-	-	-	-	-	-	0.18
Na_2O	-	-	-	-	-	0.12	-	0.72	-	0.10	-	-	-	-	-	-	-	-	-	-	-	-	-	-	-	-
K_2O	-	0.12	-	-	-	-	-	-	-	-	-	-	-	-	-	-	0.11	0.11	-	-	-	-	-	-	-	-
P_2O_5	0.91	1.01	0.79	1.05	1.36	1.76	1.35	2.48	2.08	2.02	1.85	1.55	0.83	1.17	0.52	0.69	0.92	1.48	1.68	1.66	1.43	2.04	2.69	1.70	1.18	0.95
H_2O^+	13.52	13.17	12.80	13.34	11.90	12.76	13.93	13.08	12.41	10.16	11.00	10.41	10.10	10.21	13.85	12.87	12.29	12.95	12.84	12.01	12.93	12.66	10.69	11.10	10.74	12.73
Total	99.73	100.34	99.50	100.00	99.32	99.65	100.41	99.50	99.54	99.33	99.58	100.40	99.39	100.46	101.87	99.34	99.33	99.15	99.98	99.22	99.52	99.65	99.10	99.82	99.32	99.93
Kaolinite	93.82	82.34	74.76	65.37	51.68	38.96	38.04	4.13	1.51	5.70	2.60	4.31	5.18	4.36	95.82	75.59	64.40	45.54	40.48	37.43	36.35	1.76	3.64	4.54	5.62	4.85
Goethite	4.65	16.45	23.58	46.28	50.99	53.50	77.54	77.54	82.72	81.61	88.35	90.24	92.67	94.00	5.21	22.85	32.48	45.33	50.45	53.10	54.66	81.07	81.15	86.01	88.81	92.56
Hematite	-	-	-	-	-	-	-	-	-	-	-	-	-	-	-	-	-	-	-	-	-	-	-	-	-	-
Boehmite	-	-	-	-	-	7.47	7.40	15.01	13.02	9.44	6.35	3.11	-	0.37	-	-	-	6.70	6.99	6.77	6.97	14.63	11.62	7.31	3.39	0.77
SiO_2/Al_2O_3	1.24	1.12	1.27	1.20	1.10	0.88	0.92	0.16	0.07	0.25	0.21	0.49	1.15	1.02	1.26	1.04	1.05	0.43	0.90	0.87	0.89	0.07	0.15	0.29	0.56	0.98

114

Table 11: CHEMICAL ANALYSES OF PISOIDS OF PISOIDAL PACK-IRONSTONE.

Sample No.	AG/B2b					AG/M9						AG/14a							
	PISIODS					(FERRUGINIZED)						PELIODS			(FERRUGINIZED)				
	1	2	3	4	5	6	7	8	9	10	11	12	13	14	15	16	17	18	19
SiO_2	2.39	1.59	1.29	1.02	1.02	0.88	0.29	0.39	0.30	0.22	0.22	0.45	0.32	0.27	1.39	0.95	0.62	0.60	0.35
TiO_2	0.79	0.15	0.40	0.40	0.22	0.43	0.35	0.19	-	0.22	0.26	0.31	-	0.27	-	0.15	-	-	0.30
Al_2O_3	5.72	1.42	4.27	5.40	2.43	5.65	4.42	3.91	7.92	8.75	7.17	3.45	2.60	5.96	2.57	2.09	0.98	4.87	0.65
Fe_2O_3	75.58	84.43	76.71	80.37	82.67	79.87	77.33	82.35	75.78	76.26	77.15	83.26	84.26	79.32	92.21	94.26	96.32	91.22	97.54
CaO	-	-	-	-	-	-	-	-	-	-	-	-	-	-	-	-	-	-	-
MgO	-	-	-	-	-	-	-	-	-	-	-	-	-	-	-	0.11	-	-	-
MnO	-	0.25	-	-	0.11	-	-	-	-	-	-	-	-	-	0.27	-	-	0.32	-
Na_2O	-	-	-	-	-	0.40	-	-	-	-	0.12	-	-	0.12	-	-	-	-	-
K_2O	-	-	-	-	-	0.11	-	-	-	-	-	-	-	-	-	-	-	-	-
P_2O_5	2.80	1.78	2.91	2.65	3.06	2.30	3.36	2.81	4.08	3.27	3.35	2.70	2.90	2.71	1.62	1.57	1.29	1.97	1.16
H_2O+	12.45	10.01	14.52	10.60	10.10	10.73	14.32	10.31	12.22	10.98	11.53	10.30	10.19	11.21	2.40	0.71	0.31	1.12	0.23
Total	99.73	99.63	100.10	100.28	99.82	100.29	99.91	99.77	100.52	99.74	99.85	100.16	100.27	99.84	100.46	99.84	99.52	100.10	100.23
Kaolinite	5.14	3.50	2.76	2.19	2.18	1.89	0.62	0.84	0.64	0.47	0.48	0.97	0.69	0.58	2.97	2.04	1.34	1.28	0.76
Goethite	84.10	93.95	85.36	89.42	91.97	88.87	86.04	91.63	84.32	84.84	85.85	92.63	93.75	88.25	-	-	-	-	-
Hematite	-	-	-	-	-	-	-	-	-	-	-	-	-	-	92.21	94.26	96.32	91.22	97.54
Boehmite	6.90	-	8.67	5.78	2.07	6.37	9.70	4.49	11.26	10.90	9.74	3.86	2.93	7.93	3.39	1.71	0.57	5.31	0.47
SiO_2/Al_2O_3	0.42	1.12	0.30	0.19	0.42	0.16	0.07	0.10	0.04	0.03	0.03	0.13	0.12	0.05	0.54	0.45	0.63	0.12	0.54

115

Table 12: CHEMICAL ANALYSES OF CEMENT OF THE PISIODAL PACK-IRONSTONE

Sample No.	AG/B2b				AG/M9				AG/14a				
					FERRUGINIZED								
	1	2	3	4	5	6	7	8	9	10	11	12	13
SiO_2	21.84	16.90	11.10	4.79	21.75	14.52	1.65	1.72	1.16	1.10	0.25	0.53	1.94
TiO_2	-	-	0.20	-	-	-	-	-	0.15	-	0.26	-	0.25
Al_2O_3	14.99	16.90	9.45	5.65	21.36	13.33	2.94	1.29	5.00	4.47	4.22	3.30	0.28
Fe_2O_3	41.88	52.54	62.33	73.20	42.82	55.55	80.96	84.47	78.39	79.42	80.24	83.00	86.23
CaO	-	-	0.13	-	-	-	-	-	0.14	0.33	-	-	-
MgO	-	-	-	-	-	-	-	0.12	-	0.15	-	0.11	-
MnO	-	-	-	-	-	0.12	0.11	0.38	-	-	-	-	0.26
Na_2O	-	-	-	-	-	-	0.32	-	-	-	-	-	0.11
K_2O	-	-	-	-	-	-	0.47	-	-	-	-	-	-
P_2O_5	1.94	2.17	2.82	5.10	1.84	2.08	2.88	1.12	3.84	3.06	4.21	2.70	1.07
H_2O+	19.45	11.42	12.85	10.94	11.84	14.08	10.84	9.97	12.24	12.54	10.28	10.38	9.81
Total	100.14	99.94	100.29	99.68	99.61	99.68	100.17	99.07	100.92	101.07	99.48	100.02	99.98
Kaolinite	46.90	39.31	24.75	10.94	50.13	31.18	4.18	3.26	2.49	2.36	0.55	1.14	0.72
Goethite	46.59	58.46	69.35	81.45	47.64	61.81	90.08	93.99	87.22	88.37	89.28	92.35	95.94
Hematite	-	-	-	-	-	-	-	-	-	-	-	-	-
Boehmite	4.67	-	3.04	2.19	-	4.49	2.13	-	7.02	6.80	5.16	3.72	-
SiO_2/Al_2O_3	1.46	1.00	1.17	0.85	1.02	1.09	0.56	1.33	0.23	0.25	0.06	0.16	6.93

116

TABLE 13: CHEMICAL ANALYSES OF CEMENT OF DETRITAL MUD-IRONSTONE

Sample No.	AG/15A UNFERRUGINIZED							AG/M6B FERRUGINIZED													
	1	2	3	4	5	6	7	8	9	10	11	12	13	14	15	16	17	18	19	20	21
SiO_2	49.51	35.52	35.37	56.41	32.70	24.50	15.88	1.77	1.93	3.57	4.34	3.41	2.47	2.31	6.10	4.11	3.93	2.33	1.29	2.01	10.79
TiO_2	-	-	0.12	1.11	0.10	0.23	0.49	0.27	0.25	-	-	-	0.19	-	0.12	0.11	-	0.15	-	-	0.42
Al_2O_3	23.86	28.22	24.45	5.97	24.66	22.76	13.39	3.96	2.87	1.06	0.65	0.57	1.33	0.33	3.63	1.54	1.21	0.52	0.71	0.33	7.29
Fe_2O_3	15.80	21.83	27.65	30.68	31.10	37.91	55.55	80.90	81.78	84.55	82.49	86.37	86.69	87.27	87.15	92.11	92.95	95.95	96.54	96.89	78.19
CaO	-	0.10	0.19	0.11	0.10	0.10	0.13	-	0.11	-	-	-	-	-	0.11	-	-	-	-	-	-
MgO	-	-	-	-	-	0.10	0.15	-	0.11	-	-	-	-	-	-	-	-	-	-	-	-
MnO	-	-	-	-	-	-	-	-	-	-	-	-	-	0.11	-	-	-	-	-	-	-
Na_2O	-	-	-	-	-	-	-	-	0.39	-	-	-	-	-	-	-	-	-	0.11	0.10	-
K_2O	-	0.10	0.10	-	-	0.12	-	-	0.28	-	-	-	-	-	-	-	0.11	-	-	-	0.19
P_2O_5	0.24	1.26	0.10	-	0.25	2.28	1.93	3.18	2.26	0.25	0.26	0.16	0.49	0.48	1.69	1.97	1.35	1.01	1.10	0.20	0.39
H_2O^+	10.22	12.75	11.76	5.56	12.20	11.91	10.99	10.44	13.01	9.89	12.27	9.94	10.24	9.94	1.28	0.54	0.42	0.18	0.25	0.11	2.57
Total	99.63	99.78	99.74	99.84	101.01	99.95	99.42	100.47	100.15	99.31	100.02	100.45	101.52	100.33	100.08	100.38	99.97	100.14	99.99	99.64	99.84
Kaolinite	60.42	71.78	61.91	65.12	62.43	54.94	34.01	3.87	4.11	2.67	1.64	1.43	3.37	0.83	9.18	3.91	3.05	1.31	1.79	0.83	18.45
Goethite	17.59	24.29	30.78	34.13	34.60	42.18	61.80	90.04	90.99	94.07	94.53	96.11	96.46	97.09	-	-	-	-	-	-	-
Hematite	-	-	-	-	-	-	-	-	-	-	-	-	-	-	87.15	92.11	92.95	95.95	96.54	96.89	18.19
Beohmite	-	-	-	-	-	-	-	3.17	1.65	-	-	-	-	-	-	-	-	-	-	-	-
SiO_2/Al_2O_3	2.08	1.26	1.45	9.45	1.33	1.08	1.19	0.45	0.67	3.37	6.68	5.98	1.86	7.00	1.68	2.67	3.25	4.48	1.82	6.09	1.48

117

Table 14: CHEMICAL ANALYSES CEMENT OF THE BRECIA MUD-IRONSTONE

| | UNFERRUGINIZED | | | | | | | | FERRUGINIZED | |
	1	2	3	4	5	6	7	8	9	10
SiO_2	50.72	47.78	43.99	44.96	40.89	36.14	27.83	24.14	9.22	8.42
TiO_2	-	-	5.76	0.50	0.81	0.93	1.23	0.55	0.23	0.27
Al_2O_3	35.04	35.66	32.43	29.06	31.55	30.19	25.19	22.01	9.07	7.65
Fe_2O_3	1.59	3.47	9.52	17.46	13.75	19.08	32.52	41.37	69.33	71.61
CaO	-	-	-	-	-	-	-	0.10	0.11	-
MgO	-	-	-	0.10	-	-	0.10	-	-	-
MnO	-	-	-	-	-	-	-	-	-	-
Na_2O	-	-	-	-	-	-	-	-	-	-
K_2O	-	-	-	0.12	-	0.10	0.12	-	-	-
P_2O_5	-	-	0.10	0.10	0.12	0.18	0.25	0.58	1.11	0.95
H_2O+	12.54	12.98	12.52	11.66	12.70	12.87	12.27	12.16	11.33	10.67
Total	99.89	99.89	100.24	99.05	99.82	99.51	99.51	101.18	100.40	99.57
Kaolinite	88.72	90.29	82.10	73.58	78.89	77.06	61.63	53.65	19.80	18.68
Goethite	1.72	3.86	10.60	13.86	15.31	21.24	36.18	46.03	77.14	79.67
Hematite	-	-	-	-	-	-	-	-	-	-
Boehmite	-	-	-	-	-	-	-	-	2.01	-
SiO_2/Al_2O_3	1.45	1.34	1.36	1.55	1.30	1.20	1.10	1.10	1.02	1.10

118

to 14). SiO_2 and Al_2O_3 contents are highest in the mud-ironstone varieties and lowest in the pack-ironstone varieties. This is directly related to the high percentage of clay and quartz in the mud-ironstone varieties.

Fe_2O_3 content increases from about 1.59% in the unferruginized to about 97.54% in the ferruginized varieties (Tables 7 to 12). Fe_2O_3 content increases from the ooidal pack-ironstone at the base of ironstone sequence to detrital mud-ironstone, but with the highest concentration in the pisoidal pack-ironstone. Plots of Fe_2O_3 against SiO_2 and Al_2O_3, and SiO_2 against Al_2O_3 indicate a decrease in SiO_2 and Al_2O_3 with increasing ferruginization (iron enrichment) of the ironstone (Figs. 29 to 31).

P_2O_5 values range from 0.10 in the unferruginized to 5.10% in the ferruginized components. P_2O_5 is highest in the pisoidal pack-ironstone and generally increases with increase in Fe_2O_3 (Tables 10 and 11, Fig. 32).

MnO, CaO, MgO, Na_2O and K_2O are generally less than 1.0% in all the petrographic varieties (Tables 9 to 14).

Three main groups of elements are recognised based on their similar correlation coefficients. The coefficient matrix between these elements in Table 15 were got using the computer programme. The groups are: (i) Si, Al (ii) Fe, P (iii) Ca, Mg, Mn, K.

Elements in a specific group commonly show a positive correlation between themselves and a negative correlation with the components of the other groups. Few of this significant correlations were graphically represented earlier (Figs. 29 to 31).

The minerals of the ferruginized constituents (ooids, pisoids and matrix) of all petrographic varieties were ploted into a ternary diagram developed by Aleva (1981). This makes it possible to classify the minerals associated with iron enrichment process into ferritic kaolinite, kaolinitic ferrite and ferrite (Fig. 33).

The chemistry of these mineralogical classes was used in calculating the elemental gain and loss as replacement (iron-enrichment) progresses in the ironstone. Molecular proportions of the oxides of Si, Al and Fe of the mineralogical classes were plotted into a ternary diagram with SiO_2, Al_2O_3 and Fe_2O_3 as coordinates (Fig. 34). From this ternary plot it appears that there is a decrease in the content of SiO_2 and Al_2O_3 from the kaolinitic relics to the kaolinitic ferrite with increase in Fe_2O_3 (Fig. 33). This suggests both desilicification and removal of alumina during iron enrichment of the precursor kaolinite of the ironstone.
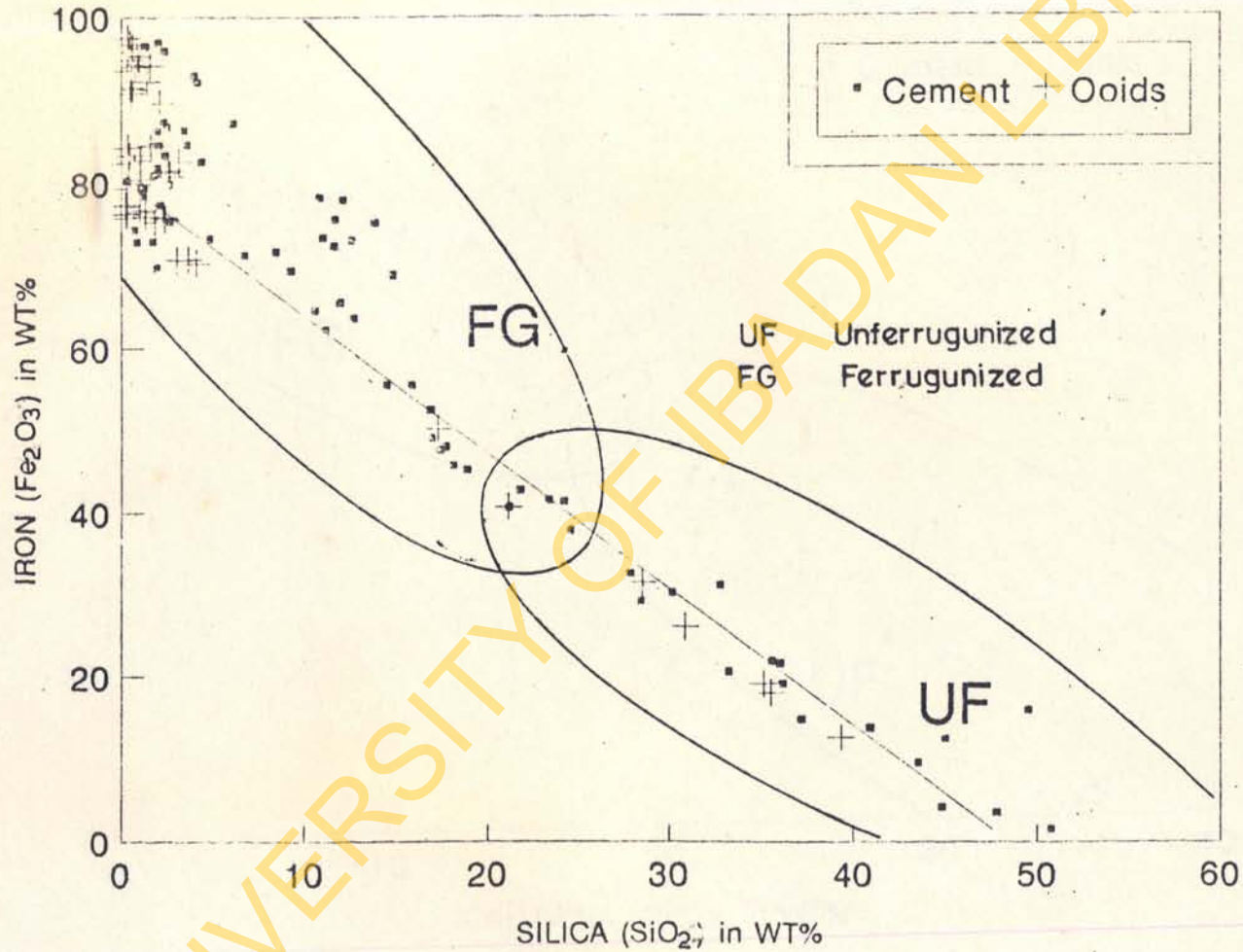
FIG 29 :   Plot of Fe₂O₃ Vs. SiO₂
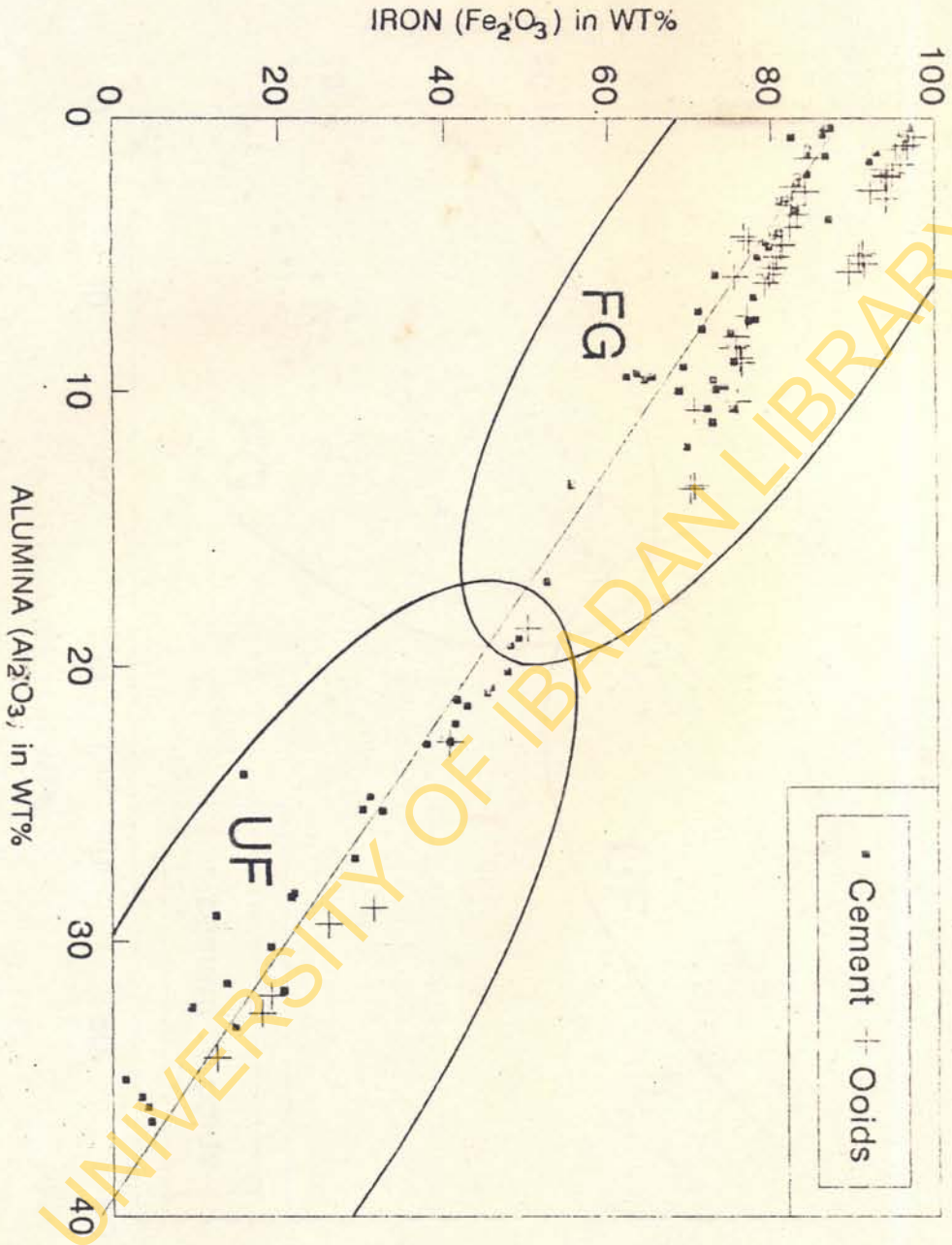
FIG. 30 : Plot of Fe_2O_3 Vs. Al_2O_3
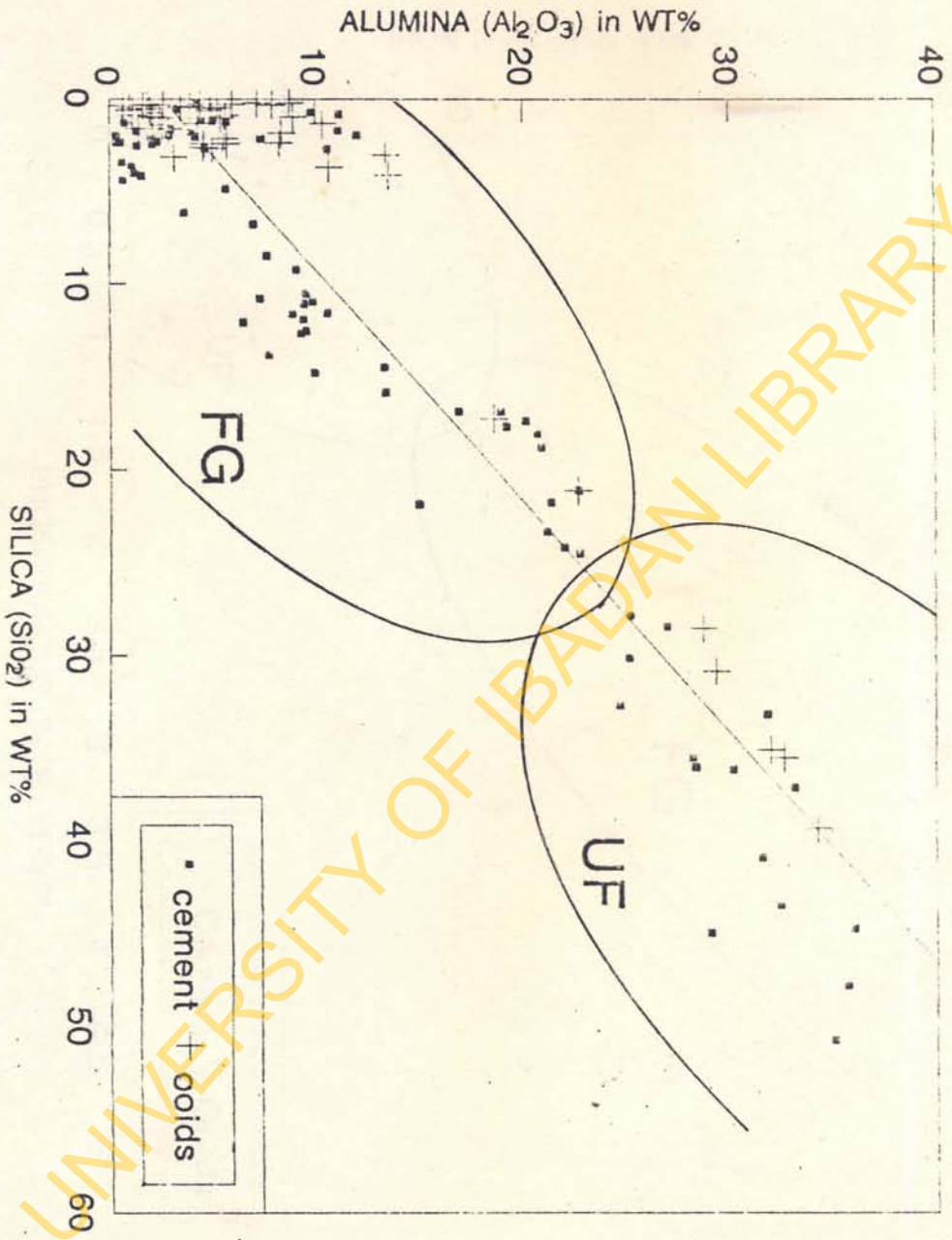
FIG 31: Plot of Al_2O_3 Vs. SiO_2
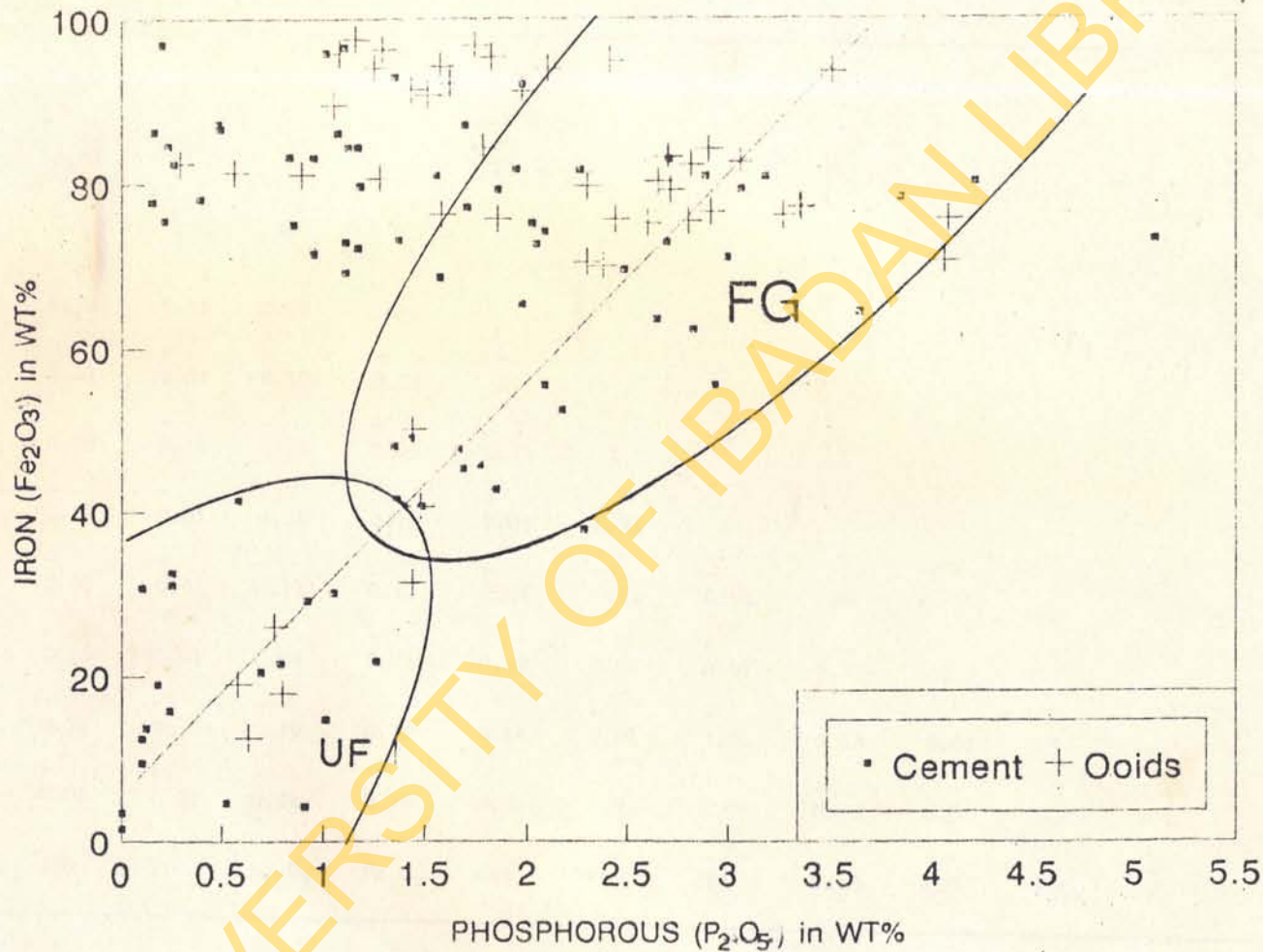
FIG· 32 :   Plot of Fe$_2$O$_3$ Vs. P$_2$O$_5$

Table 15:   CORRELATION COEFFCIENT FOR THE ELEMENTS ANALYSED FOR IN THE

AGBAJA IRONSTONE-FORMATION.

	SiO_2	TiO_2	Al_2O_3	Fe_2O_3	CaO	MgO	MnO	Na_2O	K_2O	P_2O_5	H_2O
SiO_2	1										
TiO_2	0.27	1									
Al_2O_3	0.870	0.20	1								
Fe_2O_3	-0.931	-0.25	-0.97	1							
CaO	0.01	-0.01	-0.101	-0.01	1						
MgO	0.09	-0.12	-0.01	-0.01	0.21	1					
MnO	-0.22	-0.01	-0.26	0.22	-0.01	0.31	1				
Na_2O	-0.16	-0.01	-0.11	0.11	0.01	-0.01	-0.01	1			
K_2O	0.12	0.01	0.04	-0.01	0.17	-0.01	-0.01	0.37	1		
P_2O_5	0.51	0.16	0.36	0.38	0.14	-0.01	-0.01	0.13	0.01	1	
H_2O	-0.01	-0.01	-0.01	0.36	0.01	0.01	0.01	-0.01	0.01	0.65	1
	SiO_2	TiO_2	Al_2O_3	Fe_2O_3	CaO	MgO	MnO	Na_2O	K_2O	P_2O_5	H_2O

125
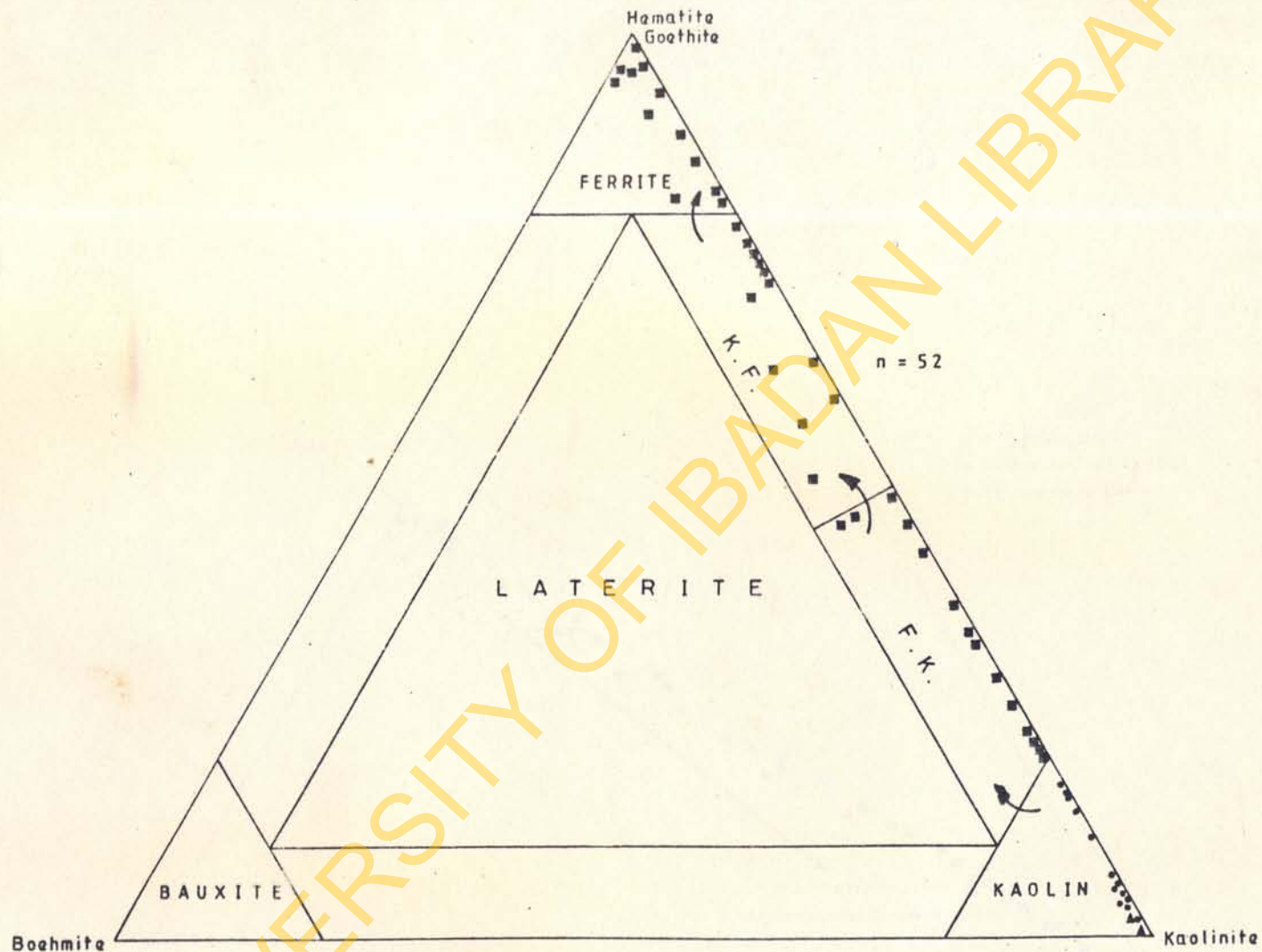
Fig. 33 : Ternary plot indicating the different minerals formed with increase in ferruginization. (▲ - Pure Kaolinite • - Unferruginized matrix ■ - Ferruginized matrix F.K: Ferritic Kaolinite K.F.: Kaolinite Ferrite ━► Ferruginization trend) (after Aleva, 1981)
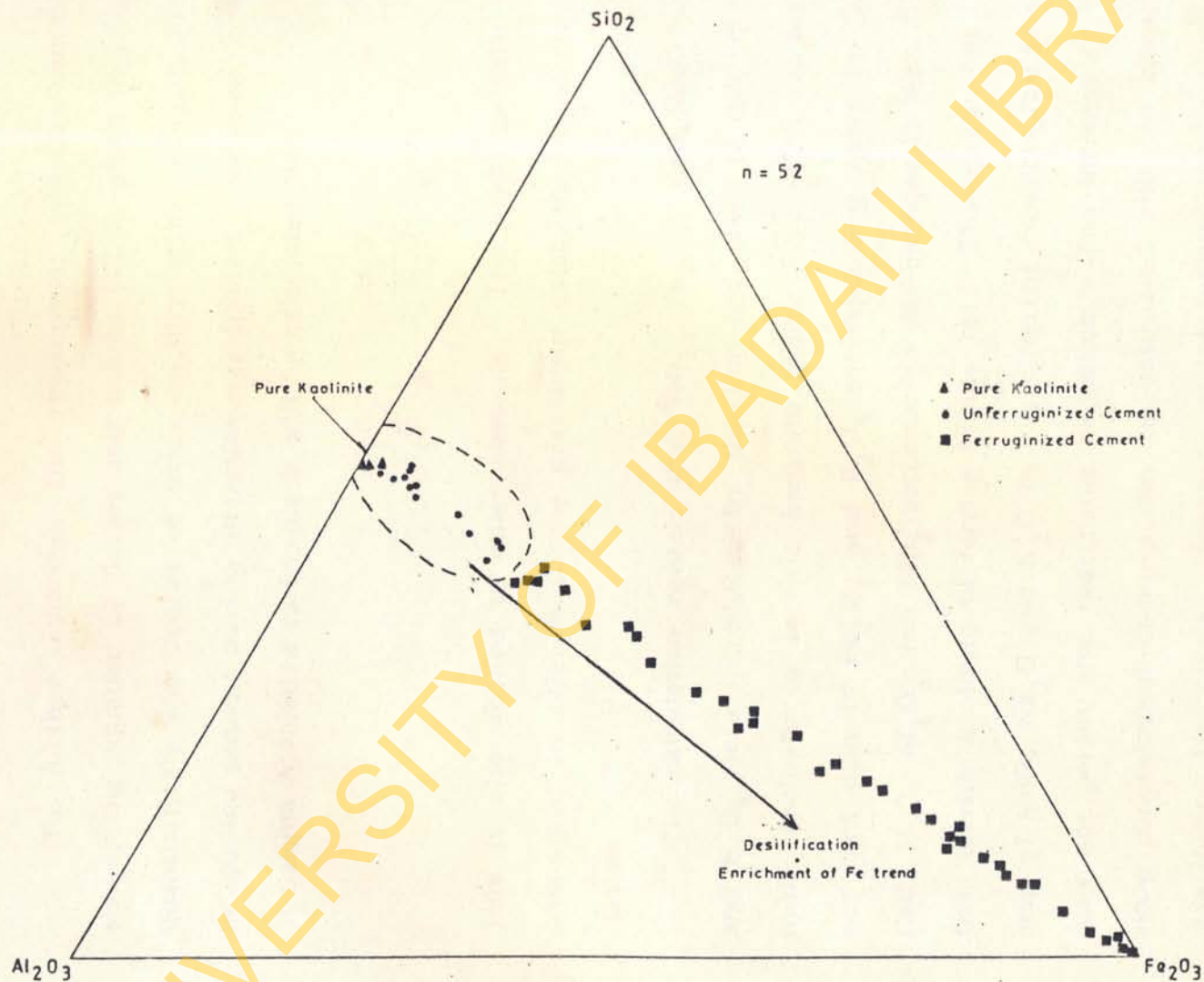
Fig. 34 : Ternary plot indicating the alteration trend from pure kaolinite – kaolinitic relics
(unferruginized cement) to ferruginized cement of Agbaja Ironstone
Note that the diagram is also applicable to ooids and pisoids

To further establish the replacement process mentioned above, the equation of Davies and Luhtas (1978) which highlights quantitatively the degree of oxide mobility with continual change in alumina content during alteration was applied. For example K_2O in Sample A relative to Sample B will be calculated thus:

$$K_2O = \frac{Al_2O_3}{K_2O}\bigg|_A \quad \frac{Al_2O_3}{K_2O}\bigg|_B$$

This is also applied to other elements. The oxide mobility was considered in relation to the previously established mineralogical classes.

The calculation reveals that TiO_2, Fe_2O_3, CaO, MgO, H_2O and P_2O_5 were introduced by the iron-rich fluid to convert the initial kaolinite to ferritic kaolinite (Table 16). With increasing per cent gain in Fe_2O_3 and P_2O_5 corresponding losses in TiO_2, CaO, MgO, Al_2O_3 and SiO_2 accompanied the changes in mineralogy from ferritic kaolinite to ferrite (Table 16). The erratic relationship of MnO, Na_2O and K_2O in the different mineralogical classes does not permit any reasonable deduction. The increase in H_2O along mineralogical changes may be associated with the elemental loss during hydrolysis. However, at the ferrite end, loss in H_2O occurs. This led to dehydration and formation of hematite.

Table 16: Mean Oxide ration and mobile oxide variations in the Mineralogical facies of the Agbaja Ironstone formation.

OXIDE RATIO	KAOLINITE	FERRITIC KAOLINITE		KAOLINITIC FERRITE		FERRITE
Al_2O_3/TiO_2	148.07	$\Delta TiO_2 = 1.78 \rightarrow$	82.98	$\Delta TiO_2 = 8.78 \rightarrow$	9.46	$\Delta TiO_2 = 0.60 \rightarrow$	15.77
Al_2O_3/Fe_2O_3	178.45	$\Delta Fe_2O_3 = 18.17 \rightarrow$	9.82	$\Delta Fe_2O_3 = 163.67 \rightarrow$	0.06	$\Delta Fe_2O_3 = 1.50 \rightarrow$	0.04
Al_2O_3/CaO	255.57	$\Delta CaO = 3.89 \rightarrow$	65.62	$\Delta CaO = 17.41 \rightarrow$	3.77	$\Delta CaO = 0.82 \rightarrow$	4.62
Al_2O_3/MgO	83.13	$\Delta MgO = 8.93 \rightarrow$	9.31	$\Delta MgO = 4.56 \rightarrow$	2.04	$\Delta MgO = 0.30 \leftarrow$	2.56
Al_2O_3/MnO	285.07	$\Delta MnO = 0.00 \leftarrow$	0.00	$\Delta MnO = 0.00 \leftarrow$	1.45	$\Delta MnO = 0.00$	0.00
Al_2O_3/Na_2O	284.96	$\Delta Na_2O = 0.00 \rightarrow$	0.00	$\Delta Na_2O = 0.00$	0.12	$\Delta Na_2O = 0.44 \leftarrow$	0.27
Al_2O_3/K_2O	0.00	$\Delta K_2O = 0.00 \rightarrow$	36.46	$\Delta K_2O = 0.00 \leftarrow$	0.00	$\Delta K_2O = 0.00$	0.00
Al_2O_3/P_2O_5	200.00	$\Delta P_2O_5 = 2.03 \rightarrow$	98.46	$\Delta P_2O_5 = 35.62$	2.75	$\Delta P_2O_5 = 1.19 \rightarrow$	2.31
Al_2O/SiO_2	0.50	$\Delta SiO_2 = 1.00 \leftarrow$	0.50	$\Delta SiO_2 = 0.29 \leftarrow$	1.88	$\Delta SiO_2 = 0.83 \leftarrow$	2.27
Al_2O_3/H_2O	0.49	$\Delta H_2O = 1.07 \rightarrow$	0.46	$\Delta H_2O = 9.20 \rightarrow$	0.05	$\Delta H_2O = 0.09 \leftarrow$	0.56

5.3   Discussion

The chemistry of the minerals of the ironstone reveals that an initial kaolinite is converted by iron-rich fluid to geothite and minor amounts of boehmite, goyazite-crandallite, bolivarite and hematite.   The initial kaolinitic material is however moderately rich in Fe and P when compared with a pure sedimentary kaolinite.   Fe and P may have been adsorbed into the kaolinite structure prior to the formation of the ooids, probably during the weathering of the parent rock.   High concentration of Al with minor enrichment of CaO, SrO, BaO and Fe_2O_3 in the phosphorus minerals also linked their source to the weathering of a parent (basement) rock. The low concentration of CaO, however ruled out a basement source for the phosphorus mineral.   The High Al concentration of the phosphorus minerals may have been absorbed from the kaolinitic matrix during the introduction of the iron-rich fluid. The plot of the minerals formed with increase in ferruginization on the Aleva, 1991 ternary diagram (Fig. 32) indicates that the iron enrichment process is not related to lateritization.

Inter-element correlation reveals that the minerals of the ironstone are formed during weathering and replacement minerals. Al, Si are the most mobile elements of minerals formed by weathering of a parent (basement) rock.   In Agbaja ironstone

these elements form the components of the precursor kaolinitic clay. The second group of elements, Fe and P are components of the iron-rich fluid. While the average values of the third group of elements, Ca, Mg, Mn and K are the same with the crustal average values.

From the elemental gain and loss calculation it is certain that the conversion of kaolinite to ferrite involves desilicification and removal aluminia plus iron enrichment (ferruginization). This process is accompanied by appreciable depletion of aluminium, silicon, calcium, magnesium, titanium, manganese, sodium and potassium, and a significant progressive gain in iron and phosphorus.

Significant depletion in alumina, calcium, potassium and sodium with increasing enrichment and gain in the H_2O content confirms the supergene nature of the replacement process. However, the loss in H_2O in the ferrite is due to dehydration and subsequent formation of hematite.

CHAPTER SIX

GENESIS OF THE AGBAJA IRONSTONE FORMATION

6.1   Previous Genetic Models

Three contrasting models have been put forward to explain the origin of the ironstone deposits of the Nupe Basin. These are the synsedimentary, lateritic and post-diagenetic models.

Authors of the synsedimentary model based their argument on evidences provided by identified ferruginous facies (coarse and fine grained varieties) and depositional patterns (Falconer, 1911; Adeleye, 1973, 1979; Agyingi, 1991). On the basis of these evidences they believed that the deposits are similar to the Minette-type ironstones. The ooids are formed within high energy, shallow marine domains. The basement source for the sedimentary materials of the Nupe Basin and the elemental charac-teristics of the ironstone deposits also support this model (Adeleye, 1973; Oresajo, 1979; Agyingi, 1991). Adeleye, 1973; Oresajo, 1979 and Agyingi, 1991 suggested a precursor, probably iron-rich kaolinitic mudstone as the source material for the Agbaja Ironstone Formation. However, the Minette-type deposits are known for their chamositic precursor.

Du Preez (1956) and Jones (1955, 1958) believed that ironstone may result from formation of concretions in lateritic soils. They also referred to ironstone formed by concretionary action as crusty deposits resulting from decomposition and superficial alteration of basement rocks. Repeated coating of earlier fractured ooids, high Al content in the allochems (Kogbe, 1978) and lack of fossils was used to support the hypothesis. This model however fails to explain the initial formation of the ooids.

Recently a post-diagenetic iron enrichment model was pro-posed for the ironstone deposits (Ladipo et al., 1988, 1993; Mucke 1993; Haase, 1993; Mucke et al., 1994). Evidences for this model were based on their ore microscopic and chemical studies, which reveal the occurrence of initial kaolinite ooids and their ferruginization mechanism. In this study, a genetic model emphasising the mechanisms of ooid formation and subsequent ferruginization of the ironstone is presented.

6.2   Agbaja Ironstone Formation: A Genetic Model

Agbaja Ironstone Formation shows characteristics which are typical of major ironstone deposits of the world, including the classical Minette-type deposits. In general Phanerozoic Ironstones have features in common, which are (1) comparable geologic

setting, (2) deposition in marine environment, (3) intercalation with sandstones, siltstone, mudstone and limestone. Others include (4) similar mineralogy and structure of iron-rich horizons, (5) repetitive horizon of iron mineralization and (6) the occurrence of ooids in iron-rich strata. These features indicate a similar genesis for all ironstone occurrences, although with some local differences and variations.

The present study confirms that the Agbaja Ironstone Formation conforms only with some of these characteristics. Lack of chamosite, presence of pure kaolinite ooids and their whole or partial replacement by geothite are few of the characteristics which distinguish the Agbaja deposit from other deposits of the world. Thus, a genetic model based on a new sedimentological approach, detailed ironstone petrography and geochemistry is being proposed for the Agbaja Ironstone Formation.

6.2.1   Formation and Deposition of the Ooids/Pisoids

Three classes of concentrically laminated or mammillary structures have been recognised in the ironstone lithofacies; these are the ooids, pisoids and peloids.

As discussed earlier, several kaolinitic mudstone beds occur in the Nupe Basin. These beds are believed to have been re-worked from older succession, transported in suspension and

redeposited in a restricted basin. The decrease in feldspar contents of the sandstone as we move up the sequence in the Patti Formation, and the general fining upwards sequence of the sediments of the Nupe Basin support the derivation of the kaolinitic mudstone from the older successions. Subsequent reworking of the kaolinitic beds to form ooids may have occurred due to sea level rising or shallowing of the basin.

Presence of pyrite pseudomorphs in the core or rings of the ooids (Plates 13, 14) and siderite pseudomorphs in the matrix (Plate 15) suggest the formation of both minerals prior to ooid formation. The presence of pyrite suggests that the ooids were formed when the environmental conditions were highly reducing while the matrix materials were introduced during a period of flooding, leading to a decrease in sulphide activity level (non precipitation of pyrite), and subsequent precipitation of siderite. The author is of the opinion that persistent flooding, probably from fluvial input may have prevented the growth of chamosite.

These kaolinitic ooids were ferruginized, fragmented and redeposited as core for the later formed pisoids which are cemented in a fresh detritus-free kaolinite matrix. This suggests a multiphase episode of ooids formation, probably due to intermittent wave action and continual fluvial input at higher

energy conditions. The present study suggests that the bog ore may have been formed due to bacterial action in the swampy environment. Evidences in support of this include the presence of organic matters as framboids (Plate 29). Pseudomorphs of hematite after pyrite (Plate 29), low content of phosphorus and high Fe concentration in the matrix (Tables 11 and 12).

The depositional history of the Nupe Basin therefore offers a model in which the three depositional periods for the ironstone may have occurred due to sea level rise often resulting in flooding and/or intermittent fluvial input. This also led to the development at different stages, of unlithified sediments consisting of (1) ooids, pisoid and peloids, (2) fine-grained kaolinite, and (3) detrital of quartz, heavy minerals and micas.

6.2.2 Ferruginization of the Agbaja Ironstone Formation

Two ferruginization periods are established from the petro-graphic study. The first ferruginization which affected the kaolinitic ooids was short-lived and probably slightly later than the initial lithification of the ooidal sediments. The reddish colour and chemical data suggest that the precursor kaolinitic materials occur as fine-grained kaolinite with adsorbed $Fe(OH)_3$ and/or FeOOH on their surfaces (Fig. 33). The presence of framboids and pseudomorphs of geothite and hematite after pyrite and

siderite are other evidences to support this period of ferruginization. A short-lived subaerial exposure and dehydration during lithification may have resulted in the oxidation of the pyrite and siderite and reconcentration of the adsorbed iron as geothite into pore spaces of the kaolinite. This ferruginization is characterised by iron enrichment along grain boundaries between ooids and cement, (Plate 19). Also common is the ferruginization of the matrix in a patchy isolating manner (Plate 15).

The second ferruginization episode starts with the fragmentation of already ferruginized ooids. These fragmented ooids are redeposited as nuclei in the formation of pisoids in a fresh detrital free kaolinite matrix. As a result of loss of water during diagenesis, desiccation cracks are developed in the pisoids. From petrographic studies it was noticed that these cracks act as path way for the iron-rich fluid during ferruginization of the pisoids and the matrix (in-filling of open-space).

The change of geothite to hematite, noticed in both periods of ferruginization is as a results of subaerial exposure and subsequent dehydration of the ferruginized ironstone. These are periods of non-deposition and exposure of ferruginized ironstone to a hot and humid climate. Generally, low content of MgO and high Al_2O_3 and SiO_2 in the unferruginized ironstone suggests a

kaolinitic precursor for the deposit. As iron is added to the kaolinitic precursor, Al, Si and other elements are removed from the deposit (Table 16). Thus an epigenetic enrichment or ferruginization of the allochem and cement is proposed for the Agbaja Ironstone Formation.

Previous authors on the Phanerozoic Ironstone assumed that the mineralogy and texture of ooids are formed during sedimentation and subsequent diagenesis (Bubenicek, 1971; Siehl and Thein, 1978, 1989; Kimberley, 1979; Nahon et al., 1980; Battacharyya, 1980; Battacharyya and Kakimoto, 1982; Delaloye and Odin, 1988; Chauvel and Guerrak, 1989). They also believed that the precursor mineral for all ironstone deposits is chamosite. For these reasons, complex mechanisms are frequently postulated for ooids generation. However, the present study does not agree with these assumptions.

Sedimentary succession of the Nupe Basin suggests an active uplift of the source area along a fault, initiating sediments deposited in a fining upward alluvial fan setting. Persistent flooding led to reworking, transportation in suspension and redeposition of clay materials within a swampy restricted bay (Fig. 23). A kaolinitic precursor for the deposit is also confirmed from mineralogical and geochemical studies. Thus, it could be inferred

that the prerequisite conditions for the formation of chamosite and/or marine source were disturbed by persistent fluvial input during the formation of the oolites.

Also in their ferruginized state, the ooids are broken as a result dehydration to form nuclei for pisoids. The fragmented ooids are reworked and redeposited in a fresh groundmass. This is in contrast to the assumed primary origin of the ferruginized ooids and pisoids of the Minette-type deposits. Presence of pseudomorphs of pyrite in the nucleus and cortex of ooids and pisoids also indicates a possible accretionary mode of formation of the allochems prior to ferruginization. The detrital nature of the deposit (especially mud-ironstone and unferruginized pack-ironstone) is further evidence of this accretionary process.

Chemical analysis revealed that the deposit is commonly depleted in Al_2O_3 and SiO_2 and enriched in Fe_2O_3 and P_2O_5. This observation does not agree with in situ lateritization mechanism and also imply possible fluid interaction under supergene condition during the ferruginization process. Vitrinite reflectance value of 0.6% Ro for the sediments of Nupe Basin (Braide, 1992c) indicates that the maximum burial temperature is below 70°C (Hood et al., 1975). This deduction confirms that the iron-rich fluids may have been introduced at very low temperature and further

supports the supergene nature of the fluids. However, the high Al content in the phosphorus minerals could be linked to leaching of the precursor kaolinitic clay. A basement source (i.e. apatite source) is ruled out in view of the low percentage of Ca in the identified phosphate minerals. However, the P present in the ironstone are probably sourced from the abundant organic matter present in the swampy environment.

Ferruginization usually resulted in a marked enrichment in iron, leading to concentration ranging from 60-90% Fe_2O_3 of the original sediment. In the first ferruginization period iron is supply as a result of oxidation of the initial fresh pyrite/siderite and reconcentration of adsorbed FeOOH of the kaolinitic clay. The source of Fe for the second ferruginization period is linked to the presence and abundance of framboids (bacteria) in the overlying bog ore. These bacterias are oxidised to form iron hydroxide of the bog ore. This iron hydroxide and the phosphorus, both found in the swampy environment combine under oxic condition to form a phosphate complex in the bog ore (Berner, 1981; Coleman, 1985; Spear, 1989). The positive correlation of Fe and P confirms a common source for both elements. Consequently under the influence of meteoric water, Fe and P of the bog ore are remobilised and deposited in the cracks and cavities (as goethite, goyazite-crandallite and bolivarite) in the pack-ironstone.

CHAPTER SEVEN

SUMMARY AND CONCLUSION

The Agbaja Ironstone Formation in the Lokoja district, Central Nigeria occurs within the Upper Cretaceous sedimentary sequence of the Nupe Basin. The Nupe Basin, also referred to as the Middle Niger Basin or the Bida Basin, is a NW-SE trending intracratonic basin adjacent to the main axis of the Benue Trough. On the basis of structural analysis the lineaments present in the basin are subdivided into three major sets oriented in a N50-60°E, N130 – 140°E and N5-15°E directions. A NW-SE fracture trend constitutes the conjugate trend to the NE-SW trend. The former trend is found to be younger, being perpendicular and often truncate the NE-SW fracture system.

From structural analysis, it is proposed that a reactivation of the NW-SE basement fractures during Santonian resulted in block faulting and formation of series of horst and graben structures beneath the present Nupe Basin. Subsequently, these horsts and grabens were filled up with Campanian-Maestrichtian sediments.

Apart from the underlying basement rocks, three lithostratigraphic units were delineated, they are the Lokoja Sandstone,

Patti Formation and the Agbaja Ironstone Formation. The Lokoja Sandstone rests unconformably on the basement complex in the Lokoja district and its overall thickness is estimated at about 30m. This formation is made up of conglomerates often overlain by sandstone units. The conglomerates occur as loosely stratified bodies, consisting of well rounded quartz, feldspar and metamorphic/igneous rock pebbles or cobbles in a whitish kaolinitic to micaceous matrix. Pebbles in the conglomerates are oriented in the north-east trend, implying a northeastern current flow direction for the sediment prior to deposition.

The Lokoja Sandstone is massive, medium to coarse grained and exhibit small-scale cross-stratification. Thickness of the Lokoja Sandstone ranges from 15 to 30m, while that of the cross-sets ranges from 2 to 30cm. Fining upward cyclotherms are exhibited by the Lokoja Sandstone with a cross-stratification azimuths showing a northeast-directed paleocurrent. Petrographic analyses of the sandstone revealed a rock with 60 to 80% monocrystalline angular to subangular quartz, 1 to 7% feldspar (mostly microcline) and less than 1% rock fragments, in a kaolinitic matrix of about 15%. Thus, this sandstone is classified as arkosic sandstone.

Patti Formation which rests conformably on the Lokoja Sand-
stone is made up of intercalations of sandstone, siltstone and
carbonaceous mudstone units. The maximum thickness estimated
for this formation if about 100m. Three sandstone facies were
recognised based on their level in the stratigraphic column of the
Patti Formation. The lower unit is massive medium to coarse
grained with whitish clay matrix overlying the intraformational
conglomerate. Middle sandstone facies, randomly found overlying
or underlying the mudstone, displays both planar and trough
cross-stratification. The sandstone is poorly sorted, medium to
coarse grained with a northeast paleocurrent direction for the
sediments. Fine to medium grained, well sorted, massive
ferruginous sandstones constitutes the upper unit. The three
sandstone facies are dominantly made up of quartz which averages
about 86% by volume and is set in a kaolinitic matrix of about 13%.
However, for the ferruginous sandstone, the kaolinitic matrix is
being replaced by goethite and hematite. These sandstone facies
are classified as quartz arenite from the petrographic studies.

Siltstone of the Patti Formation is found intercalated within
the sandstone facies. They show parallel laminations with sandy
base and clay-silt tops. Constituent minerals are clay, quartz
and feldspars, with the grains constituting about 95% in a whitish

kaolinitic matrix. Mudstones are well laminated whitish to yellowish coloured rocks intercalated with sandstones and siltstones. Towards the northern edge of the study area, the mudstone is seen to be shaly, black and highly carbonaceous. Another distinct feature of the mudstone is the presence of plant debris, pyrite and wood fragments embedded within the mudstone beds.

Field evidence and borehole logs have shown that the Patti Formation is overlain by the Agbaja Ironstone Formation. It was further revealed from the studies that the ironstone is generally coarsening upward with the ore thickness decreasing from the west to the east in the Agbaja area and the reverse for the Kotonkarifi area. Furthermore three lithofacies of the iron-stone formation are recognised. They are the oolites, pisolites and the bog ore. The oolites are friable, poorly sorted, loosely packed rocks which constitute the basal part of the ironstone formation. The pisolites, which are non-friable, well sorted, closely packed rocks, overly the oolites. Cavities within the pisoids are filled with whitish powdery materials found to be goyazite-crandallite. The bog ore is yellowish brown concretionary materials dominantly made up of rubbles and brecciated oolites.

Particle size distribution for the clastic sediments of both Lokoja and Patti Formation is unmodal. Sorting for both formations

is poor to moderate with the Lokoja sandstone being often poor. This lateral variation in the degree of sorting indicates that the Lokoja Sandstone is nearer to the source. Other textural studies show a very finely to very coarsely skewed mesokurtic sand for Lokoja Sandstone and leptokurtic for Patti Formation. These characteristics confirm a fluviatile regime for the sediments deposited under low energy conditions and short transportation.

Heavy minerals commonly found in the clastic sediments of both formations, in order of decreasing abundance, are ilmenite, zircon, tourmaline, staurolite, rutile, garnet and hornblende. The angular nature of these minerals show the textural immaturity of the sandstones of both formations. ZTR index which ranges from 61 to 89% for the Lokoja Sandstone and 83 to 95% for the Patti Formation indicates, the abundance of ultrastable heavy minerals over the metastable ones in the Lokoka district. Higher ZTR index value for Patti Formation clastic sediments indicates their relative higher mineralogical maturity than the Lokoja Sandstone. However, the heavy mineral assemblages show a basement source for both formations, but with more contribution from igneous minerals.

Depositional characteristics of the Lokoja district resemble those of modern fluvial deposits which evolved into two distinct

facies; alluvial fans and flood basin. Furthermore, sedimentological characteristics such as the lithofacies present and the regional fining upward cyclotherm also support an active uplift of the source area and development of an asymmetrically subsided basin.

On the basis of petrographic studies as revealed by thin and polished sections as well as X-ray diffraction analyses, the ironstone formation is divided into pack-ironstones and mud-ironstones. Using both the allochem types and textural characteristics, four petrographic varieties were identified: ooidal pack-ironstone, pisoidal pack-ironstone, detrital mud-ironstone and breccia mud-ironstone. The pack-ironstone corresponds to the oolite and pisolite beds while the mud-ironstone corresponds to the bog ore.

Spherical, oblong and fragmented ooids of the pack-ironstone have complex mineralogy described by their cortex and nuclei. Minerals of the ooids are kaolinite, goethite and hematite, cemented by kaolinite and goethite. Core of the ooids is also made up of pseudomorphs of goethite after pyrite of pseudomorphs of hematite after pyrite. Pisoids of the pisoidal pack-ironstone are elliptical, oval, and subspherical in shape and are composite in nature. Pisoids are dominantly goethite cemented in kaolinitic to goethitic

matrix. Clasts of the detrital mud-ironstone are quartz and heavy minerals in a kaolinitic matrix while the major constituents of the breccia are kaolinite and quartz.

Initial mineral of the ooids and the matrix in all the petrographic varieties is kaolinite with detritals of quartz, mica and few heavy minerals. However, secondary enrichment of both the ooids and matrix resulted in the formation of minerals such as goethite, hematite, goyazite-crandallite, bolivarite and boehmite. Advancing replacement and in-filling of open-space are common iron enrichment mechanisms in the ironstone. Irregular cavities within the matrix exhibit colloidal texture while those created in the ooids are sometimes filled with a milky white phosphorous mineral goyazite - crandallite. However, bolivarite occurs as disseminations within the goethitic matrix and veins of pack-ironstone and detrital mud-ironstone. From the petrographic studies two stages of iron enrichment are recognised. The first enrichment affected the kaolinite ooids of ooidal pack-ironstone while the second iron enrichment initiated through the bog ore affected the pisoidal pack-ironstone and the detrital mud-ironstone.

SiO_2, Al_2O_3 and Fe_2O_3 account for between 81 and 90% of the ironstone, SiO_2 ranges from 23.71 to 56.41% and Al_2O_3 between 22.01 and 36.54% in all the unferruginized components of the

ironstones. But both components can be as low as 0.22% in the ferruginized equivalent. SiO_2 and Al_2O_3 contents are highest in the mud-ironstone varieties but lowest in the pack-ironstone varieties. Fe_2O_3 content increases from about 1.59% in the un-ferruginized to about 97.54% in the ferruginized equivalents. Supergene Fe_2O_3 increases up the ironstone sequence with the highest concentration in the pisoidal pack-ironstone. P_2O_5 values range between 0% in the unferruginized and 5.10% in the ferruginized components. P_2O_5 is highest in the pisoidal pack-ironstone and generally increases with increase in Fe_2O_3. However, MnO, CaO, MgO, Na_2O and K_2O are generally less than 1.0% in all the petrographic varieties.

On the basis of mineral chemistry of the ironstone the secondary minerals of the ooids, pisoids and cements is classified into ferritic kaolinite, kaolinitic ferrite and ferrite. Investigation of the oxide mobility in the decomposed kaolinite suggests that the iron enrichment is accompanied by a parallel depletion in SiO_2 and Al_2O_3, moderate to extreme reduction in CaO, MgO, MnO, Na_2O and K_2O and a significant gain in P_2O_5. The significant depletion of all these elements with increasing iron enrichment and gain in the H_2O content confirms the supergene nature of the replacement process. The replacement processes can best be

described as desilicification plus iron-enrichment process (ferruginization).

Sedimentological, mineralogical and geochemical studies provided evidences to support a kaolinitic precursor for the Agbaja ironstone deposit, contrary to the general believe of a chamositic precursor as observed for other ironstone deposits. Also the presence of pseudomorphs of pyrite in the nuclei and cortex of ooids is a reliable indicator of a possible accretionary mode of formation of the ooids and pisoids prior to ferruginization. Two ferruginization periods unrelated to lateritization are established based on common depletion of Al_2O_3 and SiO_2 with increase in Fe_2O_3 in the ironstone. In the first ferruginization period iron is supply as a result of oxidation of the initial fresh pyrite/siderite and reconcentration of adsorbed FeOOH of the kaolinite. Second ferruginization period is linked to the presence of framboids (bacteria) which is oxidised iron phosphate complex in the bog ore. The Fe and P are mobilised and reconcentrated as goethite, goyazite-crandallite and bolivarite under the influence of a meteoric water.

Recommendations

(i) Data are needed on the trace and rare earth elements of the ironstone. This data will highlight more on the chemistry and identify other deleterious elements present in the ironstone.

(ii) Organic geochemistry studies of the ironstone need to be examined, so that a possible marine influence on the deposit can be deciphered.

REFERENCES

Abimbola, A.F., 1987: Genesis of the fluorite and associated sulphide mineralization At Arufu and Akwana, Middle Benue, Nigeria: a geologic, fluid inclusion and stable isotope study: M.Sc. thesis, Univ. Ilorin, 110pp.

Adeleye, D.R., 1971: Stratigraphy and Sedimentation of the Upper Cretaceous strata around Bida, Nigeria: Ph.D. Thesis, Univ. of Ibadan, 297pp.

Adeleye, D.R., 1973: Origin of ironstones, an example from the Middle Niger Valley, Nigeria: Jour. Sed Petrol., 43: 709-727.

Adeleye, D.R., 1974: Sedimentology of the fluvial Bida Sandstone: Jour. Sed. Geology, 12: 1-24.

Adeleye, D.R., 1975a: Nigeria Late Cretaceous stratigraphy and Paleogeography: Bull. Am. Assoc. Petrol. Geol., 39: 2302-2313.

Adeleye, D.R., 1975b: Derivation of fragmentary oolites and pisolites from desiccation cracks: Jour. Sed. Petrol., 45: 794-798.

Adeleye, D.R., 1976: The Geology of the Middle Niger Basin: In: Geology of Nigeria, (Ed) C.A. Kogbe, Elizabe. Publ. Co., 283-287.

Adeleye, D.R., 1979: A review of Maestrichtian paleogeography of the southern lullemmeden and Nupe Basins: Jour. Min. Geol. 16: 119-123.

Adeleye, D.R. and Badejoko, T.A., 1975: Preliminary report on the Geology of Agbaja Ironstone, Agbaja Plateau, Nigeria: Jour. Sci., 9: 3-31.

Adeleye, D.R. and Dessauvagie, T.F.J., 1972: Stratigraphy of Niger embayment near Bida, Nigera; In: Africa Geology (ed) Dessauvagie and Whiteman, U.I. Press: 181-186.

Adeleye, D.R. and Halstead, L.B., 1972: Cretaceous sediments from the shore of Lake Kainji, Nigeria: Journ. Mining and Geology, 7: 3-12.

Adeniyi, J.O., 1985: Ground total magnetic intensity in part of Nupe Basin and the adjacent Basement Complex, Niger State, Nigera: Nigerian Jour. Applied Sci., 3: 67-68.

Adeniyi, J.O., 1986: Polynomial regional surfaces and two-dimensional models in part of Nupe Basin and the adjacent Basement Complex, Niger State, Nigeria: Nigeria Jour. Applied Sci., 4: 25-34.

Agyingi, C.M., 1991: Geology of Upper Cretaceous rocks in the eastern Bida Basin, Central Nigeria, Ph.D. thesis, Univ. Ibadan.

Ajakaiye, D.E., Hall, D.H., Millar, T.W., Verhaijen, P.J.T., Awad, M.B. and Ojo, S.B., 1986: Aeromagnetic anomalies and tectonic trends in and around the Benue Trough, Nigeria: Nature, Vol. 319, ng. 6054, pp. 582-584.

Aleva, G.J., 1981: Bauxitic and other duricrusts on the Guiana Shield, South America:. In: Lateritization Processes, Proc. Intern. Sim. Laterite Processes, Trivandrum, (ed) Krishnaswany, Y.S., Rotherdam: 261-268.

Allen, J.R.L., 1970: Studies in fluviatile sedimentation: a comparison of fining-upward cyclothems with special reference to coarse member composition and interpretation. Jour. Sed. Petrol., 40: 298-323.

Astier, J.E. Donseau, M. and Nwadiale, G.G.O.O., 1989: The Lokoja oolitic ironstone deposit: possible use in the Ajaokuta iron and steel plant: Jour. Min. Geol., 25: 111-120.

Benkhelil, J., 1982: Benue Trough and Benue Chain: Geological Magazine 119: 155-168.

Benkhelil, J., 1986: Structural frame and deformations in the Benue Trough: In: Symposium on Anambra - Benue Basin, ELF Nigeria Ltd., Abstr. Vol.

Benkhelil, J., 1987: Cretaceous deformation, magmatism and metamorphism in the Lower Benue Trough, Nigeria: Geol. Journ. 22: 467-493.

Benkhelil, J., 1989: The origin and evolution of the Cretaceous Benue Trough, Nigeria: Journ. Afric. Earth Sci., 8: 251-282.

Berner, R.A., 1981: A new geochemical classification of sedimentary environments: J. Sed. Petrol., 51: 359-365.

Berry, 1974: Selected powder diffraction data for minerals; Data Book: 833p.

Bhattacharyya, D.P., 1980: Sedimentology of late Cretaceous Nubia Formation at Aswan, South East Egypt, and their origin of the associated ironstone: Ph.D. thesis, Princeton University, Princeton, NJ, 122p.

Bhattacharyya, D.P. and Kakimoto, P., 1982: Origin of ferri-ferrous ooids: An SEM study of ironstone ooids and bauxite pisoids: Jour. Sed. Petrol., 52: 849-857.

Boyle, E.A., Edmond, J.M. and Sholkovitz, E.R., 1977: The mechanism of iron removal in estuaries: Geochem, Cosmochim, Acta, 41: 1313-1324.

Braide, S.P., 1990: Sedimentation and tectonics in the southern Bida Basin, Nigeria: depositional response to varying tectonic context: Amer. Assoc. Petrol. Geol. Bull. 74: 618.

Braide, S.P., 1992a: Geological development, origin and energy mineral resources potential of the Lokoja Formation in the southern Bida Basin: Jour. Mining Geol., 28:33-43.

Braide, S.P., 1992b: Syntectonic fluvial sedimentation in the central Bida Basin: Jour. Min. Geol., 28: 55-65.

Braide, S.P., 1992c: Alluvial fan depositional model in the northern Bida Basin: Jour. Min. Geol., 28: 65-74.

BRGM, 1992: Survey, research and tests of the Agbaja-Lokoja Kotonkarifi Bassa - Nge iron ore deposits: an interim report. Fed. Govern. Nigeria, Executive Office of the President, Steel Development Department, 31p.

Brigatti, M.F., 1988: Chemistry and structural order in hydro-thermal and sedimentary Sardina Kaolinites: N. Jb. Mines, Mh., H1: 21-37.

Bubenicek, L. 1971: Geologie du gisement de fer de Lorraine: Nat. Petroles d'Aguitame Bull., 5: 223-320.

Carroll, D., 1958: Role of clay minerals in the transportation of iron; Geochim. Cosmochim. Acta, 14: 1-27.

Chauvel, J.J. and Guerrak, S., 1989: Oolitization processes in Palaeozoic ironstones of France, Algeria and Libya: In: Phanerozoic Ironstones, (ed) Young, T.P. & Taylor, W.E.G., Geol. Soc. Publ. No. 46: 165-173.

Chen, P., 1977: Table of key lines in X-ray powder diffraction patterns of minerals in clays and associated rocks: U.S. Geol. Surv. Occasional Paper 31: 67p.

Coleman, J.M., 1966: Ecological changes in a fresh water clay sequence: Trans. Gulf. Coast. Assoc. Geol. Soc., 159-174.

Coleman, M.L., 1985: Geochemistry of diagenetic non-silicate mineral: Kinentic consideration: Philo. Trans. Royal Soc. London, A315: 39-56.

Davies, J.F. and Luhita, L.E., 1978: An Archean porphyry-type disseminated copper deposit, Timmins, Ontario: Eco. Geol., 73: 383-396.

Delaoye, M.F. and Odin, G.S., 1988: Chamosite, the green marine clay from Chamasion. A study of Swiss oolitic ironstone: In: Green marine clays, Development in Sediment. ed. G.S. Odin, 45: 7-28.

Dimroth, E., 1975: Paleoenvironment of iron-rich sedimentary rocks: Geol. Rundsch., 64: 761-767.

Dimroth, E. and Chauvel, J.J., 1973: Petrography of the Sokoman iron formation in part of the central Labrador Trough, Quebec Canada: Geol. Soc. Amer. Bull. 84: 111-134.

Dunham, R.J., 1962: Classification of carbonate rocks according to depositional texture: In: Classification of carbonate rocks, Men. Amer. Ass. Petrol. Geol. 1 (ed) Ham, W.E., 108-121.

Du Preez, J.W., 1956: Origin, classification and distribution of Nigerian laterites: Proc. African Confr. Ibadan (3rd): 223-234.

Dustan, W.R., 1911: Reports on the results of the mineral survey of Northern Nigeria, 1907-1908 and 1908-1909: Colon. Rep. Misc. Ser., No. 79.

Edah, I.M., 1990: Agbaja iron ore deposit and the future of the Nigerian steel industry: In: National Seminar on Agbaja Lokoja iron ore deposit, RMRDC, Lagos.

Falconer, J.D., 1911: The geology and geography of Northern Nigeria: MacMillan London, 268p.

Gross, G.A., 1965: Geology of iron deposits in Canada Vol. 1 General geology and evaluation of ore deposits: Canada Geol. Survey, Econ. Geol. Rept. 22, 181p.

Guilbert, J.M. and Park, C.F. Jr., 1986: The geology of ore deposits. Freeman, San Francisco, Calif., 985p.

Haase, J., 1993: Vergleichende untersuchungen von eisenreichen oolithischen Kaolinit and Bauxitvorkomman mit oolithi-sche untersuchung: Doktorgrades, Georg-Angust Universitat Gottingen, 169p.

Hall, W.D.M. and Goode, A.D.T., 1978: The Early Proterozoic Nabberu Basin and associated iron formations of Western Australia: Precam. Res., 7: 129-184.

Hallam, A., 1975: Jurassic Environments: Cambridge Univ. Press, Cambridge, 269p.

Hallam, A. and Braashaw, M.J., 1979: Bituminous shales and oolitic ironstones as indicators of transgressions and regressions: Jour. Geol. Soc. London, 136: 157-164.

Harder, H., 1989: Mineral genesis in ironstone; a model based upon laboratory experiments and petrographic observa-tions: In: Phanerozoic Ironstones, Geol. Soc. London, Spec. Publ. (ed.) Young, T.P. and Taylor, W.E.G., 46: 9-18.

Haszeldine, R.S., 1983: Descending tabular crossbed sets and bounding surfaces from a fluvial channel in the Upper Carboniferous coalfield of northeast England. Special Publ. 6, Intern. Assoc. Sedi., 6: 449-456.

Holmes, A., 1975: Principles of Physical Geology. Thomas Nelson and Sons Ltd.

Hood, A., Gutjahr, C.C.M. and Heacock, R.L. 1975: Organic meta-morphism and the generation of petroleum: Amer. Assoc. Petrol. Geol. Bull. 59: 986-996.

Idowu, J.O. and Enu, E.I., 1992: Petroleum geochemistry of some Late Cretaceous shales from the Lokoja Sandstone of Middle Niger Basin, Nigeria: Jour. Afric. Earth Sci., 14: 443-455.

Iloeje, N.P., 1972: A new geography of West Africa: Longman Group Ltd., London, 170p.

James, H.E. and Van Houten, F.B., 1979: Miocene goethitic and chamositic oolites, northeastern Colombia: Sedimentology, 26: 125-133.

James, H.L., 1966: Chemistry of the iron-rich sedimentary rocks: In: Data of Geochemistry, Chapter W (ed) Fleischer, M., 61p.

Jan du Chen, Adegoke, O.S. and Adediran, S.A., 1978: Palynology and Foraminifera of the Lokoja Sandstone (Maestrichtian), Bida Basin, Nigeria: Revista Espanola De Micropaleontologia x (3): 379–393.

Jones, H.A., 1955: The occurrence of oolitic ironstones in Nigeria: Their origin, geological history and petrology: Ph.D. thesis, Oxford Univ., 232p.

Jones, H.A., 1958: The oolitic ironstones of Agbaja Plateau, Kabba Province: Records of the Geol. Survey, Nigeria, 20–43.

Jones, H.A., 1965: Ferruginous oolites and pisolites. Jour. Sed. Pet., 35: 838–845.

Kearsley, A.T., 1989: Iron-rich ooids, their mineralogy and micro-fabric: clues to their origin and evolution: In: Phanerozoic Ironstones, (ed) Young, T.P. & Taylor, W.E.G. Geol. Soc. Special Publ. No. 46: 141–164.

Kennedy, W.Q., 1965: The influence of basement structure in the evolution of the coastal (Mesozoic and Tertiary) basins: In: Salt basins around Africa, Proc. Inst. Petrol. Geol. Soc., London, Elsevier.

Kimberley, M.M., 1978: Paleoenvironmental classification of iron formations: Eco. Geol., 73: 215-229.

Kimberley, M.M. 1979: Origin of oolitic iron minerals. J. Sed. Petr., 49: 111-132.

Kimberley, M.M., 1980: The Paz de Rio oolitic inland-sea iron formation: Eco. Geol., 75: 97-106.

Kimberley, M.M., 1989: Nomenclature for iron formations: Exhalative origins of Iron Formations: Ore Geology Reviews, V. 5, p. 1-145.

Kings, 1950: Outline and distribution of Gondwanaland: Geol. Mag., 87: 353-359.

Knox, R.W., 1970: Chamosite ooliths from the Winter Gill ironstone of Yorkshire, England: Jour. Sedi. Petrol., 40: 1216-1225.

Kogbe, C.A., 1976: Palaeogeographic history of Nigeria from Albian times: In: Geology of Nigeria (ed) Kogbe, C.A., Univ. of Ife, 237-252.

Kogbe, C.A. 1978: Origin and composition of the ferruginous oolites and laterites of NW Nigeria: Geol. Rundsh, Band 67, Hert 2, pp. 662-674.

Kogbe, C.A., Ajakaiye, D.E. and Mathasis, G., 1981: Confirmation of a rift structure along the mid-Niger Valley, Nigeria. Jour. Afric. Earth Sci., 1: 127-131.

Ladipo, K.O., 1986: Tidal shelf depositional model for the Ajali Sandstones, Anambra Basin, S.E. Nigeria: Jour. Afric. Earth Sci., 5: 175-185.

Ladipo, K.O., 1988a: Paleogeography, sedimentation and tectonics of the Upper Cretaceous Anambra Basin, S.E. Nigeria: Jour. Afri. Earth Sci., 7: 815-821.

Ladipo, K.O., 1988b: Example of tidal current periodicities from an Upper Cretaceous sandstone succession (Anambra Basin): In: Tide-influenced sedimentary environments and facies (ed) P.L. de Boer et.al.: 333-340.

Ladipo, K.O., Akande, S.O. and Mucke, A., 1988: Depositional environments, ore microscopy and origin of the Agbaja oolitic ironstone: Abstr. Vol. NMGS, p.15.

Ladipo, K.O., Akande, S.O. and Mucke, A. (in Press): Genesis of oolitic ironstone from the middle Niger sedimentary basin: evidence from sedimentological, ore microscopic and geochemical studies: Jour. Min. Geol. (1993).

Madon, M.B., 1992: Depositional setting and origin of Berthierine oolitic ironstones in the Lower Miocene Terengganu Shale, Tenggol Arch. Offshole Peninsular, Malaysia: Journ. Sedi. Petrol., 62: 899-916.

Maynard, J.B., 1983: Geochemistry of Sedimentary Ore deposits: Springer, N.Y., 305p.

McPherson, J.G., Shanmugam, G. and Moiola, R.J., 1987: Fan-deltas and braid deltas: Varieties of coarse-grained deltas: Geol. Soc. Amer. Bull., 99: 331-340.

Mitchell, A.H.G. and Reading, H.G., 1978: Sedimentation and tectonics: In: Sedimentary Environments and Facies, (ed) Reading, H.G., Blackwell Sci.Publ.,Oxford, 439-476.

Mucke, A., 1993: Post-diagenetic ferruginization of sedimentary rocks (Sandstone, Oolitic Ironstone, Kaolins and Bauxites) including a comparative study of the reddening of Red Beds: In: Development of Sed., Diagenesis, 4.

Mucke, A. and Neumann, U., 1986: The genesis of the banded iron ore deposits of Itakpe area, Kwara State, Nigeria. Fortschr. Mine. 64: 187-204.

Mucke, A., Ogunbajo, M.I. and Shekwolo, 1994: The Phanerozoic Ironstones of the Bida Basin, Nigeria: Their mineralogy and genesis, Abst. Vol. NMGS.

Murat, R.C., 1972: Stratigraphy and palaeogeography of Cretaceous and Lower Tertiary in Southern Nigeria: In: African Geology, (ed) Whiteman and Dessauvagie, U.I. Press, 251-266.

Nahon, D., Carozzi, A.V. and Parron, C., 1980: Lateritic weather-
ing as a mechanism for the generation of ferruginous
ooids: Jour. Sed. Petr. 50: 1287-1298.

Oboli, H.O.N. and Harrison, R.J., 1957: A new outline geography
of West Africa: Paul Harrap Books, London.

Oguntoyinbo, J.S., 1978: Reflection coefficient of natural vegeta-
tion crops and urban surfaces in Nigeria: Quart. Jour.
Royal Met. Soc., 96: 430-441.

Ojo, S.B., 1984: Middle Niger Basin revisited, magnetic
constraints on gravity interpretation. Abstr. Vol. 20th
NMGS, 52-53.

Ojo, S.B. and Ajakaiye, D.E. 1976: Preliminary interpretation of
gravity measurement in the Middle Niger Basin Area,
Nigeria: In: Geology of Nigeria (ed) Kogbe, C.A.
Elizab. Publ. Co. Nigeria, 295-306.

Olade, M.A., 1978: General Features of a Precambrian Iron Ore
Deposit and its Environment at Itakpe Ridge, Okene,
Nigeria, T.I.M.M., 87: 881-889.

Olade, M.A. and Adekoya, J.A., 1988: Iron deposits of Nigeria:
In: Groundwater and Mineral Resources of Nigeria, (ed)
Ofoegbu, C.O., Vieweg & Sohn Publ., 101-114.

Oresajo, M.O., 1979: Petrology and Geochemistry of Bassa-Nge
Ironstone: M.Phil. thesis, Univ. of Ibadan.

Petters, S.W., 1978: Mid-Cretaceous palaeoenvironments and bio-stratigraphy of the Benue Trough, Nigeria: Geol. Soc. Amer. Bull., 89: 151-154.

Petters, S.W., 1980: Biostratigraphy of Upper Cretaceous foramini-fera of the Benue Trough, Nigeria.

Ratchiffe, N.M. and Burton, W.C., 1985: Fault reactivation models for origin of the Newark basin and studies related to eastern U.S. seismicity: Proc. U.S. Geol. Sur. Workshop on Early Mesozoic Basins, Eastern U.S.: U.S. Geol. Surv. 946: 36-45.

Ramsay, J.G. 1980: Shear zone geometry: a review. Journal of Structural Geology, vol. 2, pp. 83-99.

Siehl, A. and Thein, J., 1978: Geochemische trends in der Minette (Jurrassic, Luxemberg/Lothringen): Geol. Rundsch., 67: 1052-1077.

Siehl, A. and Thein, J., 1989: Minette-type ironstone: In: Phanerozoic Ironstones, (ed) Young, T.P. & Taylor, W.E.G. Geolog. Soc., Publ., No. 46: 175-193.

Skinner, B.J., 1969: Earth Resources: Prentice-Hall, Englewood Cliffs, N.J., 150p.

Spears, D.A., 1989: Aspects of iron incorporation into sediments with special reference to the Yorkshire Ironstones: In: Phanerozoic Ironstones, Geol. Soc. London Spec. Publ. ed. Young T.P. and Taylor, W.E.G., 46: 19-32.

Steel, R., Siedlecka, A. and Roberts, D., 1985: The Old Red Sandstone basins of Norway and their deformation: a review: In: Gee, D.G. and Sturt, B.A., John Wiley & Sons, 293-315.

Sturesson, U., 1992: Volcanic ash: The source material for Ordovician Chamosite ooids in Sweden: Jour. Sed. Petro. 62: 1084-1094.

Tattam, C.M., 1943: A review of Nigeria stratigraphy: Rept. Geol. Surv. Nigeria.

Taylor, J.H., 1949: Petrology of the Northampton Sand Ironstone Formation: G.B. Geol. Surv. Mem., 111p.

Trendall, A.F., 1983: Introduction: In: Iron-Formation: Facts and Problems, (eds) Trendall, A.F. and Morris, R.C., Elsevier, Amsterdam, 1-12.

Uwadiale, G.G.O.O., 1991: Electrolytic coagulation and selective flocculation of Agbaja iron ore: Jour. Mining Geol., 27: 77-86.

Uwadiale, G.G.O.O., 1992: Particle size and coal/ore ratio in mag-
netizing reduction of Agbaja iron ore: Abst. Vol. 28th
NMGS, p.90.

Uwadiale, G.G.O.O. and Hull, A.J., 1985: Mineralogy of ironstone
from Agbaja deposit, Nigeria, in relation to beneficia-
tion: I.M.M.: 8161-8165.

Van Houten, F.B., 1985: Oolitic ironstones and contrasting
Ordovician and Jurassic paleogeography: Geology, 13:
722-724.

Van Houten, F.B., 1986: Search for Milankovitch patterns among
oolitic ironstones: Paleoocean., 1: 459-466.

Van Houten, F.B. and Hong-Fei, H., 1990: Stratigraphic and palaeo-
geographic distribution of Palaeozoic oolitic ironstones:
Palaeozoic Palaegeo: Biogeo., (ed) Mckerrow, W.S. and
Scotese, C.R., Geolo. Soc. Mem, No. 12: 87-93.

Whiteman, A., 1982: Nigeria: Its Petroleum Geology Resources and
Potential, Vols. 1 and 2: Graham and Irotman, London,
394p.

Young, T.P., 1989: Phanerozoic ironstones: an introduction and
review: In: Phanerozoic Ironstone, (ed) Young, T.P.
& Taylor, T.P. Geol. Soci. Publ., No. 46: 9-25.

APPENDICES

APPENDIX I

PROCEDURES FOR GRAIN SIZE ANALYSES

Twenty-three well dried disaggregated clastic samples (sand-stones and siltstones) were selected for sieve analysis. 100g of each sample poured into sets of sieves were agitated by a Ro—Tap shaker for 15 mins. The retained weight of each sample is recorded against the sieve number and weight distribution data (Appendix II). From the sieve analyses data, various textural parameters were calculated.

APPENDIX II

Grain Size Analyses Data Sheets

Sample AG/K/12a   FMN: Lokoja

Sieve Size	Scale	Sample Wt. Retained (g)	Cumm. Sample Wt. (g)	Ind. Wt. (%)	Cumm. Wt. (%)
4.00mm	-2				
2.00mm	-1	0.12	0.12	0.24	0.24
1.00mm	0	1.00	1.12	2.00	2.24
600um	1	6.02	7.14	12.04	14.27
250um	2	29.92	37.06	59.84	74.12
150um	3	7.78	44.84	15.56	89.68
63um	4	4.13	48.79	8.26	97.94
63um	5	4.13	49.68	1.42	99.36
		49.68		99.36	

Sample AG/I/06   FMN: Patti

Sieve Size	Scale	Sample Wt. Retained (g)	Cumm. Sample Wt. (g)	Ind. Wt. (%)	Cumm. Wt. (%)
4.00mm	-2	8.08	8.08	16.6	16.16
2.00mm	-1	20.30	23.33	40.50	56.76
1.00mm	0	10.05	34.43	20.10	76.86
600um	1	5.48	43.91	10.96	87.82
250um	2	4.17	48.08	8.34	96.16
150um	3	0.76	48.84	1.52	97.68
63um	4	0.47	49.31	0.94	98.62
63um	5	0.10	49.41	0.20	98.82
		49.41		98.82	

Sample: AG/B/24c   FMN: Patti

Sieve Size	Scale	Sample Wt. Retained (g)	Cumm. Sample Wt. (g)	Ind. Wt. (%)	Cumm. Wt. (%)
4.00mm	−2				
2.00mm	−1	0.26	0.82	0.52	0.52
1.00mm	0	3.94	4.20	7.88	8.40
600um	1	21.98	26.18	43.96	52.36
250um	2	21.25	47.63	42.50	94.86
150um	3	1.95	49.37	3.90	97.76
63um	4	0.35	49.73	0.70	58.65
63um	5	0.05	49.77	0.10	99.56
		49.77		99.56	

Sample: AG/B/24e   FMN: Patti

Sieve Size	Scale	Sample Wt. Retained (g)	Cumm. Sample Wt. (g)	Ind. Wt. (%)	Cumm. Wt. (%)
4.00mm	−2	0.28	0.28	0.56	0.56
2.00mm	−1	1.56	1.84	3.12	3.68
1.00mm	0	6.52	8.36	13.04	16.72
600um	1	20.50	28.86	41.00	57.72
250um	2	16.70	45.56	33.40	91.12
150um	3	2.20	47.76	4.40	95.52
63um	4	1.84	49.61	3.70	99.22
63um	5	0.25	49.86	0.50	99.72
		49.86		99.72	

Sample: AG/A/20a   FMN: Patti

Sieve Size	Scale	Sample Wt. Retained (g)	Cumm. Sample Wt. (g)	Ind. Wt. (%)	Cumm. Wt. (%)
4.00mm	−2				
2.00mm	−1	0.21	0.21	0.42	0.42
1.00mm	0	1.56	1.77	3.12	3.54
600um	1	8.42	10.19	16.84	20.38
250um	2	22.60	32.79	45.20	65.58
150um	3	5.85	38.64	11.70	77.28
63um	4	6.08	44.72	12.16	89.44
63um	5	4.80	49.52	9.60	99.04
		49.52		99.04	

Sample: AG/A/20b   FMN: Patti

Sieve Size	Scale	Sample Wt. Retained (g)	Cumm. Sample Wt. (g)	Ind. Wt. (%)	Cumm. Wt. (%)
4.00mm	−2	1.00	1.00	2.00	2.00
2.00mm	−1	3.00	4.00	6.00	8.00
1.00mm	0	5.75	9.75	11.50	19.50
600um	1	9.30	19.05	18.60	38.10
250um	2	20.43	39.48	40.86	78.96
150um	3	3.06	42.54	6.12	85.08
63um	4	3.79	46.33	7.58	92.66
63um	5	3.49	49.82	6.98	99.64
		49.82		99.64	

Sample: KP/C/68a   FMN: Patti

Sieve Size	Scale	Sample Wt. Retained (g)	Cumm. Sample Wt. (g)	Ind. Wt. (%)	Cumm. Wt. (%)
4.00mm	-2	0.30	0.30	0.60	0.60
2.00mm	-1	1.58	1.88	3.18	3.78
1.00mm	0	6.40	8.18	2.68	16.46
600um	1	19.95	28.08	40.05	56.51
250um	2	16.10	44.18	32.41	88.92
150um	3	3.46	47.54	6.76	95.68
63um	4	1.84	49.38	3.70	99.38
63um	5	0.35	49.68	0.60	99.98
		49.68		99.98	

Sample: KP/c/68d   FMN: Patti

Sieve Size	Scale	Sample Wt. Retained (g)	Cumm. Sample Wt. (g)	Ind. Wt. (%)	Cumm. Wt. (%)
4.00mm	-2	0.20	0.10	0.20	0.20
2.00mm	-1	0.18	0.28	0.36	0.56
1.00mm	0	1.25	1.53	2.50	3.06
600um	1	15.95	17.48	31.97	35.03
250um	2	30.00	37.48	40.10	75.13
150um	3	7.50	44.98	15.03	90.46
63um	4	4.25	49.23	8.52	98.07
63um	5	0.65	49.88	1.30	99.
		49.88		99.98	

Sample: KP/B/56   FMN: Patti

Sieve Size	Scale	Sample Wt. Retained (g)	Cumm. Sample Wt. (g)	Ind. Wt. (%)	Cumm. Wt. (%)
4.00mm	−2				
2.00mm	−1	0.32	0.32	0.64	0.64
1.00mm	0	4.00	4.32	8.08	8.72
600um	1	2.60	25.92	43.63	52.35
250um	2	20.95	46.87	42.32	94.67
150um	3	2.00	48.87	4.04	98.71
63um	4	0.53	49.90	1.07	99.78
63um	5	0.10	49.50	0.20	99.98
		49.50		99.98	

Sample: Kp/B/55a   FMN: Patti

Sieve Size	Scale	Sample Wt. Retained (g)	Cumm. Sample Wt. (g)	Ind. Wt. (%)	Cumm. Wt. (%)
4.00mm	−2	7.91	7.91	15.85	15.85
2.00mm	−1	10.95	27.86	39.97	55.82
1.00mm	0	12.00	39.86	24.04	79.86
600um	1	4.50	44.36	9.02	88.88
250um	2	3.95	48.31	7.91	96.79
150um	3	1.00	49.81	2.00	98.79
63um	4	0.50	49.81	1.00	99.79
63um	5	0.10	49.91	0.20	99.79
		49.96		99.99	

Sample: KP/B/55c   FMN: Patti

Sieve Size	Scale	Sample Wt. Retained (g)	Cumm. Sample Wt. (g)	Ind. Wt. (%)	Cumm. Wt. (%)
4.00mm	-2	0.20	0.20	0.40	0.60
2.00mm	-1	0.55	0.75	1.10	1.51
1.00mm	0	1.60	2.35	3.22	4.35
600um	1	8.40	10.75	16.90	21.63
250um	2	21.90	32.65	44.06	65.69
150um	3	6.15	38.80	12.37	78.06
63um	4	6.35	45.15	12.77	90.83
63um	5	4.55	49.70	0.18	99.93
		49.70		99.98	

Sample: KP/A/5   FMN: Patti

Sieve Size	Scale	Sample Wt. Retained (g)	Cumm. Sample Wt. (g)	Ind. Wt. (%)	Cumm. Wt. (%)
4.00mm	-2	0.67	0.67	1.34	1.34
2.00mm	-1	3.49	4.16	6.98	8.32
1.00mm	0	7.32	11.48	19.64	22.96
600um	1	18.07	29.55	36.14	59.10
250um	2	16.11	45.66	32.22	91.32
150um	3	1.84	47.50	3.68	95.00
63um	4	1.42	48.92	2.84	97.84
63um	5	1.01	49.93	2.02	99.86
		49.93		99.86	

Sample: KP/B/51a   FMN: Lokoja

Sieve Size	Scale	Sample Wt. Retained (g)	Cumm. Sample Wt. (g)	Ind. Wt. (%)	Cumm. Wt. (%)
4.00mm	-2	0.22	0.22	0.44	0.44
2.00mm	-1	1.38	1.60	2.76	3.20
1.00mm	0	6.05	7.65	12.10	15.30
600um	1	20.00	27.65	40.00	55.30
250um	2	18.35	46.00	36.70	92.00
150um	3	1.47	47.47	2.94	94.94
63um	4	1.45	48.92	2.90	97.84
63um	5	1.00	49.92	2.00	99.84
		49.92			

Sample: KP/B/51c   FMN: Lokoja

Sieve Size	Scale	Sample Wt. Retained (g)	Cumm. Sample Wt. (g)	Ind. Wt. (%)	Cumm. Wt. (%)
4.00mm	-2				
2.00mm	-1	0.56	0.56	1.12	1.12
1.00mm	0	4.39	4.95	8.78	9.90
600um	1	22.20	27.25	44.40	54.30
250um	2	18.77	45.92	36.54	90.84
150um	3	2.00	47.42	4.00	94.84
63um	4	1.31	48.73	2.62	97.86
63um	5	1.25	49.98	2.50	99.96
		50.80		99.86	

Sample: KP/B/50   FMN: Lokoja

Sieve Size	Scale	Sample Wt. Retained (g)	Cumm. Sample Wt. (g)	Ind. Wt. (%)	Cumm. Wt. (%)
4.00mm	-2				
2.00mm	-1	0.52	0.52	1.04	1.04
1.00mm	0	4.32	4.88	8.64	9.68
600um	1	22.22	27.06	44.47	54.15
250um	2	18.25	45.31	36.52	90.67
150um	3	2.01	47.32	4.02	94.69
63um	4	1.36	48.68	2.72	97.41
63um	5	1.28	49.96	2.56	99.97
		49.96		90.97	

Sample: Kp/A/1   FMN: Lokoja

Sieve Size	Scale	Sample Wt. Retained (g)	Cumm. Sample Wt. (g)	Ind. Wt. (%)	Cumm. Wt. (%)
4.00mm	-2	0.60	0.60	1.20	1.20
2.00mm	-1	6.78	7.38	13.62	14.82
1.00mm	0	12.28	19.66	24.68	39.50
600um	1	18.15	37.81	36.48	75.98
250um	2	8.82	46.63	17.72	93.70
150um	3	1.82	48.45	3.65	97.35
63um	4	0.80	49.25	1.60	98.95
63um	5	0.50	49.75	1.00	99.95
		49.75		99.95	

Sample: AG/A/17   FMN: Lokoja

Sieve Size	Scale	Sample Wt. Retained (g)	Cumm. Sample Wt. (g)	Ind. Wt. (%)	Cumm. Wt. (%)
4.00mm	-2	0.54	0.54	1.31	1.31
2.00mm	-1	5.76	6.30	12.05	13.18
1.00mm	0	11.60	17.90	24.26	37.44
600um	1	17.00	34.90	35.56	73.00
250um	2	8.60	43.50	18.00	91.00
150um	3	2.70	46.20	5.64	96.60
63um	4	1.00	47.20	2.09	98.73
63um	5	0.60	47.80	1.26	99.98
		47.80		99.98	

Sample: AG/K/11c   FMN: Lokoja

Sieve Size	Scale	Sample Wt. Retained (g)	Cumm. Sample Wt. (g)	Ind. Wt. (%)	Cumm. Wt. (%)
4.00mm	-2	0.49	0.49	1.00	1.00
2.00mm	-1	5.72	6.21	10.72	11.72
1.00mm	0	12.00	18.21	–	36.14
600um	1	18.00	36.21	24.42	72.77
250um	2	8.40	44.61	17.09	95.97
150um	3	3.00	47.61	6.11	98.05
63um	4	1.02	48.63	2.08	98.05
63um	5	0.50	49.13	1.02	99.07
		49.13			

Sample: AG/B/23e   FMN: Lokoja

Sieve Size	Scale	Sample Wt. Retained (g)	Cumm. Sample Wt. (g)	Ind. Wt. (%)	Cumm. Wt. (%)
4.00mm	-2	0.54	0.54	1.09	1.09
2.00mm	-1	5.80	6.34	11.71	12.80
1.00mm	0	11.99	18.33	22.22	32.02
600um	1	18.08	36.41	36.52	73.54
250um	2	8.51	44.92	17.19	90.73
150um	3	3.02	47.94	6.10	96.83
63um	4	1.06	49.00	2.14	98.97
63um	5	0.50	49.50	1.01	99.98
		49.50		99.98	

Sample: AG/B/23a   FMN: Lokoja

Sieve Size	Scale	Sample Wt. Retained (g)	Cumm. Sample Wt. (g)	Ind. Wt. (%)	Cumm. Wt. (%)
4.00mm	-2	0.51	0.51	1.04	1.04
2.00mm	-1	5.75	6.36	11.76	12.79
1.00mm	0	12.05	16.36	24.64	37.43
600um	1	18.04	36.35	36.84	74.32
250um	2	8.24	44.56	16.70	91.11
150um	3	2.82	47.38	5.76	96.87
63um	4	1.04	48.82	2.03	99.00
63um	5	0.48	48.90	0.98	99.98
		48.90		99.98	

Sample: AG/B/22a   FMN: Lokoja

Sieve Size	Scale	Sample Wt. Retained (g)	Cumm. Sample Wt. (g)	Ind. Wt. (%)	Cumm. Wt. (%)
4.00mm	-2	0.60	0.60	1.21	1.21
2.00mm	-1	5.25	5.85	10.88	11.79
1.00mm	0	12.25	18.10	24.69	36.98
600um	1	18.04	36.14	36.35	72.83
250um	2	7.89	44.03	15.90	88.73
150um	3	3.51	47.54	7.07	95.80
63um	4	1.05	48.59	2.11	97.91
63um	5	1.03	49.62	2.07	90.98
		49.62		99.98	

Sample: AG/B/22b   FMN: Lokoja

Sieve Size	Scale	Sample Wt. Retained (g)	Cumm. Sample Wt. (g)	Ind. Wt. (%)	Cumm. Wt. (%)
4.00mm	-2	0.45	0.45	0.90	0.94
2.00mm	-1	5.50	5.95	11.04	11.94
1.00mm	0	11.92	17.87	23.93	35.87
600um	1	18.06	35.93	36.25	72.12
250um	2	8.34	44.32	16.84	88.96
150um	3	3.41	47.73	6.84	95.90
63um	4	1.08	48.81	2.17	97.97
63um	5	1.00	49.81	2.00	90.97
		49.81		99.97	

Sample: AG/B/22c   FMN: Lokoja

Sieve Size	Scale	Sample Wt. Retained (g)	Cumm. Sample Wt. (g)	Ind. Wt. (%)	Cumm. Wt. (%)
4.00mm	-2	0.45	0.45	0.90	0.90
2.00mm	-1	5.50	5.95	11.04	11.94
1.00mm	0	11.92	17.87	23.93	35.87
600um	1	18.06	35.93	36.25	72.12
250um	2	8.39	44.32	16.84	88.96
150um	3	3.41	47.73	6.84	95.80
63um	4	1.08	48.81	2.17	97.97
63um	5	1.00	49.81	2.00	99.97
		49.81		99.97	

APPENDIX III

PROCEDURES FOR HEAVY MINERAL SEPARATION

5g of treated dried sand fractions of sandstones and siltstones were used for the heavy mineral separation, using bromoform (s.p. 2.85). The oven-dried heavy mineral extracts were mounted on a microslide glass for necessary microscopic analyses and subsequent mineralogical description (Appendix IV). Modal analysis results were used in the calculation of ZTR index for the formations.

$$ZTR = \frac{Z + T + R}{\text{Total number of non-opaques}} \times \frac{100}{1}$$

Z = Zircon   T = Tourmaline   R = Rutile

APPENDIX IV

OPTICAL PROPERTIES OF HEAVY MINERALS

Minerals	Properties
Zircon	Colourless or pinkish in colour, prismatic high relief.
Tourmaline	They range in colour from green, light brown to brown. The crystal is subangular and seldom has an euhedral prismatic shape. Show striation, high relief and absorption under ppl.
Rutile	Reddish brown colouration, very high relief and birefringence parallel extinction.
Apatite	White or milk-white or colourless short prismatic and subrounded moderate relief, weak birefringence and parallel extinction.
Garnet	Colourless or light brown, subangular in shape.
Staurolite	Irregular grain with concoidal fracture. Yellow to reddish yellow and brown in colour. Markedly pleochroic, high R.I. and low birefringence is low.
Hornblende	It varies in colour from bluish green to yellowish green ones to yellow. It may be subangular or takes short or long prismatic shape. It shows extinction and pleochroism.
Hematite	Reddish brown under incident light.
Ilmenite	Black colour with bluish tint under incident light.

APPENDIX V

PROCEDURES FOR THE CALCULATION OF THE ANALYTICAL DATA FROM MICROPROBE STUDIES

The objectives are to:

1. calculate the amount of H_2O involved in the system.

2. establish the different mineral components in the system (starting from kaolinite, the initial mineral before replacement by FeOOH, which originally contains water).

Stages of calculation:

1. Calculate The SiO_2/Al_2O_3 ratio from the analytical result, see whether it conforms with the theoretical value of 1.2 for kaolinite.

2. If the value is equal or between 1.0 - 1.2, then calculate for H_2O from Al_2O_3 and SiO_2 respectively. The average of these values is inserted into the analytical result (as H_2O calculated).

3. If the ratio is greater than 1.2, i.e. excess SiO_2 is in the system. Calculate for the SiO_2 component in kaolinite from the analytical value of Al_2O_3. Subtract this value from the analytical value of SiO_2 to know the excess SiO_2 in the system. Then calculate for H_2O from Al_2O_3 only.

Insert all the calculated values into the analytical result.

4. If the ratio is less than 1.2, i.e. excess Al_2O_3 is in the system. Calculate for Al_2O_3 component in kaolinite from the analytical value of SiO_2. Subtract this value from the analytical value of Al_2O_3 to know the excess Al_2O_3 in the system. Then calculate for H_2O from SiO_2 only and convert the excess Al_2O_3 to AlOOH.

    Insert all the calculated values into the analytical result.

5. Convert the analytical value of FeO into FeOOH or Fe_2O_3 as appropriate to the point analysed.

    Replace FeO value with the converted value.

6. Sum all the inserted values and the other available oxides in the analytical result.

7. Finally, deduce the constituent minerals from this result.

    NB: Kaolinite $=$ $Al_2O_3 + SiO_2^k + H_2O$

    Goethite $=$ FeOOH

    Hematite $=$ Fe_2O_3

    Boehmite $=$ AlOOH
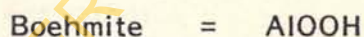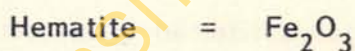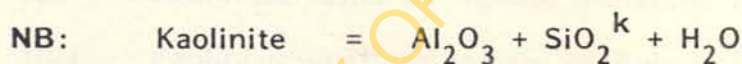
    SiO_2^k/Al_2O_3 ratio is then calculated.

APPENDIX VI

Calculated molecular proportion for:

(i)   Sedimentary kaolinite

(ii)   Kaolinitic relics of Agbaja Ironstone Formation

(iii)   Kaolinitic-goethitic matrix of Agbaja Ironstone
        Formation

(iv)   Goethitic-hematitic matrix of Agbaja Ironstone
        Formation

Table 19:   CHEMICAL ANALYSES OF SEDIMENTARY KAOLINITE (BRIGATTI 1988)

	1	2	3	4	5	6	7	8	9	10	11	12	13	14	Mean
SiO_2	46.29	47.04	48.13	45.52	45.98	46.12	46.00	45.46	45.90	46.00	47.10	46.05	45.70	45.29	46.18
Ti_2O	0.02	0.14	0.06	0.29	0.24	0.08	0.12	0.05	0.10	0.11	0.43	0.05	0.06	-	0.13
Al_2O_3	39.22	39.57	40.89	37.79	37.80	38.21	38.21	38.37	38.33	38.51	38.94	38.81	38.44	38.87	38.71
Fe_2O_3	0.12	0.10	0.08	1.18	1.78	1.24	1.13	0.99	0.50	0.36	0.67	0.15	0.56	0.26	0.65
CaO	0.04	0.14	0.06	0.10	0.08	0.07	0.11	0.13	0.04	0.08	0.15	0.09	0.25	0.13	0.11
MgO	-	-	-	0.15	0.13	0.06	0.08	-	0.15	0.18	0.17	0.11	0.27	0.11	0.11
MnO	0.13	0.14	0.08	0.11	0.08	0.11	0.09	0.09	0.03	0.11	0.07	0.04	0.04	0.04	0.08
Na_2O	-	0.07	0.08	0.11	0.06	0.05	0.04	0.05	-	0.05	0.10	0.03	0.11	0.06	0.06
K_2O	-	-	-	-	-	0.02	-	0.02	0.03	-	0.04	-	0.04	0.02	0.01
P_2O_5	-	-	-	-	-	-	-	-	-	-	-	-	-	-	0
H_2O+	14.18	12.80	10.62	14.75	13.85	14.05	14.22	14.84	14.92	14.60	12.33	14.67	14.53	14.92	13.95
Total	100.00	100.00	100.00	100.00	100.00	100.01	100.00	100.00	100.00	100.00	100.00	100.00	100.00	99.70	100.00

188

189

	1	2	3	4	5	6	7	8	9	10	11	12	13	14
SiO_2	0.012	0.009	0.026	0.006	0.008	0.035	0.014	0.008	0.008	0.005	0.010	0.006	0.022	0.013
TiO_2	-	-	0.001	0.001	-	0.001	-	0.001	0.001	-	-	0.001	-	0.001
Al_2O_3	0.020	0.019	0.028	0.016	0.009	0.055	0.011	0.049	0.051	0.018	0.010	0.006	0.007	0.023
Fe_2O_3	0.588	0.593	0.588	0.599	0.605	0.560	0.596	0.568	0.572	0.585	0.602	0.610	0.603	0.590
CaO	0.002	0.002	-	-	0.002	-	0.002	0.002	-	0.003	-	-	-	0.001
MgO	-	-	-	0.003	-	0.003	0.003	-	-	0.003	-	-	-	0.001
MnO	-	-	-	-	-	-	-	-	-	-	-	-	-	-
Na_2O	-	-	-	-	-	-	-	-	-	-	-	-	0.002	0.001
K_2O	-	-	-	-	-	-	-	-	-	-	-	-	-	-
P_2O_5	0.015	0.017	0.009	0.008	0.012	0.007	0.013	0.011	0.010	0.025	0.009	0.008	0.008	0.011
H_2O^+	0.035	0.032	0.093	0.028	0.014	0.067	0.024	0.092	0.086	0.021	0.17	0.013	0.014	0.041

Table 20: CHEMICAL ANALYSES OF THE KAOLINITIC RELICS (UNFERRUGINIZED) OF THE AGBAJA IRONSTONE FORMATION

	15	16	17	18	19	20	21	22	23	24	25	26	27	28	Mean
SiO_2	44.76	45.96	37.14	39.35	35.51	35.11	30.83	43.99	50.72	47.78	43.14	43.87	43.46	39.45	41.28
TiO_2	-	-	0.27	0.25	0.13	-	0.16	5.76	-	-	0.10	-	0.42	-	0.52
Al_2O_3	36.01	36.54	33.70	34.24	32.65	32.00	30.83	32.43	35.04	35.66	36.60	37.25	36.87	33.63	34.34
Fe_2O_3	4.18	4.68	14.78	12.57	18.00	19.08	26.00	9.52	1.59	3.47	5.53	3.86	6.18	12.48	0.08
CaO	0.17	0.10	0.15	-	-	-	0.10	-	-	-	0.15	0.11	-	-	0.06
MgO	0.18	0.22	-	-	-	-	-	-	-	-	-	-	-	-	0.03
MnO	-	-	-	-	-	-	-	-	-	-	-	-	-	-	0.00
Na_2O	-	-	-	-	-	-	-	-	-	-	-	-	-	-	-
K_2O	-	0.12	-	-	-	-	-	-	-	-	-	-	0.15	-	0.02
P_2O_5	0.91	0.52	1.01	0.63	0.80	0.58	0.76	0.10	-	-	0.92	0.56	0.17	0.54	0.53
H_2O+	13.52	13.85	13.17	13.35	13.10	13.06	12.72	12.52	12.54	12.98	13.58	13.59	13.69	12.25	13.14
Total	99.93	101.87	100.34	100.39	100.19	99.83	99.34	100.24	99.89	99.89	100.02	99.24	100.94	99.35	100.00

	1	2	3	4	5	6	7	8	9	10	11	12	13	14
SiO_2	0.029	0.032	0.017	0.008	0.005	0.027	0.005	0.004	0.019	0.018	0.016	0.044	0.043	0.021
TiO_2	-	0.001	0.002	-	-	0.001	-	-	0.001	-	0.002	-	-	0.001
Al_2O_3	0.013	0.005	0.024	0.034	0.025	0.014	-	-	0.050	0.044	0.088	0.050	0.045	0.030
Fe_2O_3	0.528	0.539	0.517	0.527	0.527	0.528	0.497	0.499	0.490	0.496	0.478	0.505	0.509	0.510
CaO	-	-	-	-	-	-	-	-	0.003	0.006	-	0.002	-	0.001
MgO	0.003	-	-	-	-	-	-	-	-	0.004	-	-	0.004	0.001
MnO	0.005	0.004	0.002	-	-	0.004	-	-	-	-	-	-	-	0.001
Na_2O	-	0.002	-	-	-	-	-	-	-	-	-	-	-	0.001
K_2O	-	-	-	-	-	-	-	-	-	-	-	-	-	-
P_2O_5	0.008	0.008	0.022	0.019	0.020	0.013	0.038	0.037	0.027	0.011	0.009	0.004	0.018	0.022
H_2O^+	0.554	0.545	0.561	0.572	0.566	0.556	0.796	0.799	0.680	0.697	0.657	0.586	0.627	0.657

Table 21:   CHEMICAL ANALYSES OF THE KAOLINITIC-GOETHITIC MATRIX OF THE AGBAJA IRONSTONE FORMATION

	1	2	3	4	5	6	7	8	9	10	11	12	13	Mean
SiO_2	1.72	1.94	1.02	0.45	0.32	1.59	0.27	0.23	1.16	1.10	0.98	2.65	2.58	1.23
TiO_2	-	0.25	0.43	-	-	0.15	-	-	0.15	-	0.47	-	-	0.11
Al_2O_3	1.29	0.28	2.43	3.45	2.60	1.42	-	-	5.00	4.47	8.93	5.01	4.55	3.03
Fe_2O_3	84.47	86.23	82.67	83.26	84.26	84.43	79.44	79.87	78.39	79.42	76.45	80.74	81.41	81.60
CaO	-	-	-	-	-	-	-	-	0.14	0.33	-	0.10	-	0.04
MgO	0.12	-	-	-	-	-	-	-	-	0.15	-	-	0.16	0.03
MnO	0.38	0.26	0.11	-	-	0.25	-	-	-	-	-	-	0.08	-
Na_2O	-	0.11	-	-	-	-	-	-	-	-	-	-	-	0.01
K_2O	-	-	-	-	-	-	-	-	-	-	-	-	-	0.00
P_2O_5	1.12	1.07	3.06	2.70	2.90	1.78	5.33	5.22	3.48	3.06	1.58	1.28	0.56	2.58
H_2O+	9.97	9.81	10.10	10.30	10.19	10.01	14.32	14.39	12.24	12.54	11.82	10.55	10.62	11.29
Total	99.07	99.98	99.82	100.16	100.27	99.63	99.36	99.71	100.92	101.07	100.23	100.33	99.96	100.00

192

	1	2	3	4	5	6	7	8	9	10	11	12	13	14	15
SiO_2	0.000	0.766	0.619	0.656	0.592	0.585	0.514	0.733	0.845	0.796	0.719	0.731	0.724	0.658	0.747
TiO_2	0.000	0.000	0.001	0.001	0.000	0.000	0.001	0.024	0.000	0.000	0.000	0.000	0.002	0.000	0.002
Al_2O_3	0.353	0.358	0.330	0.336	0.320	0.314	0.302	0.318	0.343	0.350	0.359	0.365	0.361	0.330	0.337
Fe_2O_3	0.026	0.029	0.092	0.079	0.113	0.119	0.163	0.060	0.010	0.022	0.035	0.024	0.039	0.078	0.063
CaO	0.003	0.002	0.003	0.000	0.000	0.000	0.002	-	-	-	0.003	0.002	-	-	0.001
MgO	0.005	0.006	-	-	-	-	-	-	-	-	-	-	-	-	0.001
MnO	-	-	-	-	-	-	-	-	-	-	-	-	-	-	-
Na_2O	-	-	-	-	-	-	-	-	-	-	-	-	-	-	-
K_2O	-	-	0.001	-	-	-	-	-	-	-	-	0.002	-	-	-
P_2O_5	0.006	0.004	0.008	0.004	0.006	0.004	0.005	0.001	-	-	0.006	0.004	0.001	0.004	0.004
H_2O^+	0.751	0.769	0.732	0.742	0.728	0.726	0.707	0.696	0.697	0.721	0.754	0.755	0.761	0.736	0.730

193

	1	2	3	4	5	6	7	8	9	10	11	12	13	Mean
SiO_2	0.74	0.55	1.58	0.37	0.49	2.10	0.86	0.50	0.46	0.28	0.62	0.35	1.29	0.78
TiO_2	-	-	0.16	0.11	-	0.15	-	0.12	0.14	-	-	0.30	-	0.08
Al_2O_3	2.03	2.32	2.87	1.64	0.96	5.56	1.11	4.96	5.25	1.83	0.98	0.65	0.71	2.35
Fe_2O_3	94.03	94.88	94.11	95.87	96.74	89.58	95.34	90.80	91.47	93.59	96.32	97.54	96.54	94.37
CaO	0.11	-	-	0.10	-	-	0.11	0.11	-	0.19	-	-	-	0.06
MgO	-	-	-	0.12	-	0.10	0.13	-	-	0.12	-	-	-	0.04
MnO	-	-	-	-	-	-	-	-	-	-	-	-	-	0.00
Na_2O	-	-	-	-	-	-	-	-	-	-	-	-	0.11	0.01
K_2O	-	-	-	-	-	-	-	-	-	-	-	-	-	0.00
P_2O_5	2.10	2.14	1.25	1.08	1.74	1.05	1.82	1.51	1.43	3.51	1.29	1.16	1.10	1.57
H_2O+	0.63	0.57	1.68	0.50	0.26	1.20	0.43	1.66	1.55	0.38	0.31	0.23	0.25	0.74
Total	99.64	100.46	101.57	99.69	100.30	99.84	99.80	99.60	100.30	99.90	99.52	100.23	99.99	100.00

194

	1	2	3	4	5	6	7	8	9	10	11	12	13	14	15
SiO_2	0.772	0.784	0.802	0.759	0.766	0.769	0.767	0.758	0.765	0.767	0.785	0.768	0.762	0.755	0.770
TiO_2	0.000	0.001	0.000	0.001	0.001	0.000	0.001	0.000	0.000	0.001	0.002	0.000	0.000	0.000	0.001
Al_2O_3	0.385	0.388	0.401	0.370	0.371	0.375	0.375	0.376	0.376	0.378	0.382	0.380	0.377	0.381	0.380
Fe_2O_3	0.001	0.001	0.001	0.007	0.011	0.008	0.007	0.006	0.003	0.002	0.004	0.001	0.004	0.002	0.004
CaO	0.001	0.003	0.001	0.002	0.001	0.001	0.002	0.002	0.001	0.001	0.003	0.002	0.004	0.002	0.002
MgO	-	-	-	0.004	0.003	0.002	0.002	-	0.004	0.005	0.004	0.003	0.007	0.003	0.003
MnO	0.002	0.002	0.001	0.002	0.001	0.002	0.001	0.001	-	0.002	0.001	0.001	0.001	0.001	0.001
Na_2O	-	0.001	0.001	0.002	0.001	0.001	0.001	0.001	-	0.001	0.002	0.001	0.002	-	-
K_2O	-	-	-	-	-	-	-	-	-	-	-	-	-	-	-
P_2O_5	-	-	-	-	-	-	-	-	-	-	-	-	-	0.829	0.775
H_2O	0.788	0.711	0.590	0.819	0.769	0.781	0.790	0.824	0.829	0.811	0.685	0.815	0.807	0	302.54

APPENDIX VII

Mass balance calculation for:

(i)   Sedimentary kaolinite

(ii)   Kaolinitic relics of Agbaja Ironstone Formation

(iii)   Kaolinitic-Goethitic matrix of Agbaja Ironstone Formation

(iv)   Goethitic-hematitic matrix of Agbaja Ironstone Formation

	1	2	3	4	5	6	7	8	9	10	11	12	13	14	15
SiO_2/TiO_2	0	784	0	759	766	0	767	0	0	767	392.50	0	0	0	148.07
Al_2O_3/TiO_2	0.00	588.00	0	370.00	371.00	0	375.00	0	0	378.00	191.00	0	0	377.50	359.92
SiO_2/Fe_2O_3	772.00	784.00	802.00	108.43	69.64	96.13	109.57	126.33	255.00	383.50	196.25	786.00	190.50	190.50	178.45
Al_2O_3/Fe_2O_3	385.00	388.00	401.00	52.86	33.73	46.88	53.57	62.67	125.33	189.00	95.50	380.00	94.25	377.50	518.43
SiO_2/CaO	772.00	261.33	802.00	379.50	766.00	769.00	383.50	379.00	675.00	767.00	261.67	384.00	190.50	190.50	255.57
Al_2O_3/CaO	385.00	129.33	401.00	185.00	371.00	375.00	187.50	188.00	376.00	378.00	127.33	190.00	94.25	251.67	169.32
SiO_2/MgO	0	0	0	189.75	255.33	384.50	383.50	0	191.25	153.40	196.25	256.00	108.86	127.00	83.13
Al_2O_3/MgO	0	0	0	92.50	123.67	187.50	187.50	0	94.00	75.60	95.50	126.67	53.86	755.00	577.75
SiO_2/MnO	386.00	392.00	802.00	379.50	766.00	384.50	767.00	758.00	0	383.50	785.00	768.00	762.00	381.00	285.07
Al_2O_3/MnO	192.50	194.00	401.00	185.00	371.00	187.50	375.00	376.00	0	189.00	382.00	380.00	377.00	755.00	577.79
SiO_2Na_2O	0	784.00	802.00	379.50	766.00	769.00	767.00	758.00	0	767.00	392.50	768.00	381.00	381.00	284.96
Al_2O_3/Na_2O	0	388.00	401.00	185.00	371.00	375.00	375.00	376.00	0	378.00	191.00	380.00	188.50	0	0
SiO_2/K_2O	0	0	0	0	0	0	0	0	0	0	0	0	0	0	0
Al_2O_3/K_2O	0	0	0	0	0	0	0	0	0	0	0	0	0	0	0
SiO_2/P_2O_5	0	0	0	0	0	0	0	0	0	0	0	0	0	0	0
Al_2O_3/P_2O_5	0	0	0	0	0	0	0	0	0	0	0	0	0	0.50	0.50
Al_2O_5/SiO_2	0.50	0.50	0.50	0.50	0.50	0.50	0.50	0.50	0.50	0.50	0.50	0.50	0.50	0.50	0.50

197

	1	2	3	4	5	6	7	8	9	10	11	12	13	14	15
SiO_2/TiO_2	0	0	69.00	656.00	0	0	514.00	30.54	0	0	0	0	362.00	0	155.82
Al_2O_3/TiO_2	0	0	330.00	336.00	0	0	302.00	13.25	0	0	0	0	180.00	0	82.98
SiO_2/Fe_2O_3	28.69	26.41	6.73	8.30	5.24	4.92	3.15	12.22	84.50	36.18	20.54	30.46	18.56	8.44	21.02
Al_2O_3/Fe_2O_3	13.58	12.34	3.59	4.25	2.83	2.64	1.85	5.30	34.30	15.91	10.26	15.21	9.26	4.23	9.82
SiO_2/CaO	248.67	383.00	206.33	0	0	0	257.00	0	0	0	239.67	365.50	0	0	106.04
Al_2O_3/CaO	176.50	179.00	110.00	0	0	0	151.00	0	0	0	119.67	182.50	0	0	65.62
SiO_2/MgO	149.20	127.67	0	0	0	0	0	0	0	0	0	0	0	0	19.78
Al_2O_3/MgO	70.60	59.67	0	0	0	0	0	0	0	0	0	0	0	0	9.31
SiO_2/MnO	0	0	0	0	0	0	0	0	0	0	0	0	0	0	0
Al_2O_3/Mno	0	0	0	0	0	0	0	0	0	0	0	0	0	0	0
SiO_2Na_2O	0	0	0	0	0	0	0	0	0	0	0	0	0	0	0
Al_2O_3/Na_2O	0	0	0	0	0	0	0	0	0	0	0	0	0	0	0
SiO_2/K_2O	0	0	619.00	0	0	0	0	0	0	0	0	0	362.00	0	70.07
Al_2O_3/K_2O	0	0	330.00	0	0	0	0	0	0	0	0	0	180.50	0	36.46
SiO_2/P_2O_5	124.33	191.50	77.78	164.00	98.67	146.25	102.80	733.00	0	0	119.83	182.75	724.00	164.50	302.10
Al_2O_3/P_2O_5	58.83	89.50	41.25	84.00	53.33	78.50	60.40	318.00	0	0	59.83	91.25	361.00	82.50	98.46
Al_2O_5/SiO_2	0.50	0.50	0.53	0.51	0.54	0.54	0.59	0.43	0.41	0.44	0.50	0.50	0.50	0.50	0.50

198

	1	2	3	4	5	6	7	8	9	10	11	12	13	14	15
SiO_2/TiO_2	0	32.008	8.50	0	0	27.00	0	0	19.00	0	8.00	0	0	0	
Al_2O_3/TiO_2	0	3.00	12.00	0	0	14.00	0	0	50.00	0	44.00	0	0	0	
SiO_2/Fe_2O_3	0.06	0.06	0.03	0.02	0.01	0.05	0.01	00.04	0.04	0.03	0.09	0.08	0.04	0.04	
Al_2O_3/Fe_2O_3	0.02	0.06	0.05	0.06	0.05	0.03	0	0	0.10	0.09	0.18	0.10	0.09	0.09	
SiO_2/CaO	0	0	0	0	0	0	0	0	6.33	3.00	3.00	0	22.00	3.00	
Al_2O_3/CaO	0	0	0	0	0	0	0	0	16.67	7.33	0	25.00	0	7.33	
SiO_2/MgO	9.67	0	0	0	0	0	0	0	0	4.50	0	0	10.75	4.50	
Al_2O_3/MgO	4.33	0	0	0	0	0	0	0	0	11.00	0	0	11.25	11.00	
SiO_2/MnO	5.80	8.00	8.50	0	0	6.75	0	0	0	0	0	0	0	0	
Al_2O_3/MnO	2.60	0.75	12.00	0	0	3.50	0	0	0	0	0	0	0	0	
SiO_2Na_2O	0	16.00	0	0	0	0	0	0	0	0	0	0	0	0	
Al_2O_3/Na_2O	0	1.50	0	0	0	0	0	0	0	0	0	0	0	0	
SiO_2/K_2O	0	0	0	0	0	0	0	0	0	0	0	0	0	0	
Al_2O_3/K_2O	0	0	0	0	0	0	0	0	0	0	0	0	0	0	
SiO_2/P_2O_5	3.63	4.00	0.77	0.42	0.25	2.08	0.13	0.11	0.70	0.82	1.45	4.89	10.75	0.82	
Al_2O_3/P_2O_5	1.63	0.38	1.09	1.79	1.25	1.08	0	0	1.85	2.00	8.00	5.56	11.25	2.00	
Al_2O_5/SiO_2	0.45	0.09	1.41	4.25	5.00	0.51	0	0	2.63	2.44	5.50	1.14	1.05	2.44	

	1	2	3	4	5	6	7	8	9	10	11	12	13	14	15
SiO_2/TiO_2	0	0	26.00	6.00	0	35.00	0	8.00	8.00	0	0	6.00	0	6.85	
Al_2O_3/TiO_2	0	0	28.00	16.00	0	55.00	0	49.00	51.00	0	0	6.00	0	15.77	
SiO_2/Fe_2O_3	0.02	0.02	0.04	0.01	0.01	0.06	0.02	0.01	0.01	0.01	0.02	0.01	0.04	0.02	
Al_2O_3/Fe_2O_3	0.03	0.03	0.05	0.03	0.01	0.10	0.02	0.09	0.09	0.03	0.02	0.01	0.01	0.04	
SiO_2/CaO	6.00	4.50	0	0	4.00	0	7.00	4.00	0	1.67	0	0	0	2.09	
Al_2O_3/CaO	10.00	9.00	0	0	4.50	0	5.50	24.50	0	6.00	0	0	0	4.62	
SiO_2/MgO	0	0	0	2.00	0	11.67	4.67	0	0	1.67	0	0	0	1.54	
Al_2O_3/MgO	0	0	0	5.33	0	18.33	3.67	0	0	6.00	0	0	0	2.56	
SiO_2/MnO	0	0	0	0	0	0	0	0	0	0	0	0	0	0	
Al_2O_3/MnO	0	0	0	0	0	0	0	0	0	0	0	0	0	0	
SiO_2Na_2O	0	0	0	0	0	0	0	0	0	0	0	0	11.00	0.85	
Al_2O_3/Na_2O	0	0	0	0	0	0	0	0	0	0	0	0	3.50	0.27	
SiO_2/K_2O	0	0	0	0	0	0	0	0	0	0	0	0	0	0	
Al_2O_3/K_2O	0	0	0	0	0	0	0	0	0	0	0	0	0	0	
SiO_2/P_2O_5	0.80	0.53	2.89	0.75	0.67	5.00	1.08	0.73	0.80	0.20	1.11	0.75	2.75	1.39	
Al_2O_3/P_2O_5	1.33	1.12	3.11	2.00	0.75	7.86	0.85	4.45	5.10	0.72	1.11	0.75	0.88	2.31	
Al_2O_5/SiO_2	1.67	2.11	1.08	2.67	1.13	1.57	0.79	6.13	6.38	3.60	1.00	1.00	0.32	2.27	

200